Biomass Upgrading in Staged Autothermal Reactors with Multifunctional Catalysts

A dissertation submitted to the faculty of the
Graduate School of the University of Minnesota
by

Samuel D. Blass

In partial fulfillment of the requirements for the
degree of Doctor of Philosophy.

Advisors: Lanny D. Schmidt
Aditya Bhan

December 2013

ACKNOWLEDGMENTS

One of the more unique aspects of my PhD program, besides an original contribution to science, is the opportunity to cultivate career friendships with others who have accompanied me and guided me through the trials and tribulations of academia. Many of these individuals do not appear on any of my publications, so I would like to acknowledge everyone here as I begin this coda of my time in graduate school.

In having two advisors, Professors Lanny Schmidt and Aditya Bhan, I have benefitted from multiple perspectives on my area of study and from their ideas and concepts that extend beyond the realms of catalysis and reaction engineering. Besides being experts in their fields, my advisors are also my role-models for applying discovery, creativity, critical thinking, and rigorous analysis to research problems. They have coached me on these skills which will be transferable to anything that comes my way and for that I am truly grateful.

It is more difficult to quantify what I have learned from my fellow graduate student colleagues, with whom I spent most of my time. I began my Schmidt Lab adventure with Dr. Reetam Chakrabarti's instructions on how to swage tubing, and also how to nail a ping-pong serve. Perhaps most importantly, he periodically reassured me that my reactor was not about to detonate. I am especially grateful for Reetam's practical perspective and for the many late nights spent serving as a sounding board for my ideas.

From Dr. Jake Kruger I learned how to fill out an incident report after accidentally setting a fume hood on fire. I will always admire Jake's quest to live an entirely green lifestyle, rather ironic for someone who spent three years burning hydrocarbons in a lab. I am grateful to Drs. Christine and Josh Colby for their endless supply of friendship and veggie burgers, and to Nils Persson, an undergrad Schmidtster-turned-lab technician who also served as our in-house video director and comedy writer. Chapters 5 and 6 would not have been possible without Nils' creativity and dedication. Rich Hermann, another talented undergrad, has been a great source

of both experimental ideas and free Twins tickets. Rich is partially responsible for Chapter 6 and also happens to have more publications from our group than most Schmidt graduate students. I am also grateful to Dr. Hui Sun and Michael Skinner for being excellent sources of ideas and lab supplies, and to undergraduates Corey Rosenthal, Sheila Hunter, and Eric Hansen for their assistance with experiments.

While research is an important part of any PhD program, there is certainly more to graduate school than the lab. Perhaps there has been no one better suited to teach me that than Jeremy Bedard, who embodies the principle of "work hard – play hard." His refreshing perspective was a breath of fresh air in a sometimes stifling academic environment. As the last in a long line of Schmidt students, I have watched our group dwindle down in number, but Jeremy and Nils have made the lab seem a lot less empty.

I must also acknowledge my parents for their endless support, and the Minnesota Corn Growers Association for providing me with an incredible eye-opening perspective of our country's farming industry. Contrary to popular belief, corn does not grow in the produce section. As a native of the northeast's urban wilderness, I love driving through Minnesota's farm country and I have really been taken with the Midwestern lifestyle. Smile at strangers and support your local farmers market!

ABSTRACT

Biomass contains a significant weight percentage of oxygen which must be removed to produce biofuel. In addition, the distributed nature of biomass necessitates the development of small-scale biorefineries which will also require reactors capable of processing and distributing biofuel locally. For this we turn to small-scale autothermal reactors capable of thermochemical processing of biomass to biofuel. An autothermal staged reactor consists of an upstream catalyst responsible for catalytic partial oxidation (CPO) which generates hydrogen and process heat needed to drive reactions on a downstream zeolite stage.

Reactions in an autothermal staged reactor are heat-integrated and small-scale, making these reactors potentially useful for a biorefinery. The challenge in developing autothermal staged reactors is in integrating multiple catalytic functions requiring different operating conditions such as temperature and space velocity. In this thesis, the autothermal staged reactor is developed by initially studying relatively simple systems such as butanol dehydration and isomerization in Chapter 2 and eventually extending the analysis to more complex and realistic systems such as cellulose upgrading in Chapter 5.

Integration of CPO and zeolite functionalities is discussed in Chapter 2, where butanol, considered an advanced biofuel, is dehydrated and isomerized to butene isomers. Higher butene yields were obtained from butanol when the catalyst used did not contain Brϕnsted acid sites such as γ-Al_2O_3 or when the zeolite used, such as HFER, contained pores that were too small to permit competing reactions such as oligomerization to occur. Up to a 95% butene yield was obtained with HFER at temperatures from 280-350 $^{\circ}$C.

The staged autothermal reactor concept was extended in Chapter 3 from butanol to hexane, decane, and 2-decanone which were used to probe the extent of isomerization, cracking and deoxygenation as a function of carbon chain length and oxygen

functionality. While the kinds of reactions butanol underwent were largely limited to dehydration, paraffins and alkanones can undergo isomerization and cracking over zeolites in a staged autothermal reactor. A maximum 36% aromatics yield was obtained from a 2-decanone feed at 400 °C over zeolite USY in contrast with a less than 5% aromatics yield from decane under identical conditions.

The staged autothermal reactor was applied in Chapter 5 to cellulose upgrading, a feedstock more similar to actual biomass than either butanol or paraffins. The staged autothermal reactor enables solids such as cellulose to be upgraded over heterogeneous catalysts such as zeolites by going through a pyrolysis vapor intermediate. Microcrystalline cellulose particles were fed to the reactor and pyrolyzed to volatile organic compounds that were subsequently upgraded over a second stage containing HZSM-5 at 500 °C. A maximum 24% yield of aromatics and 20% yield of C_{2-4} olefins and paraffins were obtained from the pyrolysis vapor entering the second stage.

Pyrolysis oil contains species such as ketones whose acidity and corrosiveness make chemical storage difficult. Bifunctional catalysts such as those containing both metal and acid functionality can be applied to upgrade ketones more effectively than monofunctional catalysts. Upgrading of butanone over Pt/γ-Al_2O_3 mixed with HZSM-5 is discussed in Chapter 4. A 99% selective stream of butane was obtained from butanone at 67% conversion and 160 °C with minimal C-C bond scission, an important characteristic in any biofuel process.

Glycerol conversion to olefins is possible with a three-stage isothermal reactor over a combination of HZSM-5, HBEA, and Pt or Pd catalysts and is discussed in Chapter 6. Glycerol can be converted to propanal which can undergo aldol condensation to form olefins ranging in size from C_{2-5} along with small amounts of aromatics and minimal amounts of CO. A maximum yield of 70% was obtained when propanal was reacted over HBEA in the absence of acetaldehyde at 500 °C. Catalyst lifetime was also extended from 10 min to at least 150 min for a pure propanal feed.

In this thesis, the chemical functionality of autothermal reactors and multifunctional catalysts is expanded and developed for a wide scope of applications—from dehydration of simple alcohols to cellulose upgrading. The autothermal staged reactor represents an attempt at designing a small-scale and heat-integrated system for potential use in a biorefinery.

CONTENTS

LIST OF TABLES

LIST OF FIGURES

CHAPTER

ONE

INTRODUCTION

In this section, the motivation and potential applications for biofuel production are discussed for autothermal reactors containing additional catalytic functions. Research in biofuels, the only known source of renewable carbon, is motivated by the environmental concerns of fossil fuel consumption.[1] First-generation biofuels such as ethanol and biodiesel have been successfully commercialized but have been unable to supplant a significant percentage of U.S. petroleum consumption, primarily because of the high oxygen content[2,3] and distributed nature of biomass.[4,5] Second-generation biofuels such as cellulosic ethanol originate from biomass feedstocks that are cheaper to produce but more expensive to convert to fuel.[6]

Methods such as gasification and pyrolysis have been developed to convert cellulosic feedstocks to biofuels, however, these processes require large energy inputs and can produce char or chemically unstable bio-oil.[6–9] Autothermal reactors, first developed by Hickman and Schmidt in 1993,[10] circumvent many of these problems by converting a wide-range of feedstocks, including cellulose, to syngas and pyrolysis oil with no external heat input and negligible deactivation.[10–13] While syngas can be upgraded to hydrocarbons via conventional processes such as Fischer-Tropsch,[14,15] pyrolysis oil upgrading is still an active area of research.

Biorefineries will require the development of reactors capable of small-scale biomass upgrading through techniques such as pyrolysis.[16] The theme of this thesis is the development of autothermal staged reactors containing expanded chemical functionalities in the form of additional zeolite catalysts capable of biomass upgrading. The additional compactness, heat-integrated configuration, and versatility in processing a

wide-range of feedstocks may render it potentially relevant for biomass upgrading in a biorefinery.

1.1 Fossil fuels

Diminishing stores of easily accessible petroleum is motivating research in alternative sources of energy. The peak of world oil production has been predicted by some to occur around 2020 with a subsequent decline in production in the ensuing years.[17,18] Despite the finite nature of global oil reserves, the world's energy usage is predicted to grow from 524 to 820 quadrillion BTU between 2010 and 2040[19] and sustained economic growth will require ever increasing amounts of oil. For example, China contributes 5% of the world's Gross Domestic Product yet consumes 15% of the world's energy.[20] The lack of any viable alternatives means fossil fuels will be the the world's primary energy source for at least another century,[21] however, new fossil fuel based technologies are being developed to extract oil from unconventional sources such as tar sands and shale gas.

Although the global supply of petroleum is not expected to be depleted in the next century,[21] expansion of new sources of petroleum such as tar sands present their own environmental challenges.[22] While tar sands is becoming a more significant source of petroleum, greenhouse gas emissions are approximately 176 $kgCO_2eq/bbl$ compared to 58 $kgCO_2eq/bbl$ for conventional petroleum extraction or approximately three times higher due to additional energy requirements.[23] Shale gas extraction, another technology seeing widespread development because it is a source of inexpensive natural gas, releases less greenhouse gas emissions than does petroleum, however, the environmental impact of drilling fluids are still widely debated.[24] The high energy density makes petroleum an excellent fuel, however, consumption is not sustainable indefinitely.

1.2 Biofuels

The search for a sustainable energy source has led researchers to biologically-derived fuels. An overview of the various biofuel technologies available and still under development first warrants a discussion of biomass structure and properties.

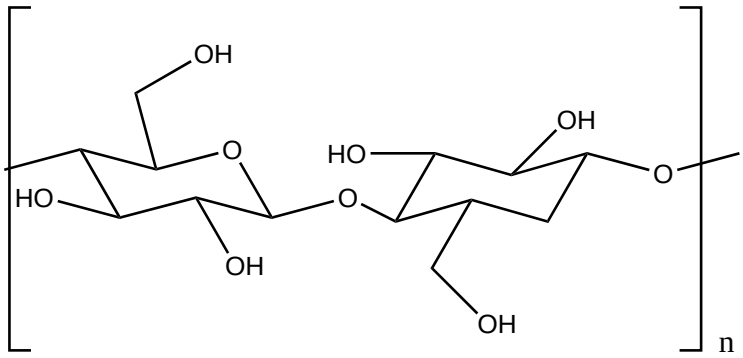

Figure 1.1: Structure of cellulose

1.2.1 Structure of biomass

Biomass is composed primarily of cellulose, hemicellulose, and lignin. Cellulose ($[C_6H_{10}O_5]_n$), a biopolymer shown in Figure 1.1, contains 5000 to 10000 anhydrous glucose residues linked by β-1,4 glycosidic bonds and comprises about 40-50 wt% of lignocellulosic biomass.[6] The equatorial configuration of the glycosidic linkages enables cellulose to form microfibers bound by Van der Waals forces and hydrogen bonding. The microfibers tend to crystallize[25] which makes cellulose insoluble in water and resistant to hydrolysis.[26] The crystallinity of the microfibers confers stiffness to plant cell walls. Hemicellulose accounts for 25 to 35 wt% of biomass and is composed of a mixture of polymerized monosaccharides.[6] Lignin, a component of biomass that has no defined structure, is composed of a branched 3D network of phenolic compounds that helps bind cellulose fibers together.[6,27]

1.2.2 First-generation biofuels

First-generation biofuels are fuels such as ethanol made from starch[28] and biodiesel made from vegetable oil.[29]

Corn ethanol

Much interest has been generated in biomass conversion to fuel because it is the only known source of renewable carbon and the only conceivable alternative fuel for applications that require liquid fuels.[1] Biofuel consumption is also more environmentally friendly than petroleum consumption and does not release as much CO_2 into the

atmosphere as fossil fuels.[28] The reduction in greenhouse gas emissions is an attractive possibility considering that, in 2011, the United States released 2.3 billion metric tons of CO_2 into the atmosphere, or approximately 20% of the global CO_2 emissions[30] despite making up only 5% of the global population.

Biofuel production in the United States consists mostly of ethanol.[28] In 2005, approximately 4 billion gallons of ethanol was produced, corresponding to usage of about 14% of the total U.S. corn harvest.[29] Correspondingly, biodiesel production was approximately two orders of magnitude lower than ethanol. Ethanol is considered a first generation biofuel and many alternatives are being sought because the energy gained from ethanol is only about 25% greater than the energy required to produce it.[29] Corn ethanol currently only becomes economically viable by selling the byproducts as animal feed.[29] Additionally, ethanol requires corn as a feedstock which has triggered a debate about corn utilization for food vs. fuel.[29,31,32]

Biodiesel

Biodiesel is synthesized by transesterification of vegetable oil with a high content of triglycerides to form one mole of glycerol and three moles of fatty acids that contain approximately 16 carbon atoms on each chain.[33] Biodiesel can yield 93% more energy than is consumed in its production compared to 25% for ethanol[29] and can be synthesized from waste vegetable oils.[34] Biodiesel also accounted for approximately 0.1% of U.S. diesel consumption in 2005.

Issues facing ethanol and biodiesel production

The distributed nature of biomass currently prevents biofuel from significantly supplanting conventional petroleum although attempts are being made to circumvent this problem. Marvin et al. determined the optimal locations of hypothetical small-scale biorefineries by taking into account factors such as biorefinery capacity, process yield, and transportation costs in a way that minimizes costs.[4,5] Even with optimized models for biorefinery locations, technologies currently under development must contend with both the distributed nature and chemical complexity of biomass. Cellulose ($[C_6H_{10}O_5]_n$) contains approximately 50 wt% oxygen—high compared to petroleum which contains only trace amounts.

Biodiesel production also faces its share of obstacles such as the high cost of veg-

etable oil.[34] Biodiesel production from waste vegetable oil is under development in an attempt to lower the price of the biodiesel precursors.[34] The surplus of glycerol byproduct is also a significant impediment to large-scale implementation of biodiesel.[35,36] Biodiesel production forms an estimated 10 wt% of crude glycerol which must be separated and refined if it is to be sold.[35,36] New markets for glycerol are being sought to prevent a glycerol excess that would reduce the price too much for biodiesel to be economically viable on a large scale.[36]

1.2.3 Second-generation biofuels

Second-generation biofuels are fuels which have not yet been mass produced but have advantages over first-generation biofuels such as reduced production costs[37] and are still an active area of research.

Cellulosic ethanol

Among the many alternatives to corn ethanol is cellulosic ethanol derived from feedstocks such as switchgrass which require less energy and fertilizer to produce. Switchgrass also does not compete with crops that could be used for human consumption and fuel derived from cellulosic sources can potentially supplant up to 30% of U.S. petroleum consumption.[31] Additionally, cellulosic ethanol has the potential to reduce greenhouse gas emissions by up to 86%.[38] Schmer et al. found that cellulosic ethanol yields 500% more energy than is consumed for its production[28] yet widespread implementation has not yet been accomplished due to the high cost of the enzymes needed to break down cellulosic biomass to ethanol.[39] By contrast, the first-generation technology used to ferment starch, a polysaccharide similar to cellulose, into ethanol has been employed since ancient times.[40]

Gasification

Gasification is being investigated as a means of converting biomass to synthesis gas (H_2 and CO)[41] which can then be upgraded to liquid hydrocarbons through a conventional process such as Fischer-Tropsch[14] discussed below. Biomass gasification requires temperatures ranging from 700 to 1000 °C[7,8] and can be accomplished with or without the use of a catalyst. Non-catalytic gasification is slower than catalytic gasification but produces more tar formation because catalysts such as nickel supported

on alumina can catalyze reforming reactions of tar to syngas.[8] Nonetheless, catalysts such as Pd or Ru supported on SiO_2, which also increase the rate of gasification,[7,42] are still susceptible to deactivation caused by tar formation[7,43] or from poisoning by inorganics such as sulfur, chlorine, or alkaline metals contained in biomass.[2,3,7]

Pyrolysis

Pyrolysis is a process in which a feedstock such as biomass is heated in the absence of oxygen to temperatures between 300 - 500 °C at which point the ordered chemical structure breaks down to form hundreds of different compounds.[6,7] The kinds of products that form depend on the pyrolysis conditions used. For example, long residence times on the order of hours cause biomass to form char and tar with a low oxygen content which can be subsequently used as a solid fuel. By contrast, biomass pyrolysis at short residence times, on the order of seconds or milliseconds, cause the ordered biomass structure to collapse into a complex and viscous solution known as bio-oil. The short residence time is insufficient for allowing char formation to occur resulting in a liquid product instead of a solid.[6] Bio-oil contains hundreds of different oxygenated compounds[9] which render it acidic and unstable.[44,45] Bio-oil still retains a sizable energy density[46] and is a liquid which facilitates transportation to reactors that can carry out further upgrading reactions to biofuels.[47,48] The advantages of fast pyrolysis include a high throughput, thermal efficiency and low production costs.[6] Oxidative pyrolysis is a process where the process heat needed to pyrolyze biomass is generated from combustion of the biomass itself and was pioneered by Salge et al. for use in short contact-time reactors.[49] The internal heat source enables the process to have a higher degree of heat transfer than more conventional pyrolysis processes and can occur over catalysts with no deactivation due to the lack of coke formation.[44,50] The specifics of cellulose pyrolysis in autothermal reactors is more fully developed below in Section 1.3.2.

1.3 Catalytic partial oxidation

One alternative method of gasification is by autothermal catalytic partial oxidation (CPO). CPO has been under development by Schmidt and coworkers since 1993 when Hickman and Schmidt demonstrated a method of producing hydrogen from methane

autothermally with no catalyst deactivation.[10] CPO, shown in Equation 1.1, is commonly carried out in short contact-time reactors (SCTRs)—reactors that operate at residence times in the domain of milliseconds. Oxidation of a hydrocarbon feedstock in a SCTR yields complete oxidation products such as CO_2 and H_2O as well as partial oxidation products, H_2 and CO, also known as syngas. Methane reacted with oxygen in the presence of nitrogen in a SCTR can form H_2 and CO in a 2:1 ratio (Equation 1.1), a ratio ideal for syngas upgrading via conventional processes such as Fischer-Tropsch.

An SCTR can couple strongly exothermic combustion of a gas like CH_4 (-802 kJ mol^{-1}) with highly endothermic steam reforming (206 kJ mol^{-1}) resulting in a steady state stream of syngas, CO_2, and H_2O.[10,51] The thermodynamics of conventional steam reforming necessitate large quantities of heat input which, in a SCTR, is supplied in a heat-integrated configuration by coupling with upstream exothermic combustion. When a small portion of the reactant stream in a SCTR is combusted in the first 2-3 mm of the bed, a region known as the oxidation zone, the process heat drives endothermic reforming over the remainder of the catalyst called the reforming zone[52] (Figure 1.2). The increased rate of endothermic reforming over Rh of a reactant such as CH_4 causes the operating temperatures to be lower and the H_2 selectivity to be higher when compared with the same reaction over Pt.[53]

$$CH_4 + \frac{1}{2}O_2 \longrightarrow 2H_2 + CO \quad \Delta H_r = -36\ \text{kJ/mol} \tag{1.1}$$

1.3.1 CPO of gases and liquids

Hydrocarbons

CPO has been extended to the oxidative dehydrogenation of ethane to ethylene[54] and liquids such as hexadecane.[11,12] At temperatures greater than 600 °C, hydrocarbons such as hexane, decane, and hexadecane can undergo thermal cracking to form α-olefins.[11,12] Reactants such as diesel[11] and octane isomers[55] also undergo both CPO and thermal cracking to form syngas, CO_2, H_2O, and α-olefins.

Oxygenates

CPO has been studied as a means of converting bio-oil[56–58] and butanol[59] into syngas. A staged reactor configuration has also been used as a means of producing high

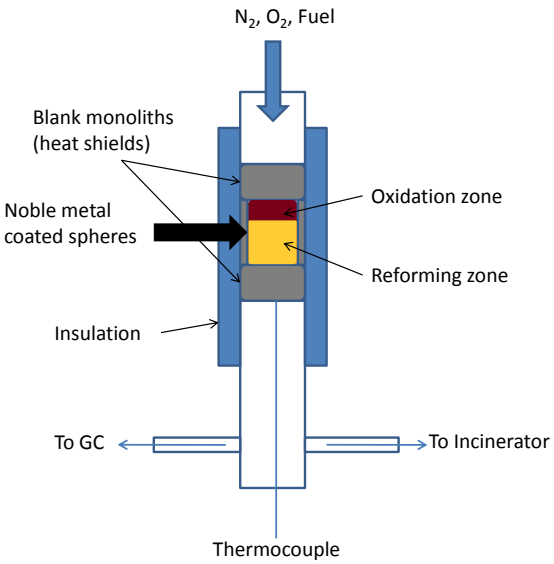

Figure 1.2: General schematic of CPO in a SCTR.

purity hydrogen from isobutanol for potential use in a fuel cell.[60] CPO of iso-butanol was carried out over a 1 wt% Rh-1 wt% Ce catalyst to produce syngas, CO_2, and H_2O. Steam addition promoted steam reforming of butanol which resulted in a H_2 selectivity of 105% at 650 °C. The effluent was passed over a second catalyst stage containing a 1 wt% Pt-1 wt% Ce catalyst optimized for water-gas-shift (WGS).[61] The additional steam helped drive the second-stage WGS reaction boosting the H_2 selectivity to 122% at 510 °C and resulting in an effluent containing a maximum 3 mol% of CO, a concentration comparable to the effluent of industrial high temperature shift catalysts.[60] The staged reactor configuration is further developed in Chapters 2, 3, and 5 but with the combination of both metal and acid functionalities, rather than two metal functionalities.

1.3.2 CPO of solids

CPO has been extended to solid feedstocks as well such as polyethylene,[62] polystyrene,[63] and cellulose.[13,50] Solids reacting over a noble metal catalyst such as Rh at 700 °C under autothermal conditions undergo a process known as reactive flash volatilization (RFV).[13,49,50] The incoming solid particle impacts the catalyst surface where it undergoes a phase transition to liquid which subsequently volatilizes and passes through

the catalyst. The vapors formed from RFV of solid feedstocks are what undergo steam reforming and thermal cracking reactions to form syngas, CO_2, H_2O, among other products. CPO of polyethylene[62] forms hydrocarbon chains ranging in length from C_{12-30} at temperature from 600-1000 °C while CPO of polystyrene results in an 80% yield of the styrene monomer at 600 °C[63] over noble metal catalysts such as Rh and Pt.

Biomass processing can also occur at high temperatures in the oxidative environment found in autothermal reactors over noble metal catalysts such as rhodium and platinum impregnated on an alumina support.[13,49,50] Cellulose fed to an autothermal reactor undergoes RFV and breaks down to form pyrolysis oil vapors containing hundreds of different compounds at temperatures around 800 °C. The pyrolysis vapors undergo reforming to syngas, CO_2, and H_2O. Minimal deactivation is observed because the heat transfer rate to the cellulose particles was too high for char formation to occur.[13] The proportions of bio-oil vapors and CPO products can be tuned by varying the fuel to oxygen ratio. A maximum 60% pyrolysis vapor yield was obtained over Pt/α-Al_2O_3 spheres at 660 °C.[44] The zeolitic-upgrading of pyrolysis vapors formed from RFV of cellulose is explored in Chapter 5.

1.4 Solid-acid catalysts

Solid-acid catalysts such as zeolites and γ-Al_2O_3 are used extensively in this thesis and a brief introduction to catalyst structure, adsorption, and the relevant classes of reactions that zeolites can catalyze are discussed below.

1.4.1 Zeolite structure

Zeolites are crystalline microporous materials composed of silica with aluminum substitutional impurities. The substitutional impurity of a 3-coordinated aluminum atom in a lattice of 4-coordinated silicon atoms creates a charge build-up on an adjacent oxygen atom. The charge build-up can attract a proton counter-ion and serve as a catalytically active Brϕnsted acid site.[64] Conversion and product formation over zeolites is strongly influenced by shape selectivity effects caused by the zeolite pore size. Shape selectivity in zeolite pores alters the types of products that form by either preventing products larger than the pore size from diffusing in to an active site or

by preventing a product larger than the pore size from forming in the pore. A well known example is the disproportion of toluene reaction to form benzene and xylene isomers. The product stream can be enriched in p-xylene if the pore size is small enough to prevent the wider o- and m-xylene isomers from exiting the pore. For example, Kaeding et al. obtained an 74% selectivity to p-xylene at 13% conversion at 600 °C and a WHSV of 2.8 h^{-1} over boron-modified HZSM-5 compared to 24% at 50% conversion over unmodified HZSM-5 under identical experimental conditions.[65] The authors suggested that boron atoms can decrease the pore openings by hindering reactant diffusion and magnifying shape selectivity effects. Large-pore zeolites like ultra-stabilized Y or HBEA are more accommodating for larger molecules because of a decreased extent of shape selectivity effects while smaller-pore zeolites like HFER have pores that restrict certain kinds of product formation.[48] The effects of zeolite pore size on product distribution are discussed for paraffin, butanone, and cellulose feeds later.

Conversion and product formation are also strongly influenced by an effect opposite to shape selectivity in which larger reactants are adsorbed more strongly than smaller reactants.[66] When alkanes of different sizes are fed to a zeolite, the larger compound will adsorb and convert preferentially over the smaller compounds because the larger compound has an increased amount of attractive forces with the pore wall.[67] For example, Denayer et al. fed a mixture of C_{6-9} linear alkanes at 233 °C and 450 kPa to USY and found preferential conversion of the larger compounds and attributed the difference to stronger adsorption of the larger reactants. Tailoring a catalyst to be optimal for selectively forming certain products is an active area of research. The effects of both shape selectivity and competitive adsorption were observed and are discussed for a paraffin feed and cellulose feed in Chapters 3 and 5.

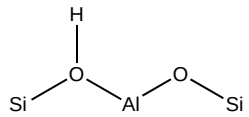

Figure 1.3: Structure of a zeolite acid site.

1.4.2 Classes of biomass upgrading reactions

Bio-oil formed from biomass pyrolysis contains hundreds of different compounds[68] which impart acidity and corrosiveness to the mixture.[44,45] Upgrading of surrogates for compounds formed in bio-oil is an active area of research and has been studied

over a variety of catalysts such as metal[56–58] and zeolite catalysts.[69–71] One focus of this thesis is the upgrading of ketones (Chapter 4), aldehydes (Chapter 6) and a complete pyrolysis vapor mixture (Chapter 5) over zeolites. Each oxygenate functionality presents unique challenges that must be fully understood before developing a large-scale bio-oil upgrading process. The classes of reactions that are observed in this thesis are discussed below.

Alcohol dehydration

Alcohols can undergo ether formation and dehydration over solid-acid catalysts such as zeolites[72–74] or γ-Al_2O_3.[75] The heterogeneous acid-catalyzed dehydration of ethanol, a common surrogate for biomass for its C-H, C-C, and C-O bonds, is a commonly studied probe reaction for biomass deoxygenation. The alcohol loses the OH group as H_2O and desorbs as an olefin. Olefins that form from dehydration of butanol, a potential second-generation biofuel, over a zeolite such as HZSM-5 at temperatures between 200-350 $^{\circ}$C can undergo subsequent chain-growth reactions to form larger compounds.[72]

Aldol condensation of ketones and aldehydes

Ketones[69,76,77] and aldehydes[78,79] contain electrophilic groups that can lead to chain-growth reactions such as aldol condensation. Under a zeolite-catalyzed mechanism proposed by Hoang et al., an aldehyde such as propanal forms an enol which attacks a second propanal and undergoes subsequent dehydration to form a diene. The olefin cyclizes and dehydrates further to form trimethyl benzene.[80] Cracking of the intermediate oxygenated species that form from propanal can produce olefins as a final product. Olefins such as ethylene that forms from methane coupling over Mo/HZSM-5 catalysts can also be cyclized to form benzene, toluene, and xylenes.[64,81,82] The production of olefins from aldehydes via aldol condensation represents one potential route for biomass deoxygenation because the oxygen leaves the molecule as water.[78,80] Oxygenates can promote uncontrolled chain-growth reactions which ultimately result in coke formation and catalyst deactivation.[69,70] Biomass deoxygenation reactions such as dehydration and aldol condensation remove the oxygen from biomass as water[72,83,84] instead of CO or CO_2 which preserves the carbon backbone structure, an important characteristic for a biomass upgrading process.

Hydroisomerization and hydrocracking

Hydroisomerization and hydrocracking, a common operation in the petroleum industry, is employed to balance the high demand for branched gasoline-range hydrocarbons with the availability of heavy oils.[85,86] In a hydroisomerization and hydrocracking process, a metal-acid catalyst such as Pt/HZSM-5 is utilized to crack and isomerize the feedstock into gasoline-range hydrocarbons. The hydrogenation capability of the metal component breaks up coke precursors, limiting deactivation, and enabling the hydroisomerization and hydrocracking catalyst to operate for several years before requiring replacement.[85] The metallic presence also increases the reactivity of the hydrocarbon feed by dehydrogenating paraffins to reactive olefins. The olefins, after isomerizing and cracking over the zeolite, are hydrogenated back to paraffins over the metal.[87] Hydroisomerization and hydrocracking is carried out on a small scale and heat integrated with CPO in a staged autothermal reactor and is the focus of Chapter 3.

1.5 Autothermal staged reactors

Research in autothermal biomass upgrading has been largely restricted to syngas formation, a reaction that results in the nearly complete breakdown of the carbon backbone structure. An alternative to CPO are processes, such as those catalyzed by solid-acid catalysts, that can also produce biofuel but break fewer C-C bonds. In this thesis, the combination of these multiple catalytic functions is explored through the use of staged autothermal reactors and multifunctional catalysts. A staged autothermal reactor consists of a heat-generating CPO stage and a downstream solid-acid catalyst stage that can catalyze upgrading reactions of the CPO stage effluent. The autothermal staged reactor was first developed by Skinner et al. for ethanol dehydration in 2011[83] followed by methanol dehydration.[88] The concept of a staged autothermal reactor is extended further for paraffin and alkanone processing in Chapters 2 and 3 and for cellulose pyrolysis vapor upgrading in Chapter 5. The combination of multiple catalytic functions in a single-pipe reactor is faced with challenges in integrating transition metal catalysts that operate autothermally over a specific range of conditions such as temperatures and space velocities with different conditions required for zeolite catalysts.

The combination of multiple catalytic functions can also be accomplished by synthesizing a catalyst containing both zeolite and metal functionalities. Multifunctional catalysts can be used to upgrade biomass more efficiently than monofunctional catalysts but each functionality requires a different set of reaction conditions to work. The development of multifunctional catalysts will also require an understanding of how each functionality works and interacts with the other functionality. A platinum catalyst combined with a zeolite can catalyze the upgrading of oxygenates more effectively than a single platinum or zeolite catalyst individually. The behavior of this bifunctional catalyst is explored for butanone, a surrogate for pyrolysis oil, in Chapter 4.

Lastly, glycerol upgrading to olefins is considered in Chapter 6. Glycerol is a byproduct of biodiesel production and constitutes a significant weight percentage of the product.[35,36] Without finding new uses or pathways for glycerol, wide-spread biodiesel production will result in a glycerol oversupply and present a potentially significant economic obstacle for larger-scale biodiesel implementation.[35,36] The staged reactor and multifunctional catalyst concepts are explored for glycerol upgrading in Chapter 6. Rather than combining multiple catalytic functions in a single stage, the different chemical functionalities of zeolites and metals are separated into individual stages. Glycerol can then be upgraded with this reactor configuration to olefins that can serve as precursors to gasoline or polymers such as polyethylene or polypropylene.

Staged autothermal reactors are small-scale, high-throughput, and heat-integrated —properties not commonly found together in conventional reactors. The CPO catalyst functions as an internal heat and hydrogen source, obviating the need for an expensive external heat and hydrogen source. Additionally, autothermal syngas production can produce heat and hydrogen from almost any source of hydrocarbons. Integration of zeolite reactions with CPO results in a reactor that can carry out conventional chemistry but with all the advantages of an autothermal system, potentially making it an important component in a small-scale biorefinery.

CHAPTER

TWO

AUTOTHERMAL REFORMING OF BUTANOL TO BUTENES IN A STAGED MILLISECOND REACTOR: EFFECT OF CATALYSTS AND ISOMERS[1]

The development of autothermal staged reactors began with a study of ethanol dehydration[83] and methanol dehydration[88] over a zeolite catalyst in a staged autothermal reactor. In this chapter, the dehydration and isomerization of butanol is studied in an autothermal short contact-time reactor containing a 1 wt% Pt stage followed by a zeolite or γ-Al_2O_3 stage downstream to convert butanol into butenes with up to 95% yield at residence times on the order of 100 milliseconds. CH_4 is fed as a sacrificial fuel to the Pt stage and butanol is fed between the stages to avoid undesired oxidation and reforming reactions of butanol over Pt. The energy released by CH_4 catalytic partial oxidation drives downstream butanol dehydration and isomerization. The effect of the catalyst is studied by comparing the performance of HZSM-5, HFER, and γ-Al_2O_3 catalysts. Higher yields (20%) of butenes were obtained with γ-Al_2O_3 and HFER than with HZSM-5. The absence of Brϕnsted acid sites in γ-Al_2O_3 and the small pore structure of HFER lead to reduced yields of large side products such as higher hydrocarbons that promote oligomerization reactions. A 95% butene yield is obtained with HFER at temperatures ranging from 280-350 °C and a 95% yield with γ-Al_2O_3 at temperatures between 320-350 °C. Only a 75% butene yield was

[1]Portions of this chapter appear in H. Sun, S. Blass, E. Michor, L. D. Schmidt, "Autothermal reforming of butanol to butenes in a staged millisecond reactor: effect of catalysts and isomers," *Appl. Catal., A* **445-446** (2012) 35-41.

obtained with HZSM-5 at 230 °C. The effect of hydrocarbon structure on product formation is studied by comparing conversions of each butanol isomer using a heated tube reactor at temperatures between 200-400 °C. The reactivity of butanol follows as: t-butanol > 2-butanol > iso-butanol > 1-butanol. Both trans-2-butene and cis-2-butene are primarily formed from linear butanol isomers, while isobutene forms from branched butanol isomers. Conversions and product distributions of butanol isomers formed over HZSM-5 in a staged reactor are comparable (<10% difference across all species) with data using a heated tube reactor at similar temperatures. We successfully demonstrate an alternative pathway to dehydrate butanol to butenes with an autothermal staged reactor when compared with conventional methods for applications in small-scale biomass utilization. The largest advantage of this reactor is the integration of highly exothermic autothermal stage and endothermic alcohol dehydration stage which provides an alternative processing technique to maintain the bed temperature.

2.1 Introduction

Significant research has focused on the development of processes to convert biomass to fuels and chemicals with the goal of decreasing dependence on fossil fuels. The production of butanol from biomass has recently attracted both industrial and academic interest.[89,90] Various processes for producing butanol isomers from biomass are described in the literature. 1-butanol can be produced by traditional ABE fermentation process with a production ratio of 3:6:1 of acetone: butanol: ethanol. Recently, Liao et al.[91] demonstrated that iso-butanol can be produced by yeast or micro-organism from sugar, such as glucose or cellulose. A biosynthetic pathway reported by Atsumi et al.[92] achieved a high yield, high-selectivity production of iso-butanol from glucose.

Butenes are currently priced lower than butanol and thermal conversion results in inevitable process inefficiencies. However, deoxygenation of butanol is investigated as a means of increasing energy density for potential use as a transportation fuel or chemical precursor in addition to a fuel additive. In addition, dehydration of butanol into butenes has a potential application on improving market acceptance of alcohols. In spite of a lot of efforts, alcohols have rarely gained acceptance beyond their inclusion as blending components in the fuel. The conversion of butanol into butenes overcomes this obstacle and results in the production of material that is

valuable as fuel intermediate and as petrochemical intermediate.

Previous studies have focused on the mechanisms of butanol dehydration over solid-acid catalysts,[93–95] and skeletal isomerization of linear butene into branched butenes.[96–99] Butene can play a prominent role in the fuel production. The butene isomers obtained from butanol dehydration can be oligomerized to liquid fuels for transportation purposes.[100–102] In the alkylation process, one mole of C_4 olefins reacts with one mole of isobutane to form an isoparaffin whose carbon number is greater by 4.[103] In addition, isobutene is also widely used as a precursor for polymers and octane-enhancing additives for gasoline.[95] Traditionally, isobutene is produced via isomerization in a heated tube from linear butene with a 40% yield with residence times up to 10 seconds.[96,98] Linear butene is obtained by catalytic cracking of petroleum products.[95]

Autothermal staged reactors have been studied as a means of deoxygenating biomass using ethanol as a model compound.[83] Our previous results demonstrated methanol dehydration to dimethyl ether (DME) with high yield (~80%) and ethanol dehydration to ethylene with a 95% yield in a staged reactor at a residence time of 100 milliseconds.[83,88] In this work, we extend this analysis to butanol because the feedstock contains a greater number of C–C bonds than methanol or ethanol thus enabling it to undergo both dehydration and isomerization reactions. Concurrent dehydration and isomerization reactions of butanol isomers to butenes are rarely reported in the literature. The novelty of the staged reactor lies in the combination of two catalytic functions in a single tube. The upstream Pt stage functions as an internal heat source by catalyzing partial oxidation reactions of CH_4. The energy released heats the downstream zeolite stage which catalyzes dehydration and isomerization reactions. The autothermal staged reactor is a departure from conventional methods of producing butene from butanol, because heat is generated internally rather than being provided externally. The largest advantage of this reactor is that it pairs exothermic and endothermic dehydration chemistry which provides an alternative processing technique to maintain an adequate bed temperature.[104] Dehydration and isomerization in a staged reactor occurs at residence times of approximately 100 milliseconds which is faster than conventional processes (residence time is ~100 times larger).[96,98] Small scale butanol processing in an autothermal staged reactor is a high throughput process and is a good candidate for replacing conventional fuel and chemical platforms in a biofuel-driven economy. In this work, 1 wt% Pt/α-Al_2O_3 was

used for catalytic partial oxidation (CPO) reactions on the first stage and HZSM-5, HFER, or γ-Al_2O_3 for butanol dehydration/isomerization on the second stage. The axial temperature gradient along the downstream stage was resolved to help explain reactor performance. The effect of hydrocarbon structure was investigated by reacting four different butanol isomers into the heated tube reactor. The product selectivities and yields obtained from experiments with a heated tube reactor and autothermal reactor containing HZSM-5 catalyst are compared. Finally, the results lead to the development of an autothermal steady state operating configuration that permits integration of CPO of CH_4 and deoxygenation of biomass derived butanol chemistry at high process feed rates.

2.2 Materials and Methods

A schematic of the staged reactor is shown in Figure 2.1. Platinum (1 wt%) was coated on ceramic foam monoliths (99.5% α-Al_2O_3) 18 mm in diameter and 10 mm length with 45 pores per linear inch (ppi) using the incipient wetness method.[50,105,106] Uncoated foams were placed at the front- and back-faces of the catalyst to reduce axial heat loss. All monoliths were wrapped with ceramic insulation to eliminate gas bypass. K-type thermocouples were placed at the center of the monolith to measure catalyst temperatures and the reactor was insulated with fiberfrax insulation. Each catalyst was used for at least 20 h with no significant deactivation or observed coke formation. All experiments were carried out at atmospheric pressure.

Commercial catalysts (Zeolyst) NH_4-ZSM-5 powder with Si/Al=25 and NH_4-FER powder with Si/Al=28 were used. The proton form of the zeolite was obtained by calcining the ammonium form in a furnace from room temperature to 500 °C with 1 °C/min temperature ramp and 5 h soak in air. Either HZSM-5, HFER, or γ-Al_2O_3 (0.6g) was mixed with 2.4 g of quartz and ituated between two 80 ppi monoliths in the reactor. The zeolite was regenerated in a furnace at 600 °C with a total flow of 1 standard liter per min (SLPM) of air for 1 h. The upstream and downstream stages were separated by 80 mm. A fused silica capillary (Agilent, 0.53 mm ID) was placed in the center of the reactor through a bottom port which was then sealed with a septum as a guide for a thermocouple. The axial temperature profile was measured by motion of the thermocouple inside the quartz capillary tube.[52,54] . CH_4 was fed as a sacrificial fuel to the Pt stage at 0.2 SLPM. The C/O ratio, defined as the molar

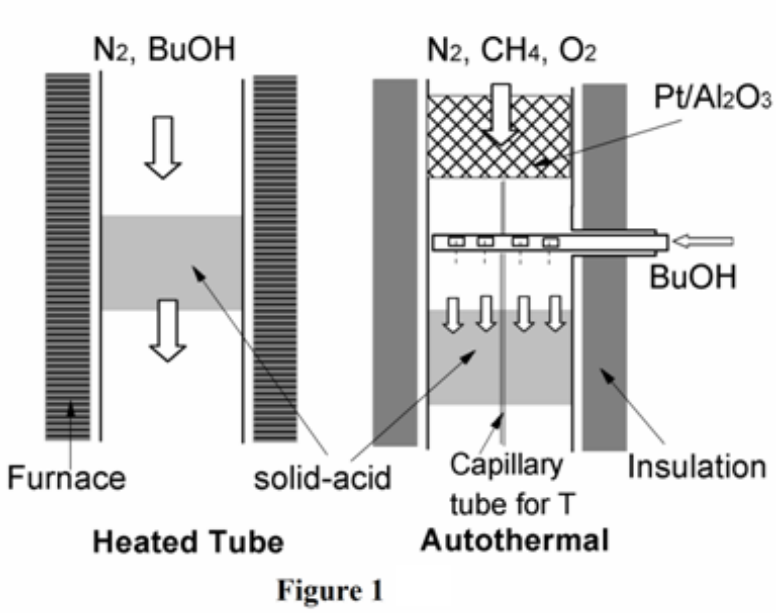

Figure 2.1: Simplified schematic of the heated tube reactor (left) and autothermal staged reactor (right) for butanol dehydration and isomerization reactions. The arrow direction indicates the direction of the flow. The dotted lines represent the flow pattern of butanol vapor.

feed rate of methane over the twice the molar feed rate of O_2, was changed by varying oxygen flow. Butanol isomers were introduced to the reactor at 0.18 ml/min. Butanol was vaporized using a syringe pump and a resistive heating element and introduced into the reactor halfway between the two stages through a 1/8 inch stainless steel tube containing 8 holes (0.016" ID) and welded shut at one end as shown in Figure 2.1. The holes allowed for more uniform dispersion of butanol vapor in the reactor. The total flow rate to the reactor was held constant at 1.7 SLPM.

Gas samples of products at steady-state were identified and analyzed by a gas chromatograph equipped with thermal conductivity and flame ionization detectors. Response factors and retention times were determined by calibrating known quantities of species relative to N_2 which was used as an internal standard. Gas flow rates were controlled by mass flow controllers (Brooks Instrument). The carbon balance is typically closed within 10%. The configuration of the heated tube reactor is similar to the staged reactor but without the Pt stage. A quartz tube (19 mm ID) placed inside a clamshell furnace as shown in Figure 2.1. The total flow rate was maintained

at 1.7 SLPM with the same amount of butanol introduced (0.18 ml/min). Reaction temperature was controlled by a temperature controller (Omega, CSC32).

2.3 Results and Discussion

2.3.1 Autothermal staged reactor: top stage

The hydrogen and CO selectivities of the top stage are plotted in Figure 2.2A. Figure 2.2A also depicts the upstream and downstream stage temperatures (right y-axis). The reaction temperature of the downstream zeolite stage is controlled by adjusting the C/O ratio on the upstream Pt stage. Higher temperatures are obtained by feeding more oxygen into the reactor to increase the amount of combustion. The kinetics of catalytic partial oxidation on Pt is too slow to enable the CPO reaction to reach equilibrium.[107] The gas samples were taken between two stages before the butanol was introduced. The methane conversion decreases as C/O is increased. Oxygen conversion was 100% because the kinetics of combustion are fast enough in Pt such that all oxygen is consumed even if the reaction is kinetically-limited.[53] The temperature regime on the Pt stage ranges from 500 °C to 825 °C as C/O is varied from 0.53 to 1.67. This resulted in zeolite temperatures ranging from 200 to 355 °C. The vertical bar in Figure 2.2A indicates that the difference in top and bottom temperature on the second stage is ~50 °C with HZSM-5. Despite the 300 °C variation in temperature of the Pt stage, the zeolite stage temperature gradient is consistently -3.3 °C/mm because the reactor is well insulated with ~0.4 J/cm^2-s heat lost as reported in previous results.[88]

The axial temperature profile in the reactor shown in Figure 2.2B with an isobutanol feed at various C/O ratios. A noticeable temperature drop (up to 70 °C) is apparent at a 55 mm distance from the Pt stage which is where butanol was introduced into the reactor. This temperature drop is attributed to heat transfer between the Pt stage exhaust at 500-700 °C to the butanol vapor at 150 °C. A steeper drop in temperature is observed at low C/O ratios where the back shield monolith temperature can reach up to 700 °C. At the C/O = 1.40-1.67, the temperature gradient is constant between the two stages while at the C/O = 0.53-1.11, the temperature gradient increases at 80 mm. At higher temperatures, a greater rate of heat transfer to the butanol vapor occurs. Butanol has to travel farther before radial heat loss

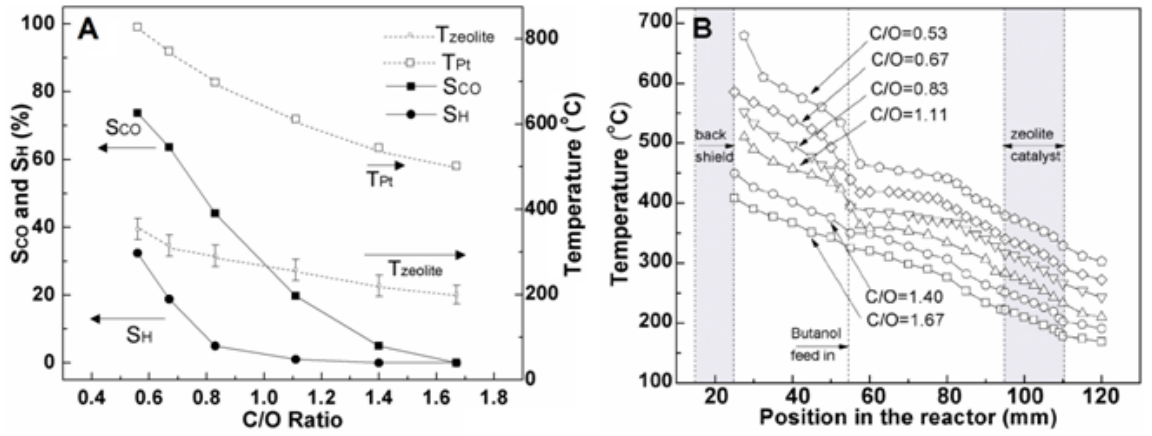

Figure 2.2: (A) Hydrogen selectivity (S_H) and CO selectivity (S_{CO}) and temperature profiles at various C/O ratio in the autothermal reactor. This shows that at higher C/O ratio, it associates with lower SH and SCO, and also lower T_{Pt} and $T_{zeolite}$. (B) Axial temperature profile at different C/O ratio vs. position in the autothermal reactor. This demonstrated that there is a significant temperature drop (< 65 °C) at where butanol is introduced. Temperature decreases as distance is increased further from the top stage. In both figures,the catalyst is HZSM-5 with an isobutanol feed.

becomes significant again. At 80 mm, the temperature gradient returns to its original value. The temperature gradient is approximately linear in the zeolite region, suggesting radial heat loss might be dominant and any thermal contribution from dehydration/isomerization reaction may be negligible.

2.3.2 Autothermal staged reactor: effect of catalysts

Figures 3 and 4 depict C_4 olefins yields and butanol conversion over γ-Al_2O_3, HFER and HZSM-5 catalysts in the autothermal staged reactor. The axial downstream stage temperature is averaged (T_{avg}). The corresponding C/O ratio is shown on the top axis. As shown in Figure 2.3, the total C_4 olefin yield over HFER and γ-Al_2O_3 increases with T_{avg} and reaches a maximum of 90-95% between 280 and 350 °C. Over HZSM-5, the C_4 olefin yield goes through a maximum of 75% at 230 °C after which it decreases with increasing temperature. The temperature at which a maximum C_4 olefin yield is obtained over HFER is 40 °C lower than yields over γ-Al_2O_3.Over all three catalysts studied, the C_4 olefin yield from 1-butanol followed the same trends as those from isobutanol but required an additional 20 °C to reach same yields.

Figure 2.4 shows 1-butanol and isobutanol conversion and the selectivities of all observed C_4 species over each catalyst studied as a function of T_{avg}. As seen in Fig 4A-D, conversion of isobutanol over γ-Al_2O_3 reaches 100% at 320°C and over HFER at 280 °C, while the total C_4 selectivity remains constant at 90-95%. On γ-Al_2O_3 and HFER, no isobutene is formed from 1-butanol feed, while 50-60% selectivity of isobutene was observed from isobutanol over γ-Al_2O_3 (Figure 2.4A and 40-50% over HFER (Figure 2.4C). HZSM-5 has the highest activity compared to HFER and γ-Al_2O_3 since the conversion reached 100% at 250 °C which is lower than 280 °C for HFER and 320 °C for γ-Al_2O_3.However, the total C_4 selectivity decreased by 50% over HZSM-5 with increasing temperatures as larger compounds were formed. The selectivity of isobutene increased by 15% over HZSM-5 (Figure 2.4F), indicating the occurrence of isomerization reactions.

As evidenced by the conversion of butanol, the presence of Brϕnsted acid sites in the catalysts make zeolites more active than γ-Al_2O_3 which primarily contains Lewis acid sites. The high activity of HZSM-5 limited the range of temperatures over which a high C_4 selectivity can be obtained. A high C_4 selectivity was only obtained over HZSM-5 between 200-250 °C but it can be reached over the entire range of T_{avg} studied with HFER and γ-Al_2O_3. The 10-membered ring (10-MR) HZSM-5 has larger cavities that exist in place of channel intersections which make it more active than HFER which has only 10x8 MR pores.[96] γ-Al_2O_3 primarily has Lewis acid sites which are too weak to catalyze oligomerization and isomerization reactions. Therefore C_4 olefin yields were higher over HFER and γ-Al_2O_3 because C_4 olefins were not consumed in oligomerization and isomerization reactions. In addition, HFER is suggested to be optimal for isomerization of linear butenes to isobutene due to shape selectivity effects.[98,108,109] HFER has a pore size enabling isobutene diffusion but suppressing dimer and oligomer formation which are byproducts and cause catalyst deactivation.

While there is precedence for isomerization reactions of C_4 hydrocarbons over HFER, the conditions used previously are significantly different than ours. Menorval et al. reported isomerization of n-butene to isobutene on HFER with residence times ranging from 1 min to 4.7 min, and achieving conversions of 15.3% to 43.8% at 350 °C, respectively.[110] In Figure 2.4C, the C_4 selectivity over HFER remained relatively constant indicating the lack of isomerization reactions, however, this might simply be due to the short residence times used (100 milliseconds compared with 1 minute

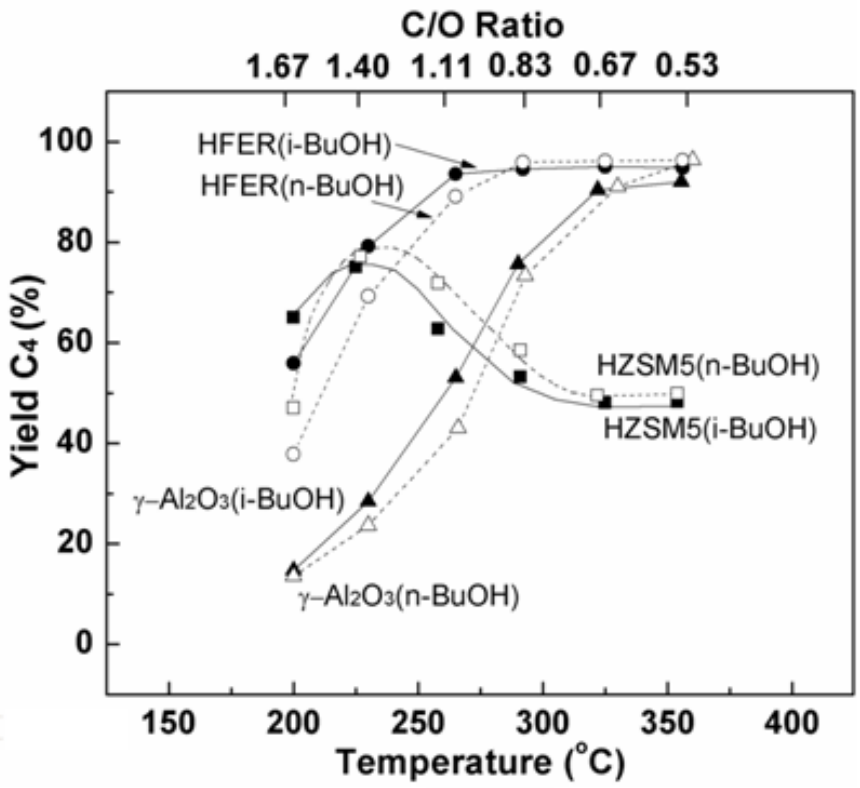

Figure 2.3: C_4 olefin yield in autothermal staged reactor at various C/O ratios for three catalysts, (●)HFER catalyst, (■) HZSM-5 catalyst and (▲) γ-Al_2O_3 catalyst with isobutanol feed; (○)HFER catalyst, (□) HZSM-5 catalyst and (△) γ-Al_2O_3 catalyst with 1-butanol feed. Open symbols are C_4 yields with 1-butanol feed, while closed symbols are those with isobutanol feed. We take the average temperature of the top and bottom temperature to represent the average temperature (T_{avg}) of the second stage. Here, the temperature of every data point is the average temperature, and it has a corresponding C/O ratio shown on the top axis.

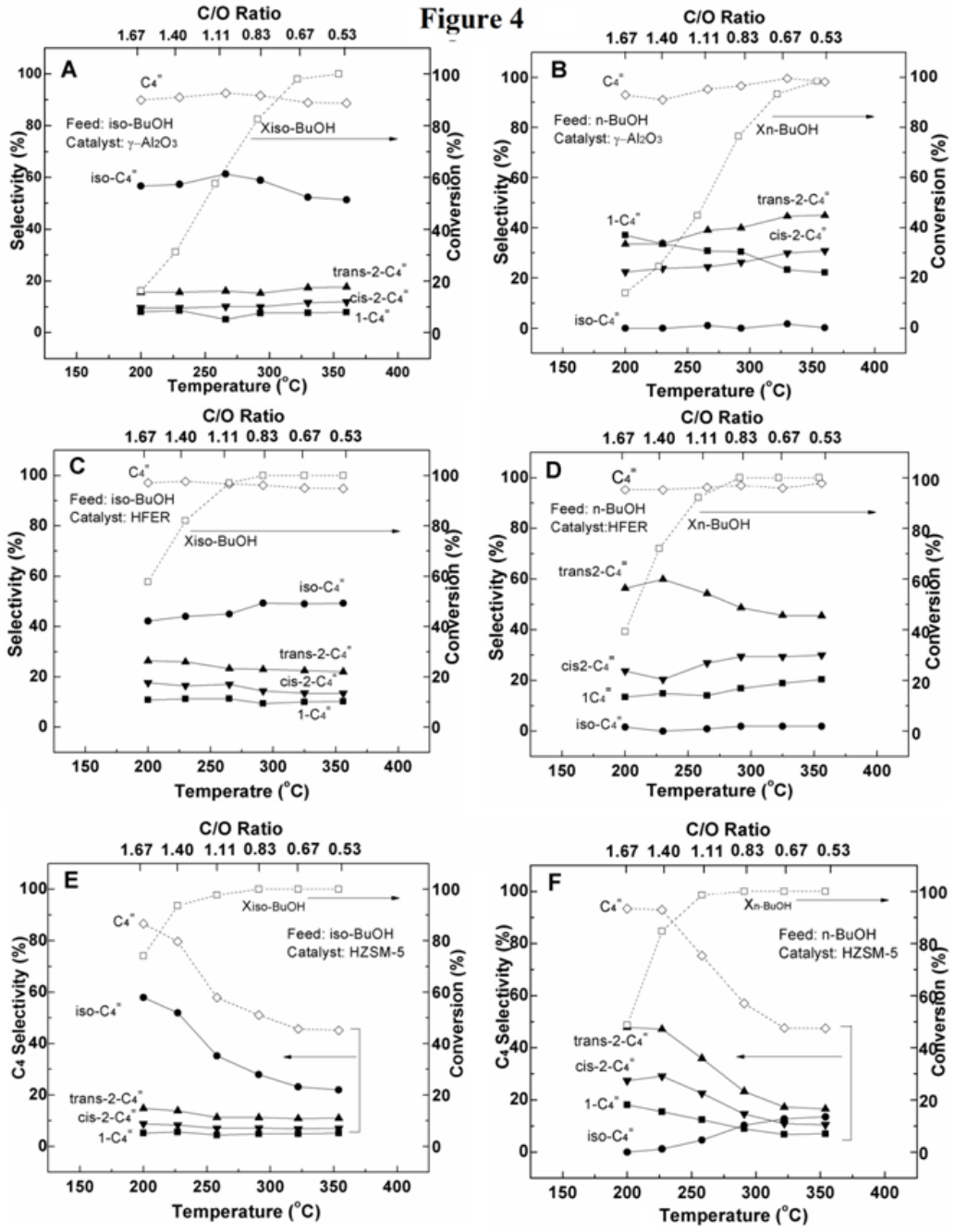

Figure 2.4: C_4 olefin selectivity, conversions for autothermal reforming of iso-butanol(left panel) and n-butanol (right-panel) with three catalysts. (A)-(B) show C_4 selectivity and conversion with catalyst γ-Al_2O_3, (C)-(D) is with catalyst HFER and (E)-(F) is with catalyst HZSM-5; total C_4 selectivity ($\diamond$), iso-C_4 selectivity ($\bullet$), trans-2-C_4 selectivity ($\blacktriangle$), cis-2-C4= selectivity ($\blacktriangledown$), 1-C_4 selectivity ($\blacksquare$), conversion with different butanol feeds ($\square$). X represents conversion.

used by Menorval et al.). In Figure 2.4D, trans- or cis-isomers shows a slight change in selectivity (~13%), indicating the presence of double bond isomerization between trans- and cis-isomers, but with no isobutene formation. Comparing the performance of HFER and HZSM-5, which have the same Si/Al ratio, the extent of isomerization over HZSM-5 catalyst is more apparent than on HFER and may be attributed to the larger pore size of HZSM-5.

The deactivation test carried out for three catalysts shows that the conversion of isobutanol at 400 °C over HZSM-5 decreases by ±20% over 2 h, due to pore blockage by carbonaceous deposits formed over Brϕnsted acid sites. The conversion of isobutanol over HFER decreased by 10% after 4 h and remained constant over γ-Al_2O_3 for 8 h. The small pore size of HFER and the lack of strong acid sites on γ-Al_2O_3 minimize the production of side products such as higher hydrocarbons which deactivate the catalysts. This also demonstrates that HFER and γ-Al_2O_3 are more suitable catalysts for autothermal staged reactors than HZSM-5. These catalysts have a slow rate of deactivation and require temperatures between 280-350 °C to achieve a high C_4 yield. High temperatures are not an issue for autothermal staged reactors due to an internal heat source which enables high temperatures to be easily achieved.

2.3.3 Heated tube reactor: effect of isomers

HZSM-5 was chosen as the catalyst to study the effect of isomers because it catalyzes the formation of a greater range of products than HFER or γ-Al_2O_3 enabling us to probe a larger number of reactions. In Figure 2.5A, t-butanol had the highest reactivity since the temperature at which it reached 98% conversion (200 °C) was lower than temperatures for other isomers. At 200 °C, 2-butanol, isobutanol, and 1-butanol reacted with 88%, 72%, and 39% conversion respectively. This result is also consistent with the higher activation energies of 1-butanol, 2-butanol and isobutanol dehydration over Na-HZSM-5 catalyst 135-160 kJ/mol, compared to 80 kJ/mol for t-butanol dehydration at 60-185 °C.[93,111–114] A lower activation barrier for t-butanol means a lower temperature is needed to reach 100% conversion. In Figure 2.5B, it can be observed that 1-butanol was mainly transformed into linear butenes between 250-300 °C, while butenes were transformed into higher olefins and paraffins above 300 °C. The yields of C_5 and C_{6+} species went through a maximum at 300 °C, while the concentration of propylene and ethylene continually increased with temperature.

This suggests that C_{5+} products are intermediates while C_2 and C_3 species are final products. The amount of linear butenes, which are primary products in the dehydration reaction, initially decreased due to oligomerization to higher olefins. The butene yield became constant at temperatures greater than 300 °C. Product distributions from 2-butanol, t-butanol and isobutanol shared the same trends as 1-butanol except below 250 °C where the total C_4 yields were different according to butanol isomer reactivity. Dehydration reportedly takes place at temperature less than 150 °C while skeletal isomerization occurs at temperatures between 300-500°C with primarily dimerization mechanism over HZSM-5.[109] In our studies, the selectivity of C_3 was larger than that of C_5 at 300-400 °C. We postulate that C_5 is the intermediate product which will be further cracked into C_{2-3}.

In Figures 5C and 5D, the selectivities of C_4 olefins with 2-butanol and t-butanol feed are plotted, while those with isobutanol and 1-butanol feed are plotted in Figures 6C and 6D (closed symbol). In Figure 2.6D, trans-isomer which has a ΔH_f = -10.8 kJ/mol is thermodynamically preferred over the cis-isomer which has a ΔH_f = -7.7 kJ/mol even though the cis-isomer is more structurally favored on a catalyst surface due to reduced steric hindrance.[99] In addition, the selectivity of isobutene increased from 0 to 15% (T = 200-400 °C) indicating the occurrence of isomerization. Figure 2.5C shows that the C_4 olefin selectivities from 2-butanol dehydration are similar to 1-butanol dehydration (Figure 2.6D). In Figure 2.6C, the selectivity of isobutene decreased from 64% to 20% (T=200-400 °C) with isobutanol feed. t-Butanol was converted to isobutene with greater ease than other butanols, resulting in a high isobutene selectivity (90% selectivity at 200 °C as shown in Figure 2.5D).

It is suggested in the literature that a carbenium-ion transition state forms over the Brϕnsted acid site in the dehydration/isomerization proccess.[74,96,115,116] Willams et al. suggest the presence of an alkoxide intermediate for butanol dehydration at temperatures less than 150 °C.[93] In our experiments, dibutyl ether was not observed due to its instability at high temperature (>200 °C). The differences in products formed from each butanol isomer are attributed to the different intermediate structures that form. We postulate that butanol forms an alkoxide intermediate by eliminating water. The alkoxide structure then isomerizes to another alkoxide structure via a carbenium-ion-like transition state. The lack of isobutanol formation from 1-butanol reactions over all catalysts is evidence of a series reaction in which dehydration to an alkoxide is followed by isomerization. Branched products (isobutene)

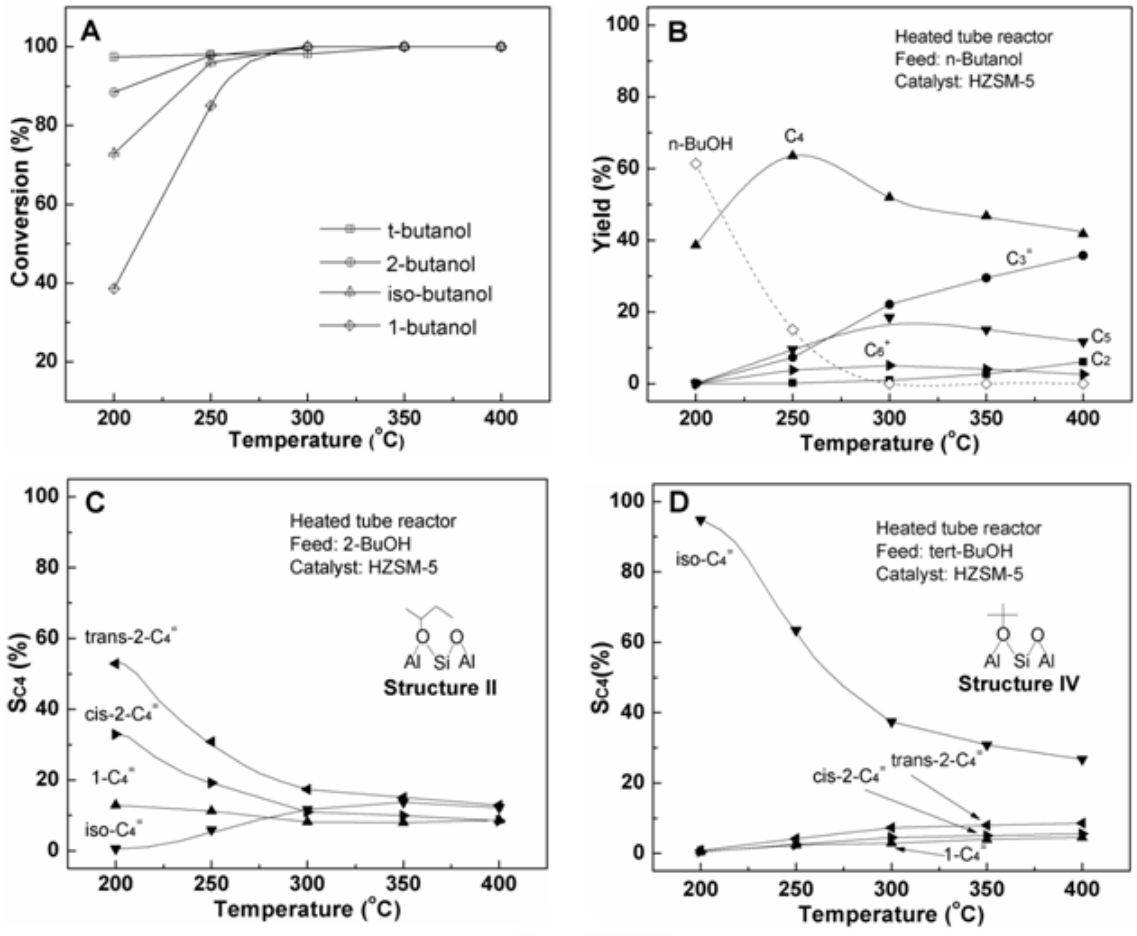

Figure 2.5: (A) Conversion of 4 butanol isomers in a heated tube reactor over HZSM-5 at various temperatures. (B) Product yield of heated tube reactor over HZSM-5 catalyst with 1-butanol feed at various temperatures, (C) C_4 species selectivity for 2-butanol in a heated tube reactor over HZSM-5 catalyst. The C_{2-3} and C_{5-6+} are not shown here for simplicity. (D) C_4 species selectivity for t-butanol in a heated tube reactor over HZSM-5 catalyst. Structures II and IV are corresponding alkoxide structures formed in isomerization process.

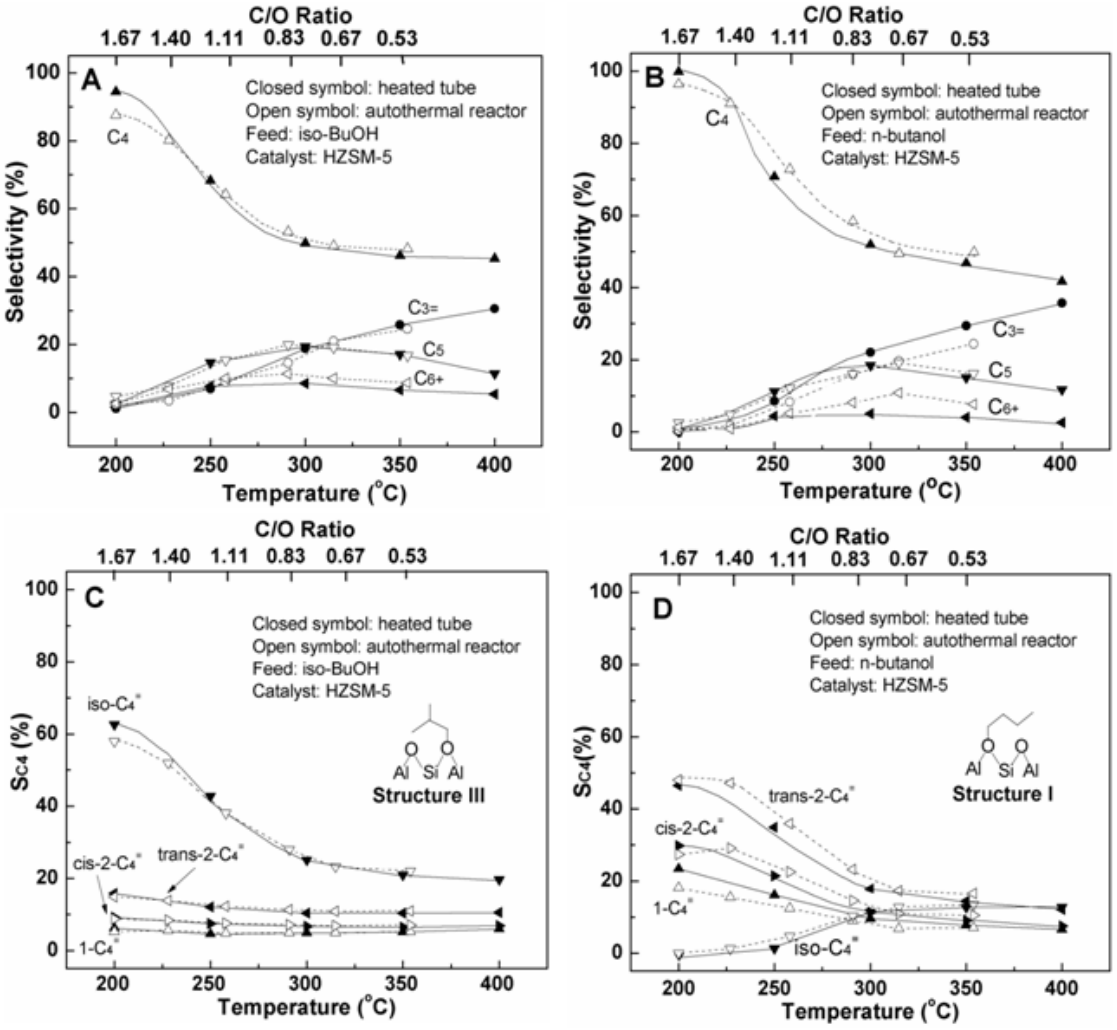

Figure 2.6: (A-B) Comparison between autothermal staged reactor (open symbol) and heated tube reactor (closed symbol) in terms of product distribution and C_4 selectivity (C-D). Autothermal reaction product selectivity is plotted vs. T_{avg} (bottom x-axis) and C/O ratio (top x-axis). The C_{2-3} and C_{5-6+} selectivities are not shown here for simplicity. Structures I and III are corresponding alkoxide structures formed in the isomerization process.

form from branched butanol isomers such as t- and isobutanol while linear products (1-butene, 2-butene) form from linear butanol isomers such as 1- and 2-butanol. We postulate that linear alkoxide intermediates (structure I in Figure 2.6D and II in Figure 2.5C) are isomerized into branched products (structure III in Figure 2.6C and IV in Figure 2.5D) via a methyl-cyclopropyl carbenium-ion-like transition state before desorbing as olefins.[74,115] Greater stability in branched alkoxides compared with linear alkoxides leads to a decrease in isomerization to linear products.

2.3.4 Autothermal reactor vs. heated tube reactor and its implication

Product selectivities from the autothermal staged reactor experiments are plotted against those from the heated tube experiments in Figure 2.6. With an isobutanol feed (Figures 6A and 6C), the selectivities of all products (C_{3-6+}), trans- and cis-isomers, isobutene and 1-butene) from the autothermal experiments are comparable to those from the heated tube experiments. With a 1-butanol feed (Figure 2.6B), the total selectivity of C_4 and C_5 are comparable, while the C_3 selectivity was lower in the heated tube experiments by about 8% and the C_{6+} selectivity was higher by the same amount. In Figure 2.6D, the selectivity of trans- and cis-isomers was ~8% higher in the autothermal experiments, while 1-butene was lower by the same amount.

The differences in product selectivities between the heated tube and autothermal reactors may be due to the temperature gradients found in the autothermal reactor. The temperatures previously reported here are representative of all temperatures in the zeolite stage. The product selectivity between the autothermal and heated tube reactors with isobutanol and 1-butanol feed were comparable to each other (<10% difference). The differences can primarily be attributed to the similarity in the dehydration activation energy of isobutanol and 1-butanol. Williams et al. reported that the activation energy of isobutanol to isobutene is 138.1 ± 8.4 kJ/mol,[93] while the activation energy of 1-butanol to n-butene is 133.9 ± 8.4 kJ/mol at 105-185 °C with Na-HZSM-5 catalysts.[112] This shows that the dehydration reaction rate of isobutanol and 1-butanol have similar sensitivity to temperature. Therefore, the deviation from heated tube reactor to autothermal staged reactor is comparable with both isobutanol and 1-butanol feed. Additionally, linear butanol isomers undergo isomerization reactions while branched isomers do not. These isomerization reactions may be more

sensitive to temperature changes than alcohol dehydration. This increased sensitivity would result in linear butanol isomers displaying a greater difference in product selectivities when comparing products formed on a zeolite with a temperature gradient as in the autothermal reactor or without a gradient as with the heated tube reactor. The ability to sufficiently preheat the butanol by direct contact with hot exhaust gases implies that it is not necessary to employ a fired heater or a combustion chamber to preheat butanol. This could potentially reduce the capital cost of the process.

2.4 Conclusions

Autothermal reforming of butanol isomers were investigated in a staged reactor with an upstream stage consisting of 1 wt% Pt catalyst on α-Al_2O_3 and a downstream stage consisting of either γ-Al_2O_3, HFER, or HZSM-5 catalysts. The reactivity of the butanol isomers was studied by comparing their conversions over a range of temperatures. HFER and γ-Al_2O_3 have a 90-95% C_4 yield while the maximum C_4 yield over HZSM-5 is 75% due to its pore structure and acid strength effects. In the heated tube reactor, the reactivity of the butanol isomers was as follows: t-butanol > 2-butanol > isobutanol > 1-butanol. Both trans- and cis-isomers were obtained from linear butanol isomers, while isobutene was formed from branched butanol isomers. With HZSM-5, the product selectivities in the autothermal staged reactor were comparable to those from a heated tube reactor with a difference of <10%. We demonstrate with the autothermal staged reactor the integration of exothermic and endothermic chemistry. The direct contact between butanol and hot exhaust gas has the potential to replace the fire heater or the combustion chamber, reducing the capital cost of the process.

CHAPTER

THREE

HYDROCONVERSION OF LIQUID HYDROCARBONS IN A STAGED AUTOTHERMAL REACTOR[1]

In Chapter 2, butanol dehydration and isomerization was studied in an autothermal staged reactor. In this chapter, the autothermal staged reactor concept is applied to paraffin hydroisomerization and hydrocracking and 2-decanone deoxygenation. In contrast with the reactor used in Chapter 2 and for ethanol[83] and methanol[88] dehydration, the H_2 produced from CPO is now consumed in downstream reactions over a bifunctional zeolite. An autothermal staged reactor was assembled containing a top stage of Rh-Ce/α-Al_2O_3 which generated heat and H_2 by reacting CH_4 and air that passed through a downstream stage containing 0.5 wt% Pt/γ-Al_2O_3 mixed with either HBEA, HZSM-5, or USY in a heat-integrated non-isothermal reactor. The H_2 produced subsequently reacts in a $20:1$ ratio with a co-feed of hexane or decane or 2-decanone fed to the reactor between the stages. The large-sized pores of HBEA and USY allowed deoxygenation of 2-decanone to form decene isomers which can crack or cyclize to form up to 36% methylated and ethylated monoaromatics. The medium-sized pores of HZSM-5 restricted decene formation from 2-decanone by catalyzing cracking reactions to C_{2-6} compounds which can cyclize to form aromatics. By contrast, the reactor effluent from non-oxygenated reactants decane and hexane contained less than 5% aromatics. Thus, we extend the scope of staged autothermal reactor functionality to hydrocracking and hydroisomerization of higher saturated

[1]Portions of this chapter appear in S. D. Blass, A. Bhan, L. D. Schmidt, "Hydroconversion of liquid hydrocarbons in a staged autothermal reactor," *Appl. Catal., A* **451** (2013) 153-159.

and oxygenated hydrocarbons.

3.1 Introduction

The transition from a petroleum-based economy to one centered around biofuels faces a number of technical hurdles. The distributed nature of biomass sources for the production of biofuel necessitates smaller local refineries use portable and high-throughput reactors for processing fuel on-site.[16] Autothermal reactors show promise in this regard[11,12,117–120] by carrying out processes similar to those done in conventional refineries such as thermal cracking but at millisecond contact times while using no external heat input.

Autothermal reactors have been developed to carry out dehydration of methanol[88] and ethanol[83] as surrogates for biomass. In this work, we investigate hydrocracking and hydroisomerization of hexane, decane, and 2-decanone as a means of miniaturizing conventional processes and addressing the demand for high-octane transportation fuels. A biomass surrogate 2-decanone was studied in place of 14-heptacosanone, a promising alternative fuel source.[121,122]

Hydrocracking and hydroisomerization reactions are typically carried out over bifunctional catalysts with Pt[123] or Pd[124] and a zeolite solid acid catalyst. Weisz et al.[125] proposed that, in presence of excess H_2, a paraffin is dehydrogenated to an olefin over the Pt catalyst. The olefin then diffuses to an acid site and isomerizes after which the *i*-olefin diffuses back to the Pt and is hydrogenated to an *i*-paraffin.[115,126–128] Catalyst lifetime is extended because the concentration of olefins, known to be coke precursors,[129–131] is limited by Pt under high H_2 partial pressures.

Hydrocracking and hydroisomerization was incorporated into an autothermal reactor by situating a bifunctional zeolite stage in series with a noble-metal catalyst stage. The catalytic partial oxidation reaction (CPO) on the noble-metal (or CPO) stage generates both the H_2 needed for downstream isomerization as well as the process heat to enable hydroprocessing reactions to occur. Skinner et al. studied dehydration of ethanol fed between two stages of an autothermal reactor containing 1 wt% Pt on α-Al_2O_3 beads on one stage and a thin film of HZSM-5 coated on four monoliths 1 mm in length comprising a second stage and showed that heat loss through the walls of the quartz tube reactor results in a temperature difference of approximately 130 $^{\circ}$C between the front-face of the zeolite bed closest to the noble metal stage and the

back-face.[83] Hydroisomerization and hydrocracking in a conventional reactor is carried out under isothermal conditions,[132] however, the zeolite in a staged autothermal reactor experiences an axial thermal gradient. Hydrocracking is more pronounced at higher temperatures while hydroisomerization is more pronounced at lower temperatures.[133,134] We show that careful control of the hydroisomerization and hydrocracking product distribution is attainable despite non-isothermal operation because selectivity is primarily a function of conversion. We also demonstrate a staged reactor capable of accessing a wide range of conversions using conventional zeolites by carrying out upstream CPO and downstream hydrogenation/dehydrogenation, hydrocracking, hydroisomerization, and aromatization in an autothermal one-pot system.

3.2 Materials and Methods

3.2.1 Catalyst Synthesis

A staged reactor was loaded with two stages (Figure 3.1), a CPO stage consisting of a noble metal-based catalyst and a zeolite stage consisting of a bifunctional Pt/γ-Al_2O_3 zeolite catalyst. The CPO stage consisted of a 1 wt% Rh - 1 wt% Ce catalyst that was synthesized from $Rh(NO_3)_3$ and $Ce(NO_3)_3 \cdot 6\,H_2O$ (Sigma Aldrich) on α-alumina spheres (1.3 mm ID from Saint-Gobain Norpro) by incipient wetness, calcined at 800 °C for 6 h, and loaded into the reactor according to the method by Bodke et al.[135] The zeolites used were HBEA (CP814E*; Si/Al=12.5), USY (proton-form CBV720; Si/Al=15), and HZSM-5 (CBV 2314; Si/Al=11.5). All zeolites were obtained from Zeolyst International. The zeolites were treated in 100 ml·min^{-1} of dry air (20-21% O_2, <10ppm H_2O, Minneapolis Oxygen) and heated at a rate of 1.5 °C/min to 500 °C and held for 2 h. A 0.5 wt% Pt on γ-Al_2O_3 was made from Pt precursor (H_2PtCl_6, 8wt% in H_2O from Sigma Aldrich) dissolved in a slurry of γ-Al_2O_3 powder (99.97%; Alfa Aesar) and dried in a vacuum oven at 80 °C overnight. The powder was treated in 5% H_2 in Ar (200 ml·min^{-1}) by heating to 350 °C (1.5 °C/min) and held for 2 h to decompose the Pt precursor. The Pt/γ-Al_2O_3 sample was crushed and 5 g were added to 10 g of the proton-form zeolite. The mixture was pressed into 1" ID discs at 5000 psi and crushed into pellets which were sieved to select for 599-710 μm particles (24-30 mesh).

3.2.2 Reactor Configuration and Analysis

A schematic of the staged reactor is shown in Figure 3.1. Rh-Ce/α-alumina spheres (3 g) were loaded into the reactor for a bed-length of 10 mm between two 80 pores per linear inch (ppi) α-alumina foam monoliths. A thermocouple was fixed by friction at the back-face of the sphere bed. The Pt/γ-Al_2O_3 + zeolite mixture (12 g) was placed between two 80 ppi monoliths and situated 170 mm from the CPO stage. K-type thermocouples were wrapped around the front- and back-face monoliths to measure temperatures at either end of the zeolite stage. The zeolite stage had dimensions of 19 mm ID and 40 mm in length. All elements in the reactor were fixed in place with a ceramic paper liner to minimize heat loss and gas bypass. The length of the reactor was insulated with ½" of FiberFrax to minimize axial thermal gradients by reducing radial heat loss. The reactor was connected to a vaporizer made from a stainless steel coil wrapped with heating tape. The end of the coil was attached to a ⅛" stainless steel tube that was situated 5 mm below the back-face of the CPO stage. The tube contained four 0.016" holes drilled through both tube walls to enable even dispersion of the reactant over the catalyst and aid in mixing the reactant stream with the CPO stage effluent. Skinner et al. showed that as much as 40% of ethanol can be lost in undesired oxidation and thermal decomposition reactions when fed to the CPO stage.[83] Therefore, the reactant was fed between the two stages to eliminate undesired oxidation and thermal decomposition that would ordinarily occur on the CPO stage. Samples were taken from the center of the reactor tube below the zeolite stage to ensure a uniform dispersion of reactant was obtained through the catalyst bed. The space between the zeolite and sampling point was wrapped with heating tape to ensure condensation of the sampling stream did not occur prior to reaching the GC column. Samples were fed to the GC by a Pfeiffer DUO 1.5 rotary vane vacuum pump through a sample line heated to 250 °C. Carbon balances closed to within 10%.

Composition analysis was conducted with an online HP 5890 Series II gas chromatograph (GC) equipped with thermal conductivity and flame ionization detectors (TCD and FID). The GC contained a parallel dual column setup consisting of a packed Alltech HayesepD column (30×0.125×0.85) to separate permanent gases and an Alltech Heliflex capillary AT-1 column (60×0.32×1.0) to separate hydrocarbons. The HayesepD column was connected to the TCD while the Heliflex column was connected to the FID. Gas samples were injected on both columns from two sample loops

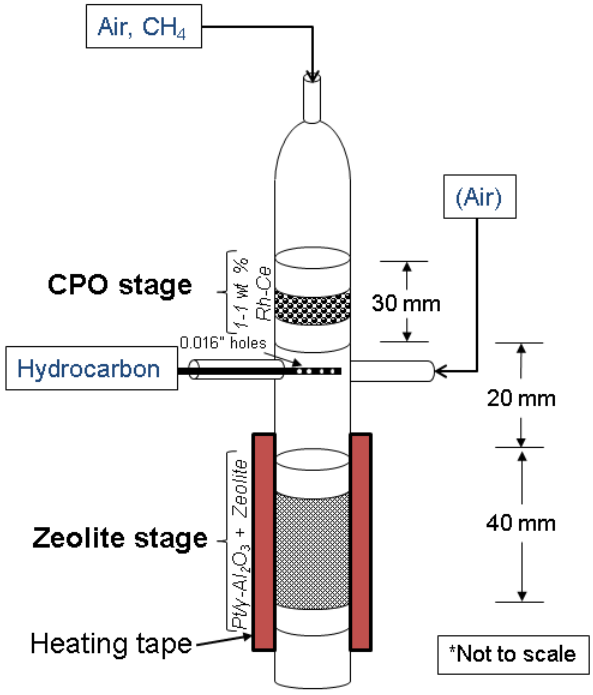

Figure 3.1: Schematic of staged reactor. Note the interstage distance shown is 60 mm. CH_4 co-fed with air reacted over the CPO stage to form partial oxidation products including H_2 and heat. The heated CPO stage effluent passed through the zeolite stage where H_2 and the side-feed reactant formed products from hydroisomerization and hydrocracking.

simultaneously. Nitrogen was used an internal standard on the TCD to calculate the molar output of permanent gases including CH_4 which was used as an internal standard on the FID. Peak identification was conducted in parallel with a HP 5890 Series II gas chromatograph containing a HP-1 column (50×0.32×1.05) connected in series with a HP MSD 5970 mass selective detector.

3.2.3 Experimental Procedure

N_2, O_2, and CH_4 were fed to the reactor at a CH_4/O_2 of 2.0 for a total flow of 2.36 standard liters per minute (slpm). All gas flows were modulated by Brooks 5850i mass flow controllers and a Labview interface. The reactor was lit off and allowed

to reach a steady state temperature. An injection was taken with no side-feed to determine the molar output of H_2 from the CPO stage. Decane, hexane, and 2-decanone were fed to the vaporizer at 0.2 ml·min^{-1} for a molar H_2 to hydrocarbon ratio of 20 after the zeolite reached a steady-state temperature. The initial zeolite stage position was 170 mm from the CPO stage as defined by distance between the CPO stage back-face to the zeolite stage back-face. Three samples of reactor effluent were injected on the GC at each experimental condition after which the zeolite stage was regenerated. During regeneration, the heating tape was connected to an Omega PID controller and heated to 500 °C for 30 minutes. The port opposite the vaporizer was attached to a compressed air source through which 0.1 slpm of air was fed. The feed to the CPO stage was reduced to 0.2 slpm of N_2 to prevent backwards diffusion of air. After 30 minutes, the zeolite stage was cooled by switching off the heating tape and increasing N_2 and air flow rates to 2.0 slpm. Care was taken to ensure the zeolite temperature was below 120 °C before lighting off again to prevent light-off from occuring over the Pt in the zeolite stage. At each position, three reactants were fed to three zeolites with regeneration after each set of three injections. The separation distance was incrementally decreased to 50 mm in 40 mm increments (the distance of the bed length). After data were collected at the smallest interstage distance (50 mm), the zeolite stage was extracted and situated at 150 mm (20 mm below the initial position of 170 mm). The separation distance was again incrementally decreased by 40 mm allowing data to be acquired at bed positions staggered by 20 mm to reduce the possibility of systematic error.

3.3 Results and Discussion

3.3.1 Effect of zeolite topology

Temperature variation

In all experiments, the axial bed position is changed in fixed intervals causing changes in temperature and, consequently, changes in conversion. Selectivity (defined on a molar basis) is primarily a function of conversion so data are plotted as such to account for thermal gradients and experimental variations in temperature. All flow rates to the reactor are constant so the residence time in the zeolite (~130 milliseconds) is approximately the same for all experimental conditions.

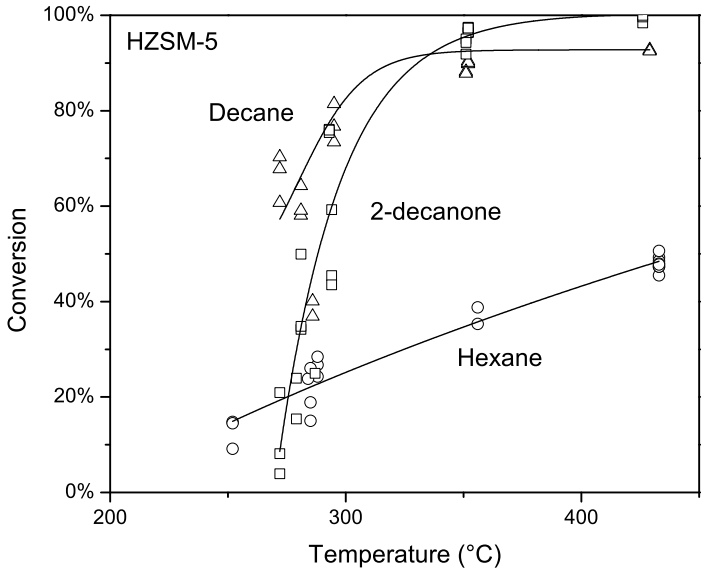
HZSM-5
Decane
2-decanone
Hexane
Conversion
Temperature (°C)
100%
80%
60%
40%
20%
0%
200
300
400

(a)

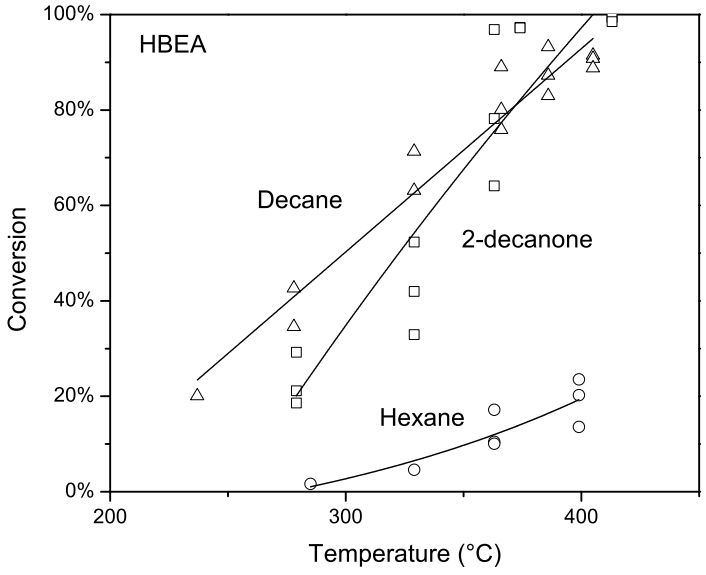
HBEA
Decane
2-decanone
Hexane
Conversion
Temperature (°C)
100%
80%
60%
40%
20%
0%
200
300
400

(b)

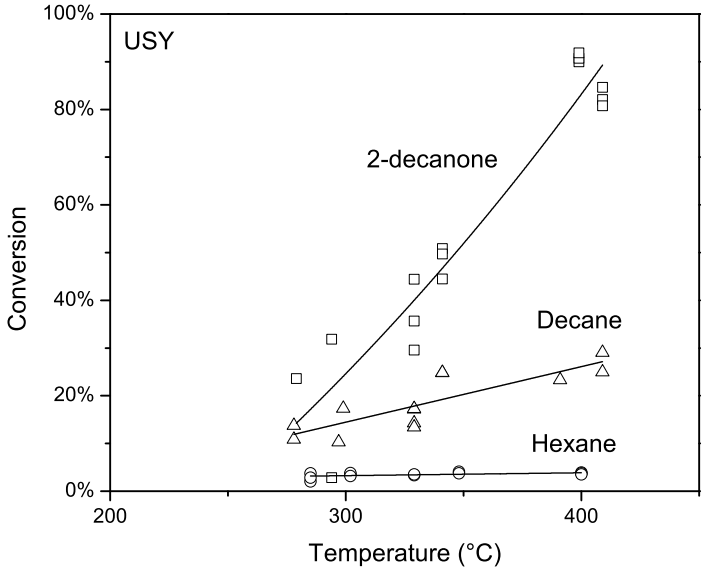

(c)

Figure 3.2: Conversion vs. zeolite temperature in the autothermal reactor. ◯ hexane △ decane □ 2-decanone.

In previous work on staged reactors the axial thermal gradient was reduced to one temperature by calculating an arithmetic mean of the front-face and back-face temperatures. However, rates of reactions are exponential with temperature so a better way to reduce the thermal gradient into an isothermal temperature is by Equation 3.1 in which the rate constant is integrated over the length of the bed and normalized by a rate constant at a calculated temperature in which the ratio of both equals unity. As a first order approximation, the surface is assumed to be saturated so the rate is only proportional to the rate constant. Skinner et al. measured a linear axial temperature profile through a 40 mm zeolite bed composed of four 10 mm 45 ppi foam monoliths coated with a thin film of HZSM-5 in an autothermal staged reactor,[83] hence a linear equation is used here. T_{iso} is calculated in Equation 3.1 where $T(z) = \frac{T_{tf}-T_{bf}}{40}z + T_{tf}$ and 40 is the length of the zeolite bed in millimeters.

$$T_{\text{iso}} = \frac{-E}{R}\left(\text{Ln}\left[\int_{-40}^{0}\exp\left(\frac{-E}{R\,T(z)}\right)\text{d}z\right]\right)^{-1} \tag{3.1}$$

The temperatures obtained from Equation 3.1 are the temperatures at which the conversion would be the same as the experimental conversion had the reactor been isothermal and are typically no more than 5% different than the arithmetic mean of the front- and back-face temperatures. Data are plotted below as a function of temperatures calculated by Equation 3.1.

Conversion as a function of reactant size

As shown in Figure 3.2, conversion increases over all zeolites with temperature. Conversion at each temperature increases with carbon number of the reactant due to the increased number of induced dipole van der Waals interactions with lattice oxygens that increase the heat of adsorption and, hence, coverage.[136] The effect of carbon number on the rate as a function of temperature was also noted by Froment et al.[134] at 130-250 °C and 5-100 bar total pressure on zeolite Y for hydroisomerization and hydrocracking of octane, decane, and dodecane. Conversion also increases with decreasing pore size due to confinement effects that are more pronounced on HZSM-5 than HBEA or USY due to differences in pore structure. HZSM-5 has 10-MR pores with intersecting three-dimensional straight and sinusoidal channels while HBEA and USY have three-dimensional straight 12-MR pores although USY also has a larger pore volume due to the presence of supercages. With decreasing pore size, the distance between lattice oxygens and the reactant decreases leading to an increase in confinement effects and, consequently, larger heats of adsorption. Larger heats of adsorption lead to a decrease in the apparent activation energy and an increase in the rate of reaction and conversion. For example, the heat of adsorption of hexane on HZSM-5 was calculated to be -92 kJ/mol,[137] -64 kJ/mol on HBEA,[138] and -53 kJ/mol on FAU (USY).[139] A low conversion of hexane over USY is consistent with the findings of Kotrel et al. who observe a hexane conversion of about 5% at 350 °C and 5.3 kPa over dealuminated Y[138] which is similar to our value of 4% at 340 °C at 4.8 kPa at a H_2:C_6H_{14} ratio of 20 at atmospheric pressure.

Conversion as a function of oxygen functionality

As shown in Figure 3.2a, conversions of decane and 2-decanone are similar over HZSM-5 and are higher than the conversion of hexane at all temperatures. By contrast, differences in conversion are more distinct when reacting hexane, decane, and

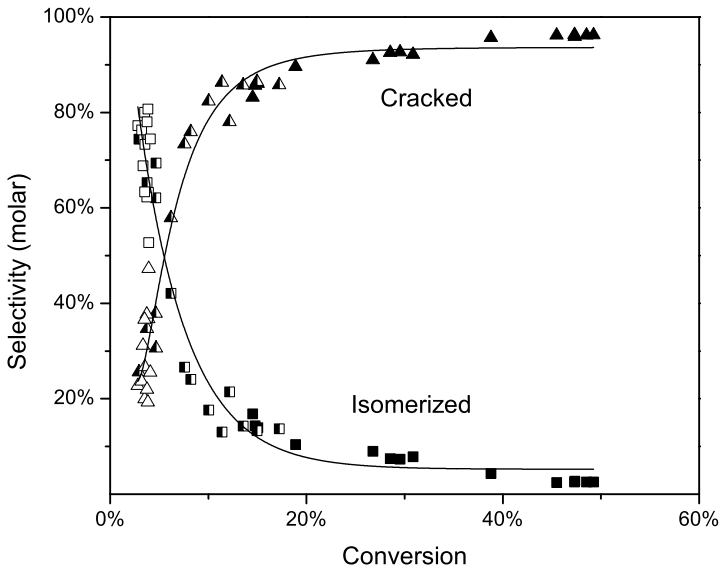

Figure 3.3: Product distributions for hexane hydroisomerization and hydrocracking. Filled symbols: HZSM-5 open symbols: USY half-filled symbols: HBEA. △ cracked products □ isomerized products

2-decanone over USY as shown in Figure 3.2c. We speculate that the appreciable difference in conversion between 2-decanone and decane over USY compared to HBEA and HZSM-5 may be attributed to the USY supercages which may permit bimolecular reactions to occur. Like acetone,[69,140] 2-decanone may also undergo condensation reactions through an enol intermediate which can attack the carbonyl carbon of another 2-decanone molecule. Bimolecular reactions over HZSM-5 between two acetone molecules has been shown to form mesityl oxide, a condensation product that ultimately cracks to isobutene.[69] The zeolite pore structure must be able to accomodate condensation reactions between 2-decanone molecules. The additional pathways provided by the ketone group may result in an increased conversion of 2-decanone when compared with decane over USY.

3.3.2 Extent of hydrocracking and hydroisomerization

Hexane

Selectivities of branched products 2-methylpentane and 3-methylpentane tend towards 100% at low conversions while selectivities for products smaller than C_6 increase with increasing conversion (Figure 3.3) indicating that a series reaction occurs over the bifunctional catalyst. Hydrocracking and hydroisomerization occur via a mechanism where a reactant is isomerized twice and then cracked to avoid the creation of primary carbenium species. The hydrocarbon is unlikely to directly crack without first undergoing structural rearrangement to an isomer.[141] Steijns et al. reacted decane and dodecane over 0.5 wt% Pt on USY at pressures ranging from 5-100 bar and temperatures between 130-250 °C and found that selectivities are unique functions of conversion regardless of the temperatures or pressures used and only depend on the type of catalyst.[142] Hydroisomerization and hydrocracking reactions in the staged reactor follow the same mechanism regardless of the temperature because all steps have similar activation energies.[142] If activation energies were dissimilar, isomerization and cracking would display different sensitivities to temperature and result in product distributions that were not functions of conversion. The temperature and, consequently, the conversion is changed as the bed position in the staged reactor is varied. Consistent with the findings of Steijns et al., selectivities in Figure 3.3 are functions of conversion and independent of temperature.

Decane

As shown in Figure 3.4, selectivities from decane hydroisomerization and hydrocracking do not change appreciably until conversion is approximately 80% possibly due to competitive adsorption effects. Denayer et al. co-fed C_{6-9} hydrocarbons over USY at 233 °C and 450 kPa and measured the adsorption equilibria and intrinsic rate constant for each hydrocarbon. The authors showed the larger reactant is preferentially converted and attributed the difference to a greater sensitivity of the adsorption constant to carbon number than the instrinsic rate constant.[143] In the staged reactor, secondary cracking of initial cracking products does not occur while an appreciable amount of large reactant molecules are still present in the catalyst. At higher conversions, the number of large reactant molecules decreases leading to a diminished effect of competitive adsorption and an increase in conversion of primary products

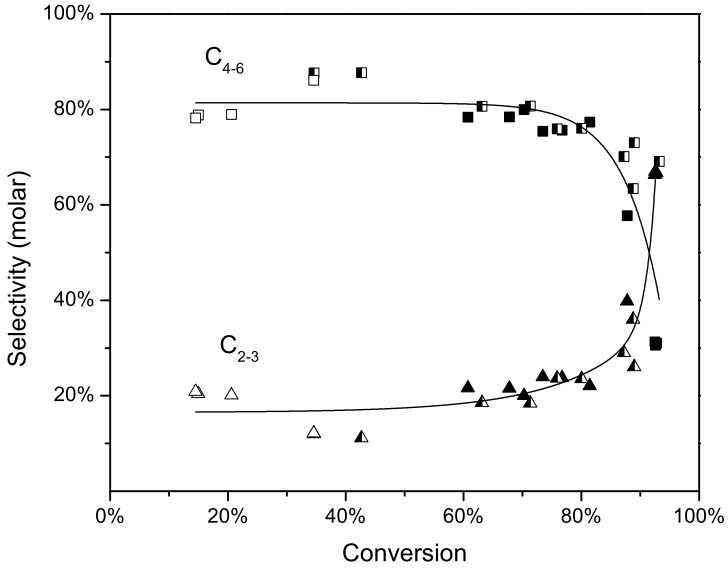

Figure 3.4: Product distribution for decane hydroisomerization and hydrocracking. Filled symbols: HZSM-5 open symbols: USY half-filled symbols: HBEA. △ C_{2-3} □ C_{4-6}

is observed. Secondary cracking is dominant at the conditions used in our system and can be observed from the data in Figure 3.4 to follow a trend indicating the occurence of a series hydrocracking reaction. Smaller products such as C_{2-3} increase with conversion while larger products such as C_{4-6} decrease with conversion. The rise in C_{2-3} selectivities with conversion indicates that small products are formed from tertiary cracking reactions. Such trends are consistent with a mechanism by which a reactant is isomerized and then cracked into a product about half the initial size.

No C_{10} isomers such as methylnonane were found at any conversions observed in contrast to Steijns et al. who reacted decane on 0.5 wt% Pt/USY over a range of temperatures and pressures and found an 85% selectivity of decane isomers at 20% conversion.[142] The discrepancy may be due to two factors: the ease of cracking in C_{7+} compounds compared with C_6 compounds and experimental limitations on H_2 partial pressure leading to an increased olefin concentration. In the staged reactor, C_{4-6} compounds appear to be primary products of decane hydroisomerization and hydrocracking. Hydrocarbons which have a carbon number of 7 or greater are able to form an intermediate structure containing a tertiary carbenium ion leading to

increased rates of β-scission via the A, B_1, or B_2 mechanism.[144] The lack of C_{10} isomers may also be attributed to experimental limitations. A few differences exist between conditions used in traditional hydroisomerization and hydrocracking such as those by Steijns et al. and those used here. Typical H_2 to hydrocarbon molar ratios are about 20 at pressures ranging from 1 - 100 bar.[142,145] Safety considerations with operating an autothermal staged reactor at CPO stage temperatures in excess of 650 °C limited the pressure to one atmosphere. Mixing problems were observed in the form of carbon errors greater than 15% at hydrocarbon flow rates below 0.2 ml/min. The reactant was not well-dispersed over the catalyst below a threshold flow rate likely due to uneven flow through the 0.016" holes in the tube situated directly below the CPO stage.

As a result of the aforementioned experimental limitations, the propene to propane ratio (Figure 3.5) was far greater than 10^{-9} to 10^{-6} predicted by equilibrium calculations performed using HSC software over 250-460 °C. Deactivation and a low C_{10} isomer selectivity for decane were therefore observed because the hydrogenation/dehydrogenation functions were unequilibrated resulting in higher olefin concentrations. Degnan et al. found that for systems in which hydrogenation/dehydrogenation was unequilibrated, the isomer yield maximum as a function of conversion shifted towards lower conversions.[146] The high olefin concentration in our system may account for the lack of C_{10} isomers due to pronounced secondary cracking reactions. The traditional mechanism proposed by Weisz[147] did not include olefins as reactive intermediates which were assumed to be immediately hydrogenated to the corresponding paraffin after isomerization without undergoing subsequent reactions. By contrast, olefins in unequilibrated systems are not necessarily immediately hydrogenated back to corresponding paraffins and may, therefore, undergo subsequent cracking reactions which reduce the selectivity to branched products.[146] Bhasin et al. showed the heat of adsorption of a hydrocarbon on platinum increases with hydrocarbon size for ethane to n-hexadecane over a temperature range of 350 °C to 550 °C[148] and Thybaut et al. showed the same effect for n-octane to n-hexadecane from 220 °C to 280 °C.[149] We postulate that large molecules may limit the extent of propene hydrogenation resulting in a higher propene/propane ratio. As conversion is increased, the number of large competitively adsorbing reactant molecules decreases, leading to a reduction in competitive adsorption and allowing more propene to be hydrogenated to propane.

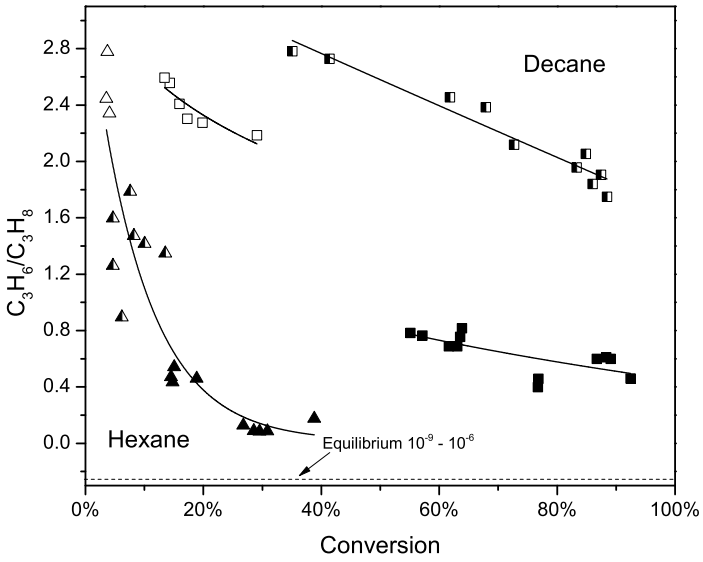

Figure 3.5: Molar ratio of propene to propane. Equilibrium concentrations are calculated for the temperature range measured in the zeolite stage (250 - 460 °C) Filled symbols: HZSM-5 open symbols: USY half-filled symbols: HBEA. △ hexane □ decane

3.3.3 Deoxygenation and aromatization of 2-decanone

General reaction pathway

Various isomers of decene were observed to form from 2-decanone deoxygenation. The selectivities of C_{10} products over HBEA and USY were 80% and 90% respectively at low conversion as shown in Figures 3.6b and 3.6c. The products at conversions less than 60% consisted of a mixture of linear decene isomers. As conversion is increased by moving the zeolite stage closer to the CPO stage, the selectivity of C_{10} compounds decreased as the initial products underwent hydrocracking reactions to form smaller C_{2-6} products. Products formed from hydroisomerization and hydrocracking reactions over HZSM-5 contained greater amounts of aromatics than products formed over HBEA and USY at conversions less than 60% (Figure 3.6. The selectivity to aromatics over HZSM-5 is about 9% at low conversions and increases to 26% at 40% conversion (Figure 3.6a). At high conversions over all zeolites studied, C_{4-6} compounds dimerize and/or cyclize to form aromatics such as benzene, toluene, and xylenes (BTX) by conventional aromatic formation mechanisms as well as monoaromatics larger than

C_8.[64]

Effect of zeolite topology on product distribution

Shape selectivity in 10-MR pores of HZSM-5 may limit the extent of methylated and ethylated monoaromatic formation. Methylated and ethylated monoaromatics have been shown to form in zeolites containing 12-, 10-, and 8-MR pores and cavities by Min et al. who showed the ethylbenzene disproporation reaction at 316 °C to 427 °C and WHSV = 5.2 h^{-1} to be an effective probe of large pore vs medium pore zeolites.[150] Zeolites with larger pore structures permit bulkier products to form from ethylbenzene such as diethylated diphenylethane while smaller pore zeolites only permitted diethylbenzene and benzene to form. Aromatics may be products of 2-decanone deoxygenation and cyclization because the 12-MR pores of HBEA and USY are large enough to limit shape selectivity effects and permit large methylated and ethylated monoaromatic products to form. The aromatics that form over HZSM-5 consist mostly of BTX with large methylated and ethylated monoaromatics like 1-methyl-4-ethylbenzene comprising less than 5% of the effluent. The 10-MR pores of HZSM-5 may be too small to allow methylated and ethylated monoaromatics to form like those produced by reactions over HBEA and USY.

We propose that deoxygenation reactions occur before cracking and cyclization reactions because no oxygenated products were observed over any catalyst. Products such as 2-decene are primarily formed from 2-decanone before any aromatics are formed from cyclization reactions (Figure 3.7). No studies of 2-decanone chemisorption on a zeolite can be found in the literature although acetone has been shown to adsorb in protonated form where it undergoes a condensation reaction with another acetone to form mesityl oxide and eventually isobutene.[151] Products formed from hydroisomerization and hydrocracking of 2-decanone over HZSM-5 consisted of aliphatics and aromatics but no observable C_{10} products even at low conversion. The 10-MR pore size may be preventing a C_{10} olefin from leaving the pore without first hydrocracking. We hypothesize that confinement effects in HZSM-5 may cause reactive double bonds in deoxygenated 2-decanone to react over an acid site and crack to form a product that can more easily traverse the pore. Reduced confinement effects in large 12-MR pore zeolites such as HBEA and USY may allow C_{10} olefins to exit the catalyst without further reacting.

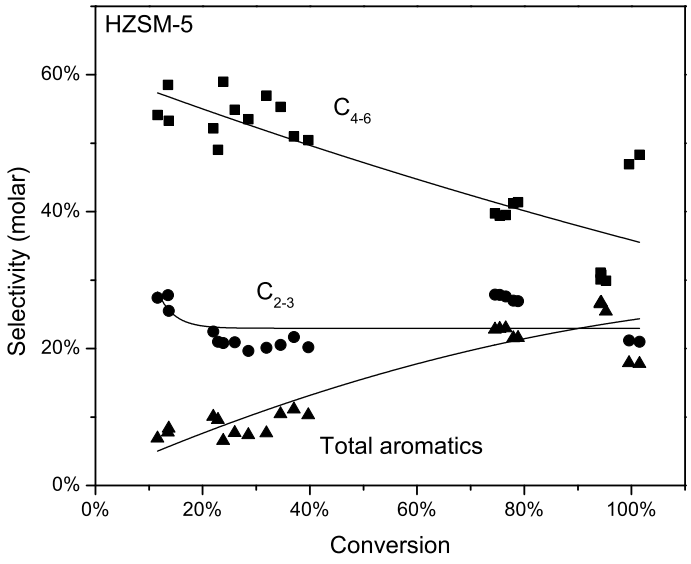

(a) Product distribution formed from 2-decanone over HZSM-5.

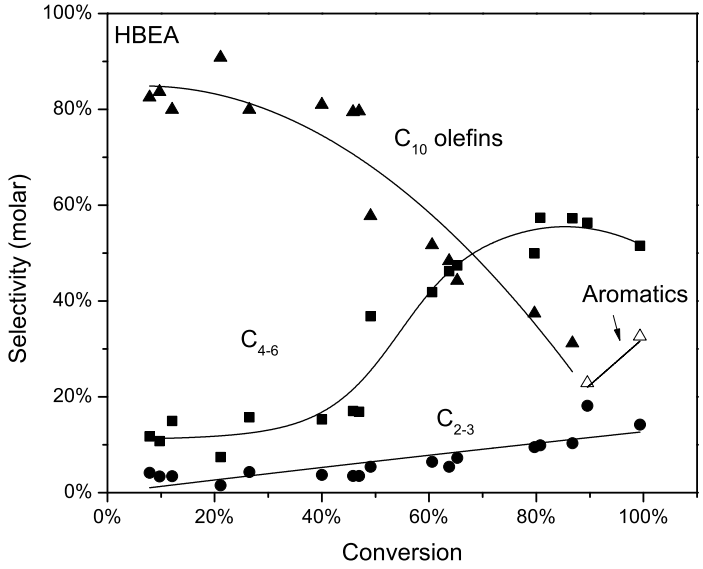

(b) Product distribution formed from 2-decanone over HBEA.

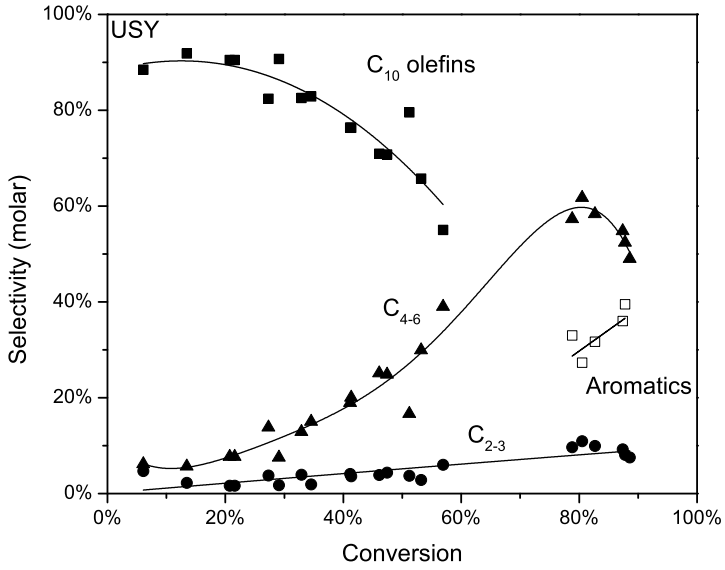

(c) Product distribution of aromatics formed from 2-decanone over USY.

Figure 3.6: Product distributions for hydroisomerization and hydrocracking of 2-decanone over HBEA, USY, and HZSM-5.

Possible mechanisms for aromatic formation

As seen in Figure 3.6, the selectivity to C_{4-6} compounds increases with conversion as C_{10} selectivity decreases. C_{4-6} compounds are secondary products of 2-decanone hydroisomerization and hydrocracking which form primarily from hydrocracking of C_{10} olefins. Similar sized compounds formed from hydroisomerization and hydrocracking of decane are primary products of hydrocracking and decrease with conversion. Aromatics are more likely formed from C_{4-6} rather than C_{2-3} oligomerization and cyclization. Larger hydrocarbons will adsorb preferentially over C_{2-3} compounds on the zeolite due to increased heats of adsorption.[152] As shown in Figure 3.6c, the selectivity to aromatics increases to 37% at conversion greater than 80% as C_{4-6} compounds are consumed to form aromatics. Note the C_{2-3} selectivity does not decrease as rapidly with conversion as C_{4-6} lending support to the notion that aromatics are formed preferentially from C_{4-6} rather than C_{2-3}. Hydroisomerization and hydrocracking of decane, by comparison, produces only trace amounts of aromatics. Fewer olefins are

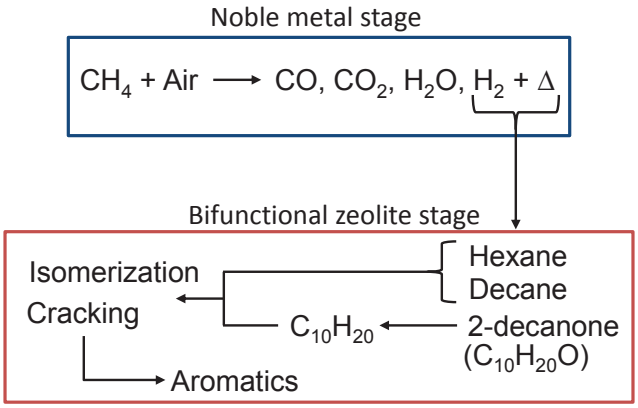

Figure 3.7: Possible routes for aromatics formation

observed to form from hydroisomerization and hydrocracking of decane resulting in a reduced selectivity to aromatics.

3.4 Conclusions

Hydrocracking and hydroisomerization have been incorporated into a single-pipe heat integrated reactor with applications in high throughput systems for biomass processing. A wide range of conversions and product distributions was obtained with the staged reactor configuration. Branched products are observed to form from hexane over all zeolites studied. The branched products decomposed to form C_2 through C_4-sized products as conversion increased. C_{10} branched products were not observed with decane hydroisomerization and hydrocracking because hydrogenation/dehydrogenation was not equilibrated. Selectivities to methylated and ethylated monoaromatics of ~40% are observed by reacting 2-decanone at high conversion over HBEA and USY zeolites containing Pt/γ-Al_2O_3. The large 12-MR pores of HBEA and USY permit 2-decanone to deoxygenate and cyclize to form aromatics while the medium 10-MR pores of HZSM-5 hamper C_{10} olefin formation by catalyzing cracking reactions. The cracked olefins can cyclize to form a maximum 26% selectivity of BTX at high conversion over HZSM-5.

CHAPTER

FOUR

REDUCTIVE DEHYDRATION OF BUTANONE TO BUTANE OVER Pt/γ-Al_2O_3 AND HZSM-5[1]

A bifunctional catalyst was used for hydroisomerization and hydrocracking of paraffins and alkanones in Chapter 3. In this chapter, a bifunctional zeolite is now used to upgrade butanone,a surrogate of bio-oil, to butane more effectively than would be possible over a monofunctional catalyst such as HZSM-5. We show butanone can be reacted to form n-butane in an isothermal reactor containing a 1 wt% Pt/γ-Al_2O_3 and an HZSM-5 catalyst (total mass of 12-400 mg, Si/Al=11.5) below 160 $^{\circ}$C with up to 99% selectivity and 67% yield. The catalyst loading (12-400 mg) and temperature (100-250 $^{\circ}$C) were varied to obtain primary products whose selectivities decreased with conversion and secondary/tertiary products whose selectivities increased with conversion. As conversion increased, the selectivities of butanol and butene decreased, showing the formation of butane from butanone through a series reaction pathway: butanone $\rightarrow$ 2-butanol $\rightarrow$ butene $\rightarrow$ butane. Butane selectivity increased as the temperature was increased from 100-200 $^{\circ}$C when compared at similar conversions due to higher dehydration rates over the zeolite. Processing ketones at low temperatures over bifunctional catalysts may be an efficient means of obtaining high yields of stable paraffins from reactive oxygenates.

[1]Portions of this chapter appear in S. D. Blass, C. Rosenthal, A. Bhan, L. D. Schmidt, "Reductive dehydration of butanone to butane over Pt/γ-alumina and HZSM-5," *Catal., Commun.* **42** (2013) 54-57.

4.1 Introduction

Significant interest has been generated in synthesizing and processing bio-oil for use as fuels or chemicals in a biofuel-driven economy. However, bio-oil contains a mix of oxygenated species such as aldehydes, ketones, esters, and other functional groups whose acidic and corrosive properties render them unsuitable for use as stable energy-carriers.[44,45] Ketones[69,76,77] and aldehydes,[78,79] in particular, contain electrophilic carbonyl groups that are prone to nucleophilic attack from other molecules, leading to condensation reactions that increase the size of the product. Uncontrolled condensation reactions result in coke formation, leading to catalyst deactivation.[69] For example, conversion of acetone decreased over HZSM-5 at 400 °C from 55 to 20% after 300 min on stream when forming coke precursors such as olefins and aromatics.[69] Therefore, a method is needed to deoxygenate ketones or convert them to more stable functional groups that do not deactivate as quickly such as alcohols.[69] The first step in one possible deoxygenation route is the reduction of a ketone group to an alcohol. Hydrogenation of carbonyl groups to alcohol groups in an enriched H_2 atmosphere has been studied over Ru,[153] Ag,[154] and Pt[155] catalysts; however, a common challenge in hydrogenolysis is selectively cleaving C–O bonds over C–C bonds.[156] Meanwhile, dehydration of alcohols to olefins over zeolites such as HZSM-5 has been shown to produce high yields of olefins with minimal C–C bond scission.[72,83,84] For example, Sun et al. achieved a 75% yield of butene from 1-butanol over HZSM-5 at 225 °C and a 92% yield over HFER at 300 °C.[72] One possible strategy that may afford more control over C–O bond scission involves incorporation of dehydration into the deoxygenation process by means of a bifunctional catalyst.

Alotaibi et al. observed a 22% yield of 2-methylpentane from methyl isobutyl ketone over 0.5 wt% Pt/SiO_2 at 200 °C and predicted a bifunctional series reaction pathway that converts methyl isobutyl ketone to 4-methyl-2-pentanol and eventually 2-methylpentane.[155] However, the pathway was proposed on the basis of a catalyst survey and experiments at one zeolite loading. We provide a more focused study across multiple space velocities and H^+/Pt ratios to help confirm and elucidate the bifunctional mechanism for butanone.

4.2 Materials and Methods

4.2.1 Catalyst Synthesis

NH_4-ZSM-5 from Zeolyst (CBV 2314; Si/Al=11.5) was calcined in 200 ml min^{-1} dry air (20-21% O_2, < 10ppm H_2O, Minneapolis Oxygen) and heated at a rate of 1.5 °C min^{-1} to 500 °C and held for 2 h. A 1 wt% Pt on γ-Al_2O_3 sample was made from a Pt precursor (H_2PtCl_6, 8 wt% in H_2O from Sigma Aldrich) dissolved in a slurry of γ-Al_2O_3 powder (99.97%; Alfa Aesar) and dried at 80 °C overnight. The powder was mechanically mixed with the calcined zeolite to obtain a zeolite to platinum molar ratio (H^+/Pt) of 20. The mixed powder was heated in dry air at 1.5 °C min^{-1} to 500 °C and held for two hours. The catalyst was then treated in 5% H_2 in Ar (200 ml min^{-1}) at 400 °C for two hours and cooled. The sample was then pressed into discs at 2000 psi and crushed into pellets which were sieved to select for 599-710 μm particles (24-30 mesh). The H^+/Pt ratio was altered by varying the Si/Al ratio at constant zeolite loading. The Si/Al ratio was changed by using CBV 2314 (Si/Al=11.5), CBV 3024E (Si/Al=15), CBV 5524G (Si/Al=25), and CBV 8014 (Si/Al=40) zeolite samples.

4.2.2 Reactor Configuration and Analysis

A 10 mm ID quartz tube was fabricated and connected to a vaporizer consisting of a ¼" stainless steel tube heated to 200 °C with heating tape as shown in Figure 4.1. The vaporizer inlet was sealed to a stainless steel nebulizer consisting of concentric ⅛" and 1⁄16" tubes. Butanone was fed through the nebulizer at 0.042 ml min^{-1} and N_2 and H_2 were fed through the nebulizer each at 0.70 standard liters per minute (slpm) for a H_2 to butanone molar ratio of 60.

Composition analysis was conducted with an online HP 7890A gas chromatograph (GC) equipped with a thermal conductivity detector and flame ionization detector in series. The GC contained a HP PLOT/Q column (30×0.32×20). N_2 was used as an internal standard. Peak identification was verified with a HP 5890 Series II gas chromatograph containing a HP-1 column (50×0.32×1.05) connected in series with a HP MSD 5970 mass selective detector. Carbon balance closed to within 15%.

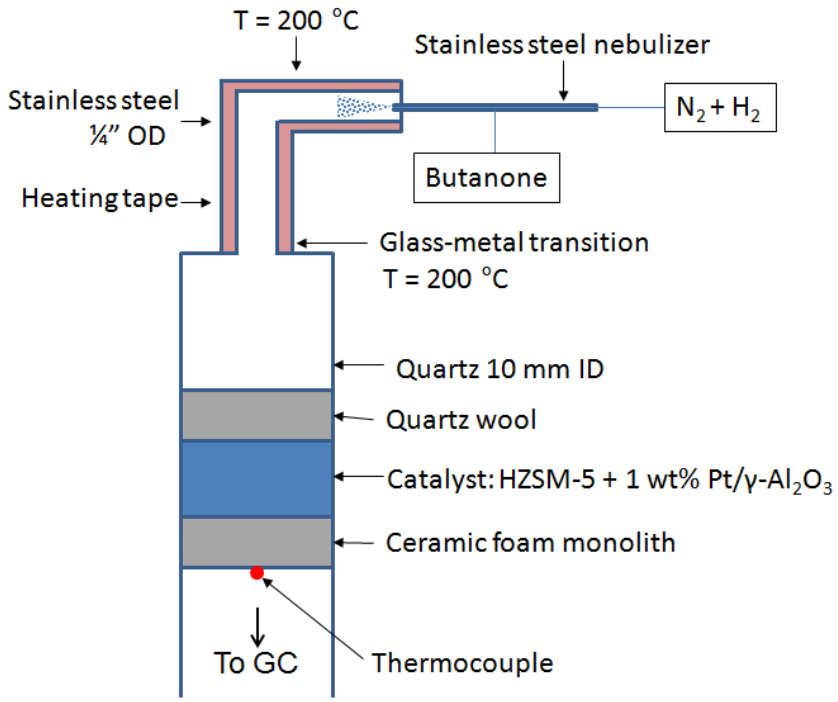

Figure 4.1: Reactor schematic

4.2.3 Experimental Procedure

The catalyst was pretreated at 500 °C for 20 minutes in dry air at 0.3 ml min^{-1} and 20 minutes in H_2 at 0.70 slpm. A constant N_2 flow rate was maintained at 0.70 slpm during pretreatment and throughout the course of the experiments. After pretreatment, the reactor was cooled to the desired temperature while maintaining constant flow rates. Three injections were analyzed at a time-on-stream of 7, 22, and 37 minutes. The catalyst temperature was varied from 100-250 °C. The catalyst was regenerated under the pretreatment conditions between each temperature. Space velocity was changed by varying the total catalyst loading from 12-400 mg at a constant reactant flow rate. Data at all loadings are plotted without consideration of bypass, which occurred at loadings below 30 mg, because the conversion did not exceed 10%. The WHSV was varied from 27-850 h^{-1} or a residence time from 3-33 milliseconds calculated on a gas hourly basis. Besides the bifunctional catalyst, monofunctional catalysts consisting of solely HZSM-5 or Pt/γ-Al_2O_3 were synthesized using the methods described above.

4.3 Results and Discussion

4.3.1 Reactivity of Butanone Over HZSM-5

Butanone was initially unreactive over HZSM-5 without Pt/γ-Al_2O_3 at temperatures up to 250 °C with conversions less than 1%. Similarly, Chang et al. reacted acetone over HZSM-5 and reported a conversion of 3.9% at 250 °C and a LHSV of 8.0 h^{-1}.[157] While acetone and butanone have been shown to be reactive over HZSM-5 to form C_{2-5+} products at temperatures exceeding 370 °C through aldol condensation and cracking,[158] the temperatures in our reactor may be too low for this to occur. The extent of bimolecular reactions is a function of partial pressure, which relates to surface coverage and temperature.[76,159] Higher temperatures are needed at lower surface coverages to initiate an aldol condensation reaction. Aldol condensations of acetone are typically done in the vapor phase from 250 to 400 °C.[69] The partial pressure of butanone used in our experimental conditions (0.83 kPa) may have been too low to achieve a minimum surface coverage needed to initiate significant bimolecular reactions such as aldol condensations, explaining the low observed reactivity.

4.3.2 Evidence for Series Reaction over Pt/γ-Al_2O_3 and HZSM-5

While butanone was inactive over HZSM-5 alone, the addition of Pt/γ-Al_2O_3 to the zeolite lead to yields of butane up to 67% with less than 2% selectivity to butene and 2-butanol. The catalyst loading was varied at each temperature to change space velocity and conversion. Only trace amounts of ethylene and propylene were observed, indicating that cracking reactions were negligible. Less than 1% selectivity to products larger than C_4 was observed, possibly because the partial pressure of butanone was low enough to limit bimolecular reactions. When product selectivities were plotted as a function of conversion, as shown in Figure 4.2, butane selectivity decreased as conversion decreased while butene increased. Butanol selectivity decreased from 15% to 10% at 100 °C as conversion increased from 2 to 60%. Increasing selectivity of butanol and butene at low conversions suggests these species are intermediates in a series reaction that ultimately converts butanone to butane. In a series reaction that can be explained with Figure 4.2, we propose that butanone was reduced over a Pt site to form 2-butanol. The butanol likely diffused to a zeolite acid site and

subsequently dehydrated to an olefin. The olefin likely diffused back to a Pt site where the C=C bond was hydrogenated to form a paraffin compound. No butanol was observed at temperatures greater than 160 °C, possibly because it was consumed rapidly by the dehydration reaction. When compared across different temperatures at similar conversions, butane selectivity increased with temperature while butanol selectivity decreased, likely because zeolite-catalyzed dehydration rates increased with temperature,[72] limiting the concentration of butanol. Deactivation was also observed as shown by a decrease in butanone conversion by 5% at 100 °C and 20% at 160 °C at the same time-on-stream. It is possible coke formation may occur more readily at 160 °C causing greater changes in conversion than at 100 °C. Selectivities did not change with time-on-stream by more than 5% at any loading.

4.3.3 Reactivity of Butanone over Pt/γ-Al_2O_3

When butanone was reacted over Pt/γ-Al_2O_3, the butane selectivity increased with temperature while butanol selectivity decreased, as shown in Figure 4.3. As the temperature was increased, dehydration catalyzed by Lewis acid sites on γ-Al_2O_3 became important. γ-Al_2O_3 containing Lewis acid sites has been shown to be an active dehydration catalyst for isobutanol from 160 to 300 °C.[160] Lewis acid-catalyzed dehydration likely explains the decrease in butanol selectivity and subsequent increase in butane selectivity. When Pt/γ-Al_2O_3 was combined with HZSM-5, both Brϕnsted and Lewis acid sites likely carried out dehydration.

In our experiments with Pt/γ-Al_2O_3 shown in Figure 4.3, butane selectivity was less than 1% at 100 °C, suggesting that direct hydrogenation of butanone to butane over Pt is unlikely even in the bifunctional case. While Alotaibi et al. obtained higher yields of alkanes than methyl isobutyl ketone than we did from butanone, a higher yield of butane could have been obtained from butanone had the catalyst loading been increased.[155]

4.3.4 Effect of metal-acid balance

At constant Pt and zeolite loading, the H^+/Pt ratio was changed by varying the zeolite Si/Al ratio. Measurements were taken at 100 °C and 37 minutes on-stream. Changing the metal acid balance had a minimal effect on conversion because the molecule was only activated over Pt sites (Figure 4.4). At a relatively constant conversion of

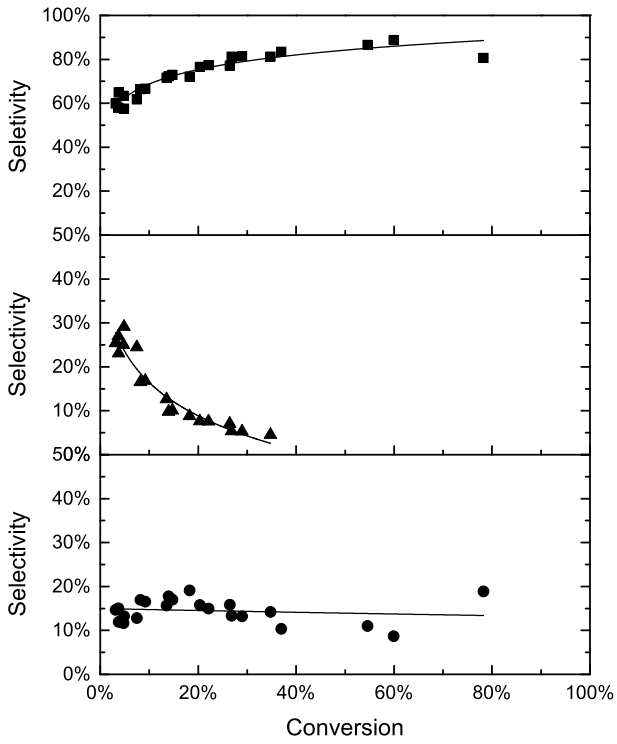
Seletivity
100%
80%
60%
40%
20%
50%
Selectivity
40%
30%
20%
10%
50%
Selectivity
40%
30%
20%
10%
0%
0%
20%
40%
60%
80%
100%
Conversion

(a) 100 °C

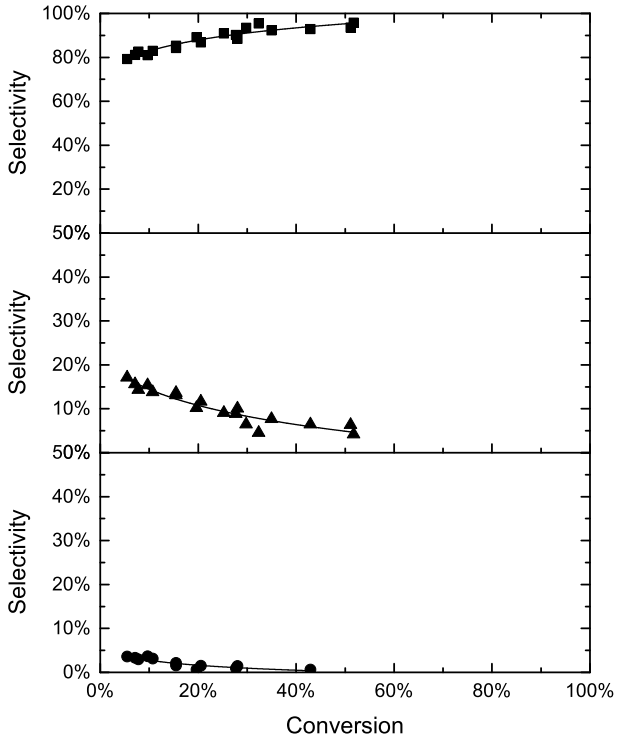

(b) 160 °C

Figure 4.2: Butane (■), butene (▲), and butanol (●) selectivities as a function of butanone conversion at different temperatures over Pt/γ-Al_2O_3 with HZSM-5. Loading: 12-400 mg.

~75%, the butane selectivity increased with acid site density while butanol selectivity decreased, showing that the H^+/Pt ratio had little effect on the conversion, leading us to postulate that initial activation of butanone over Pt/γ-Al_2O_3 to butanol is the slow step. Butanol selectivity decreased and butane selectivity increased as the acid site density was increased because the higher number of acid sites increased the rate of consumption of butanol. At the highest H^+/Pt ratio (20), the butanol selectivity increased from 8 to 20% while butane selectivity decreased from 92 to 80% at constant conversion. It is unclear why this occurred, but if coke formation occurs naturally with dehydration reactions, then an increase in the dehydration rate with acid site density will also result in an increase in coke formation. Coke formation would cause pore blockage and prevent butanol from reaching a Brϕnsted acid site

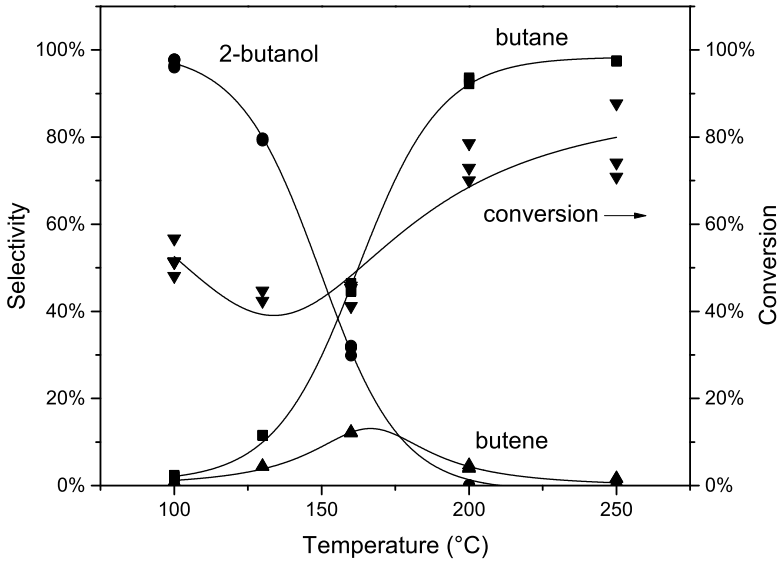

Figure 4.3: Butane (■), butene (▲), and butanol (●) selectivities and butanone conversion (▼) as function of temperature for Pt/γ-Al_2O_3 without HZSM-5. Loading: 0.20 g.

to be dehydrated, explaining the observed butane/butene ratio in Figure 4.4.

4.3.5 Deactivation

Over Pt/γ-Al_2O_3 with HZSM-5, the maximum conversion at each temperature increased (Figure 4.5) from 34% at 100 °C to 67% at 130 °C due to faster rates at higher temperatures. However, the conversion decreased to 5% when increasing the temperature from 130 °C to 250 °C. Coke is formed when acid sites catalyze the formation of species that do not desorb. The highly active nature of the solid acid site may explain the tendency to form coke faster over a Pt/γ-Al_2O_3 and HZSM-5 catalyst than on Pt/γ-Al_2O_3 alone. In an experiment intended to confirm coke formation, butanone was reacted over Pt/γ-Al_2O_3 and HZSM-5 at 250 °C for 37 minutes at which point the conversion was measured at 16% as shown in Figure 4.5. Following reaction at 250 °C, the temperature was dropped to 100 °C without regeneration, at which point the conversion increased to 40% with an additional 37 minutes on stream. By contrast, the conversion of butanone increased further to 77% when reacted at 100 °C

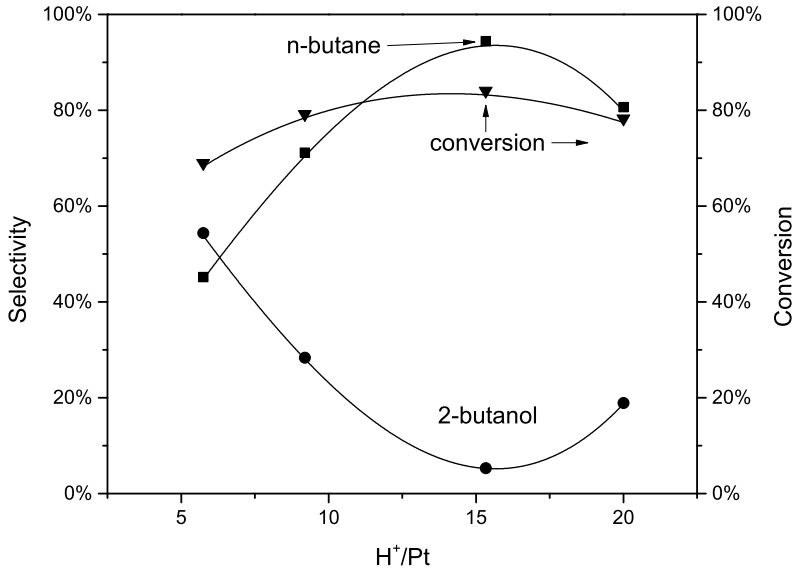

Figure 4.4: Butane (■) and butanol (●) selectivities and butanone conversion (▼) as function of metal-acid ratio for Pt/γ-Al_2O_3 with HZSM-5 at 100 °C with a total catalyst loading of 400 mg.

following regeneration with no pretreatment at 250 °C. The differences in conversion at 100 °C between catalysts with and without pretreatment may be attributed to coke formation at 250 °C which likely blocked active sites.

The decrease in conversion with temperature, however, may also be due to a decrease in the adsorption constant. When the catalyst was reacted at 250 °C followed by 100 °C, the conversion increased from 16% to 40% even without regeneration. We expect adsorption to decrease with increasing temperature because adsorption is exothermic and was measured using microcalorimetry by Sepa et al. to be -140 kJ/mol for acetone over HZSM-5.[159] Therefore, the low conversion at 250 °C may be due to both coke formation and a decrease in adsorption at higher temperatures. Both coke formation and adsorptive properties of potential reactants may be important factors to consider when designing a catalytic bio-oil upgrading process.

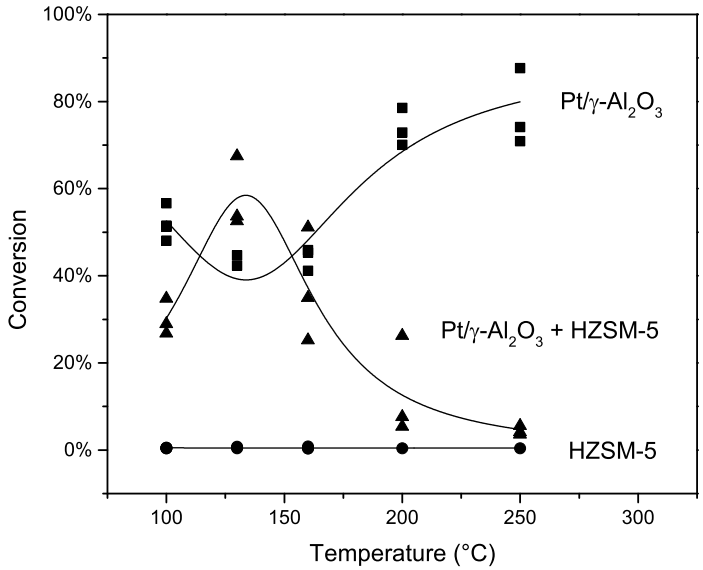

Figure 4.5: Conversion of butanone over 400 mg of HZSM-5 (●), Pt/γ-Al_2O_3 (■), and Pt/γ-Al_2O_3 with HZSM-5 (▲).

4.4 Conclusions

We have demonstrated that conversion of butanone to butane can be accomplished through a bifunctional route more efficiently than through a monofunctional one. Over a bifunctional pathway, butanone is reduced to 2-butanol over a Pt site. The alcohol is then dehydrated over a zeolite acid site to butene and, subsequently, hydrogenated to butane over a Pt site as evidenced by 99% selectivity to butanol over Pt/γ-Al_2O_3 without HZSM-5. Over a monofunctional catalyst, butanone either does not react when exposed to HZSM-5 or forms only butanol when Pt/γ-Al_2O_3 without HZSM-5 is used at temperatures below 130 °C. Minimal C–C bond scission occurred as evidenced by the negligible production of C_{2-3} compounds. The chemical complexity of bio-oil compounds necessitates the development of multifunctional catalysts such as bifunctional zeolites to produce paraffins from oxygenated species. Reductive dehydration of butanone to butane over a bifunctional zeolite may represent a new pathway to upgrading reactive ketones to biofuels.

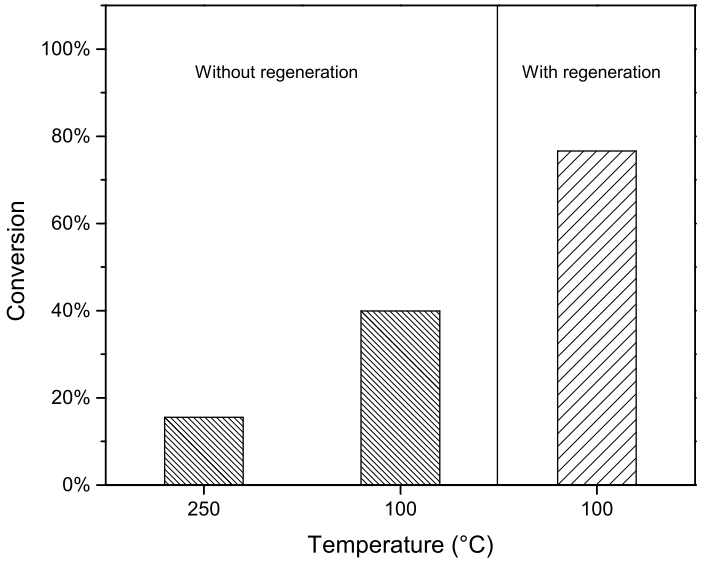

Figure 4.6: Butanone conversion with 400 mg of Pt/γ-Al_2O_3 with HZSM-5 at 100 °C with treatment at 250 °C and without treatment at 80 minutes on stream.

CHAPTER

FIVE

ON-LINE DEOXYGENATION OF CELLULOSE PYROLYSIS VAPORS IN A STAGED AUTOTHERMAL REACTOR[1]

Biomass upgrading in autothermal staged reactors has, thus far, been limited to simple systems such as ethanol[83] and paraffins (Chapter 3). In this chapter, the autothermal staged reactor is applied to cellulose, a feedstock more similar to actual biomass than feedstock previously studied. In particular, we demonstrate the coupling of oxidative cellulose pyrolysis with zeolite-catalyzed upgrading of pyrolysis vapors in a staged autothermal reactor over bifunctional combinations of HZSM-5, HFER, or USY with Pt/γ-Al_2O_3. The pyrolysis vapors formed from oxidative decomposition of cellulose passed through a downstream bifunctional zeolite stage to form a mixture of aromatics, C_{2-4} olefins and paraffins, CO, CO_2, and CH_4. A comparison of the bifunctional staged reaction with that of monofunctional zeolite catalysts revealed a ~13% increase in conversion of pyrolysis vapors to deoxygenated products. Of the pyrolysis vapor entering the zeolite catalyst, 24% was converted to aromatics while an additional 20% was converted to C_{2-4} olefins and paraffins. Complete conversion of cellulose to CO, CO_2, light hydrocarbons and aromatics was obtained at 500 °C upon addition of Pt/γ-Al_2O_3 to HZSM-5. Deactivation of the catalysts reduced the conversion of pyrolysis vapors to deoxygenated products as indicated by an increase in

[1]Portions of this chapter appear in N. E. Persson, S. D. Blass, C. Rosenthal, A. Bhan, L. D. Schmidt, "On-line deoxygenation of cellulose pyrolysis vapors in a staged autothermal reactor," *RSC Advances* **3** (2013) 20163-20170.

the oxygenate yield with time-on-stream. Oxygenate yield measured after the zeolite stage increased to 6% after 30 minutes on stream over bifunctional HZSM-5/Pt, and increased from 13% to 31% at the same time-on-stream over monofunctional HZSM-5. Pt likely promoted hydrogenation of the coke precursors produced in the staged reactor while the 10-MR pore size of HZSM-5 limited the formation of polyaromatic species. A 6% increase in CO_2 yield and 5% increase in CH_4 yield was observed when Pt/γ-Al_2O_3 was added to each zeolite, indicating the possible presence of water-gas-shift and methanation reactions, respectively, over Pt sites. The small-scale high-throughput autothermal reactor that we describe here is capable of carrying out cellulose depolymerization and upgrading in a single-pipe process.

5.1 Introduction

Research in biofuel production is motivated by diminishing hydrocarbon reserves and global climate change caused by carbon dioxide emissions.[161,162] Gasification to syngas and subsequent upgrading is one possibility, but requires large vessels, high pressures, and capital-intensive facilities.[41,163] An alternative route is pyrolysis, a bio-oil production process that can be accomplished in smaller vessels and lower pressures. Pyrolysis is also conventionally carried out as a batch process but a continuous process would yield advantages in throughput and scalability.[164] Balonek et al. showed that bio-oil can be obtained from the oxidative pyrolysis of biomass in a continuous, autothermal reactor by reacting cellulose with air over a platinum catalyst.[44] The combustion and partial oxidation reactions at the front face of the catalyst bed cause the temperature to be maintained at ~700 °C, enabling reactive flash volatilization of the microcrystalline cellulose particles impacting the surface.[105] Molecular oxygen is consumed in combustion and partial oxidation reactions providing the heat to volatilize incoming cellulose and drive the homogeneous pyrolysis reactions.

The pyrolysis vapors that form from cellulose are condensable as bio-oil yet contain a product spectrum replete with reactive oxygenated compounds such as cyclic furans, pyrans, phenols, ketones, aldehydes, and other acids. These oxygenates render bio-oil thermally unstable, acidic, and corrosive.[6,165] As a result, much interest has been stimulated in developing processes to convert bio-oil to products that can be integrated with existing chemical infrastructure. Upgrading of bio-oil compounds formed at high temperature can be made more energy-efficient by not allowing con-

densation to occur. The absence of condensation removes the need to collect and store toxic and unstable bio-oil for further processing. We explore the possibility of integrating continuous oxidative pyrolysis with downstream zeolite-catalyzed upgrading in a staged autothermal reactor. The process heat from a catalytic partial oxidation stage has previously been used to promote upgrading reactions over a downstream zeolite stage for methanol,[88] ethanol,[83] butanol,[72] and paraffin feeds.[47] A staged reactor processing cellulose circumvents the problem of reacting a solid feedstock over a zeolite by first converting the feedstock into a vapor. This solution also limits concerns over the storage of bio-oil, such as phase separation and the formation of precipitates.[6,165]

Oxygenated compounds in the bio-oil have been deoxygenated over zeolites such as HZSM-5 through a combination of dehydration, decarbonylation, and decarboxylation.[71,166–169] Aromatic yields as high as 30% have been obtained from bio-oil over HZSM-5 with Si/Al ratios of 30 - 60 at temperatures between 400 and 600 °C.[168,170,171] The high selectivity of gasoline-range hydrocarbons and aromatics has been attributed to the 10-member-ring (-MR) pore size of HZSM-5, which restricts the ability of large polyaromatics to form within the pores.[172,173]

However, extensive coke formation that blocks zeolite active sites is still observed over most zeolites from 200-500 °C and up to 100 bar in both continuous and batch systems.[71,169,174] This buildup causes catalyst deactivation, characterized by a reduction in both the formation of monocyclic aromatics and conversion of oxygenates over time.[169] Thermal degradation of aldehydes, oxyphenols, and furfural has been identified as one source of coke formation.[71] Catalytic coke is thought to be due to cyclization reactions that cause buildup of polycyclic aromatic species.[175] Coke deposits that block acid sites can be removed through oxidative regeneration of the catalyst, but this process has been shown to produce localized high temperature regions that irreversibly remove acid sites from the catalyst.[176]

Bifunctional catalysts containing platinum mixed with zeolites have been shown to increase catalyst lifetime during hydroprocessing at temperatures ranging from 200 - 500 °C by hydrogenating compounds such as aromatics and olefins that are known coke precursors.[47,115,130,131] Bifunctional HZSM-5/Pt and HY/Pt catalysts were also shown by Hong et al. to be effective at 200 - 250 °C for the conversion of phenol, a major component of lignocellulosic bio-oils.[177] We chose to introduce bifunctional catalysts downstream of the combined catalytic partial oxidation (CPO)/pyrolysis

stage in a position where temperatures ranged from 450 - 500 °C. The resulting system continuously converts cellulose to fuels and chemicals with no external energy input at contact times of about 70 milliseconds, at least one order of magnitude faster than conventional pyrolysis processes.[50] The zeolite catalyst experiences deactivation three times slower than conventional zeolites and a yield to solid carbon products of less than 3%. Thus, we demonstrate a small-scale, high-throughput, and heat-integrated reactor capable of processing cellulose at shorter contact times with lower rates of deactivation than conventional reactors.

5.2 Materials and Methods

5.2.1 Catalyst Preparation

H_2PtCl_6 (8 wt% in H_2O from Sigma Aldrich) was impregnated on α-Al_2O_3 spheres (1 wt% Pt, 1.3 mm α-Al_2O_3) by the incipient wetness technique as described in previous publications.[44] This catalyst was used in the catalytic partial oxidation (CPO) stage. Bifunctional HZSM-5/Pt was prepared by the following method. A sample of 1 wt% Pt on γ-Al_2O_3 was made from H_2PtCl_6 dissolved in a slurry of γ-Al_2O_3 powder (99.97%; Alfa Aesar) and dried at 80 °C overnight. NH_4-ZSM-5 from Zeolyst (CBV 2314; Si/Al=11.5) was calcined in dry air (20-21% O_2, <10ppm H_2O, Minneapolis Oxygen) and heated at a rate of 1.5 °C/min^{-1} to 500 °C, held for 2 h and cooled. The powder was mechanically mixed with the calcined zeolite to obtain an H^+/Pt molar ratio of 20. The mixed powder was heated in dry air at 1.5 °C/min^{-1} to 500 °C, held for two hours, then treated in 5% H_2 in Ar at 400 °C for an additional two hours and cooled. The sample was pressed into disks at 2000 psi and crushed into pellets that were sieved to select for 599-710 μm particles (24-30 mesh). The same procedure was followed for the preparation of ultra-stabilized H-Y (USY), H-Ferrierite (HFER) catalysts and their bifunctional Pt-loaded variants (USY/Pt, HFER/Pt).

5.2.2 Apparatus

Cellulose (9.6 g/h) and gases (2 SLPM N_2, 1 SLPM H_2, 0.2 SLPM O_2) were fed to an insulated quartz tube reactor (19 mm ID). Mass flow controllers (MKS Mass-Flo) fed the gases, with feed locations indicated in the illustration of the apparatus in Figure 5.1. N_2 was fed at 2.0 standard liters per minute (SLPM) as an inert

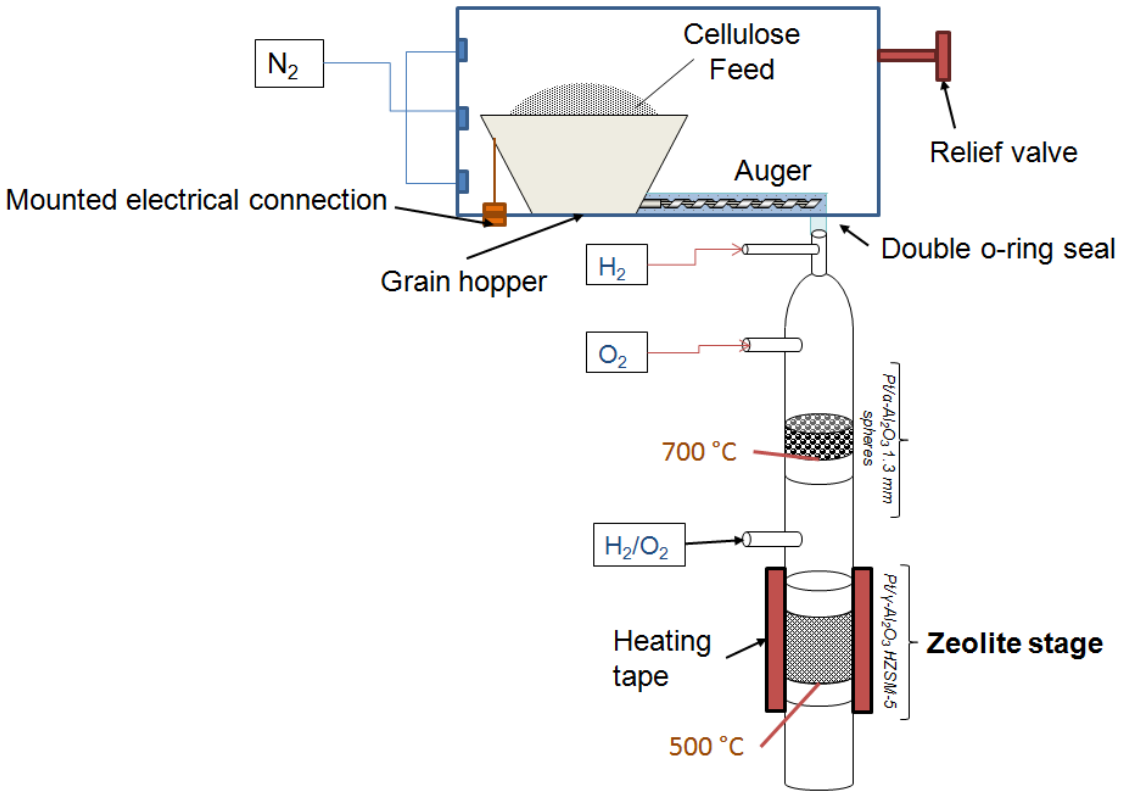

Figure 5.1: Reactor schematic. T= thermocouple.

diluent and internal standard and was used to purge the atmosphere in the solids feeding box to mitigate the potential for grain fires. H_2 and O_2 were fed upstream of the CPO stage under fuel-rich conditions to ensure complete O_2 consumption in the CPO stage and to eliminate the occurrence of homogeneous H_2 combustion prior to the front face of the CPO stage. Ignition of the CPO catalyst with a H_2 feed occurred at room temperature. Solid microcrystalline cellulose (FMC BioPolymer, 300µm average particle diameter) was loaded into a grain hopper situated in an airtight polycarbonate box that was fitted with a pressure relief valve (10 psi max) and a mounted electrical connection to the auger. The auger fed cellulose at a rate of 9.6 g/h to the reactor inlet, corresponding to a weight hourly space velocity (WHSV) of 4.8 h^{-1} and a H_2/cellulose molar ratio of approximately 42. Gas residence times were 30 milliseconds and 80 milliseconds in the first and second stages, respectively.

The first catalytic stage of the reactor over which CPO and pyrolysis occurred consisted of a 4 mm-thick layer of 1% Pt on α-Al_2O_3 spheres (1.3 mm o.d., 1.5 g), supported by a ceramic foam monolith (65ppi, 2.8 g, α-Al_2O_3), with a K-type

thermocouple located at the back face of the sphere bed. Temperature at the back face of the catalyst remained relatively constant at ~730 °C. This catalyst remained the same for every run. A second stage that was comprised of a zeolite or bifunctional Pt-loaded zeolite was wrapped with heating tape and situated downstream of the pyrolysis stage between two ceramic foam monoliths (65ppi, 2.8 g, α-Al_2O_3) and K-type thermocouples used to measure temperature at the front and back face. A side feed located between the stages was used to feed O_2 during zeolite regeneration. An Omega CSC32 Benchtop Controller controlled the zeolite back face temperature. The total catalyst loading (Pt/γ-Al_2O_3 and zeolite) was varied by changing the bed length from 0 to 20 mm. All zeolite reactions were carried out at 500 °C, a temperature indicated as optimal for conversion of oxygenates over zeolites.[70,168,178] The zeolite back face temperature was held at 500 °C while the front face temperature varied between 450 and 480 °C.

Products in the reactor effluent were analysed qualitatively by syringe injection to GC/MS (HP 5890 GC / 5970 MSD, He carrier). The major compounds identified through GC/MS were quantified via syringe injection to a GC equipped with both thermal conductivity and flame ionization detectors (HP 6890, Ar carrier). Response factors were calibrated in reference to the nitrogen peak. Coke was quantified with an online quadrupole mass spectrometer (QMS, UTi 100C). The burn-off was carried out under 1.0 SLPM Ar / 0.1 SLPM O_2 with a temperature program of 10 °C/min ramp to 500 °C and a 2 hour hold. Carbon was quantified by integrating the CO_2 peak measured at m/z of 44 and converted to a weight percent of the total cellulose fed.

5.3 Results and Discussion

5.3.1 Results of Control Studies

Control runs were carried out to analyze the content of the pyrolysis vapor formed over the pyrolysis stage of the reactor in the absence of a zeolite stage. Conversion of cellulose was always 100% due to the lack of solid accumulation on the front face of the pyrolysis stage. CO and CO_2 yields measured after the pyrolysis stage were 35% and 15% respectively, with the remainder of the carbon still contained in oxygenated pyrolysis products, which we define as any carbon-containing molecule besides CO

and CO_2. Balonek et al. carried out oxidative pyrolysis of cellulose over Pt on α-Al_2O_3 spheres at 660 °C at an atomic C/O of 1.7 with a H_2 co-feed in a similar reactor and obtained a maximum 55% yield to C_{2+} products,[44] consistent with our value of a 50% oxygenate yield. CO and CO_2 were not considered upgradable oxygenates for the purposes of this study, although CO could be considered a recoverable product for upgrading processes such as Fischer Tropsch.[179]

It is difficult to distinguish between CO and CO_2 formed from steam reforming, combustion, and thermal decomposition reactions. Graham et al. carried out non-oxidative pyrolysis of cellulose from 750 to 900 °C at residence times from 250 to 450 milliseconds and obtained less than 3 mol% of CO_2.[180] By contrast, Balonek et al. obtained a CO_2 yield of 18%.[44] Although H_2 has been shown to preferentially oxidize over cellulose,[44] we obtained a 15% CO_2 yield indicating that some cellulose is being consumed in combustion reactions despite being diluted with H_2 in a 40 to 1 ratio. H_2 was combusted as a sacrificial fuel to allow operation with low cellulose flow rates and small amounts of catalyst, while still permitting the quantification of all carbon-containing compounds in the system.

The pyrolysis vapor composition generated over the pyrolysis stage is similar to the composition of a typical cellulosic bio-oil: C_2 and C_3 acids, aldehydes, furans and pyrans, among others.[6,165,180] Phenols, produced mainly from the pyrolysis of lignin, represented less than 1% yield of the oxygenate distribution.[181,182] Therefore, the results of this study are not directly comparable with the upgrading of lignin-based bio-oils or phenolic compounds.

5.3.2 Deoxygenation capability of HZSM-5 and HZSM-5/Pt

HZSM-5 is the one of the most extensively studied catalysts for bio-oil upgrading due to its resistance to deactivation and high selectivities obtained for gasoline-range hydrocarbons and aromatics.[71,167–170,183] Hydrocarbon products commonly formed from the conversion of bio-oils over HZSM-5 at 200 - 500 °C include the olefinic light gases ethylene and propylene, as well as benzene, toluene, xylene, and ethylbenzene. As shown in Table 5.1 and Figure 5.2, C_{2-4} hydrocarbons accounted for 10% of the yield from cellulose over monofunctional HZSM-5, while aromatics accounted for 12%. Oxygen in biomass was rejected largely as CO and H_2O because the CO_2 yield remained constant at 15% upon addition of a zeolite stage. Diebold and Scahill

		C Yield (%)								
Catalyst	**TOS (min)**	**CO**	**CO_2**	**CH_4**	**Total C_{2-4}**	C_2	C_3	C_4	**Aromatics**	**Oxygenates**
None	5	34	15	1	2	2	0	0	0	49
γ-Al_2O_3	5	46	16	1	4	2	1	1	0	33
	30	39	15	1	3	2	1	0	0	42
Pt/γ-Al_2O_3	5	41	26	9	4	2	1	0	0	20
	30	44	20	3	4	2	1	1	0	30
HZSM-5	5	50	14	1	10	6	4	1	12	13
	30	43	16	1	5	2	2	1	4	31
HZSM-5/Pt	5	54	20	6	15	8	6	1	5	0
	30	56	17	4	13	6	5	2	3	6
HFER	5	45	16	1	9	5	3	1	0	29
	30	39	16	1	3	2	1	1	0	39
HFER/Pt	5	47	27	16	8	6	1	0	1	1
	30	53	17	8	7	5	1	0	0	15
HUSY	5	47	19	2	5	3	2	1	0	28
	30	40	18	2	4	2	1	1	0	37
HUSY/Pt	5	60	15	5	11	5	4	2	2	7
	30	54	15	4	8	4	3	1	0	20

Table 5.1: Carbon yield to products for each second stage catalyst tested at 5 and 30 minutes on stream.

upgraded the pyrolysis vapors from sawdust over HZSM-5 at 485 °C and a WHSV of 2.44 h^{-1} and observed a combined 16% CO and CO_2 yield.[167] Similarly we observed an increase of 16% in the CO yield when taking the difference between values measured before and after the HZSM-5 stage, as shown in Table 5.1 and Figure 5.2. The water yield from cellulose upgrading was not quantified because water was produced both by H2 combustion over the pyrolysis stage and from cellulose decomposition and subsequent upgrading.

To compare our results with literature values, we recalculated product yields by subtracting the CO and CO_2 yields from the first stage when considering that, in our experiments, approximately 50% of the carbon in cellulose is converted to CO and CO_2 from the initial pyrolysis. Subtracting CO and CO_2 formed through pyrolysis enables us to better illustrate the effect of the zeolite on the pyrolysis vapor stream. Adjaye et al. studied bio-oil upgrading over a fixed bed of HZSM-5 at a WHSV of 7.2 h^{-1} and a temperature of 410 °C. Selectivity to aromatics was approximately 28%, which is considerably higher than the 12% yield to aromatics observed in our reactor.[184] However, upon adjusting our value to exclude CO and CO_2 formed from pyrolysis, we obtain a comparable aromatics yield of 24%. Other products consisted of mostly oxygenates making further direct comparison difficult.

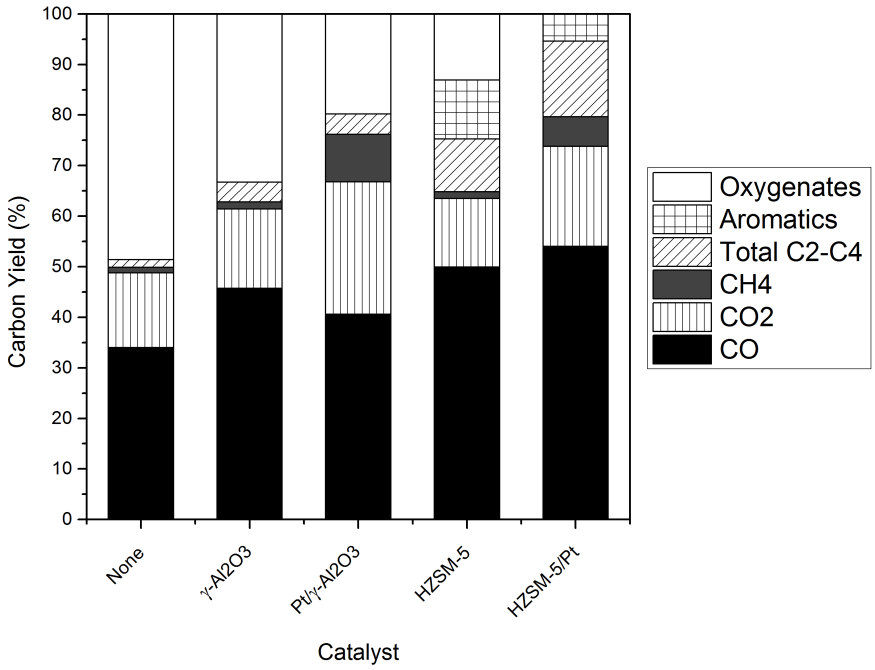

Figure 5.2: Carbon yield of reactor products over various catalysts. Products were measured at 5 minutes on stream.

5.3.3 Performance over Pt/γ-Al_2O_3

In addition to upgrading over HZSM-5, pyrolysis vapors were reacted over γ-Al_2O_3 and Pt/γ-Al_2O_3 to assess individual deoxygenation capabilities before being combined with a zeolite. As expected, little change in products occurred over γ-Al_2O_3 except an 8% increase in CO yield. While not unexpected, as γ-Al_2O_3 has been shown to be an ineffective bio-oil deoxygenation catalyst,[185] the addition of Pt to γ-Al_2O_3 further reduced oxygenate yield by another 22%, producing increased amounts of CO_2 and CH_4, as shown in Figure 5.2. We attribute the formation of CO_2 and CH_4 to methanation and water-gas-shift reactions on Pt sites because these gases are not formed in significant quantities over HZSM-5 in the absence of additional Pt. Fisk et al. demonstrated the deoxygenation of synthetic bio-oil over Pt catalysts in a heated, pressurized batch reactor at 100 psi and 350 °C and showed that Pt/γ-Al_2O_3 was active for reforming by rejecting oxygen as CO_2 through water-gas-shift, yielding 25% CO_2 by weight.[186] Their observed molar yield of methane was approximately

half that of CO_2, and little to no CO formation was observed over Pt.

As shown in Figure 5.2, the formation of CO_2 in our system was also accompanied by an increase in CH_4 yield and a decrease in CO yield when compared with results obtained over γ-Al_2O_3 and Pt/γ-Al_2O_3, consistent with the presence of methanation and water-gas-shift reactions. While our experiments were carried out at atmospheric pressures, ideally, higher pressures would be used to obtain higher conversion of oxygenates. For example, Nimmanwudipong et al. carried out hydrodeoxygenation of guaiacol (a common component of bio-oil) over Pt/γ-Al_2O_3 at 300 °C and found that, upon increasing the hydrogen partial pressure to 140 kPa, conversion increased from 0.6% to 8%.[187]

The zeolite bed length was varied, as described previously, to illustrate the evolution of cellulose pyrolysis products formed by zeolitic upgrading (Figure 5.3). Decarbonylation appears to be the predominant deoxygenation process, as evidenced by the simultaneous increase in CO yield from 35% to 55% and decrease in oxygenate yield from 50% to 10% with variation in zeolite bed length from 0 to 20 mm. Light hydrocarbon formation increases steadily over the course of the bed, as evidenced by the increase in C_{2-4} yield with increasing oxygenate conversion shown in Figure 5.3. Equal yields of saturated (ethane and propane) and unsaturated (ethylene and propene) compounds were obtained at the beginning of the bed but ethane and propane represent 75% of the C_{2-4} compounds at the end of the bed. The presence of paraffins suggests that Pt not only carries out C–C bond scission but also hydrogenates unsaturated compounds. This could explain the 7% reduction in aromatic formation with the addition of Pt to monofunctional HZSM-5 (Table 5.1), because the mechanism of aromatic formation requires olefinic hydrocarbons which could be hydrogenated to paraffins.[178,188]

5.3.4 Performance of HFER-based catalysts

Determining the effect of zeolite pore size on the product distribution of oxygenates is difficult due to the complexity of the reactant and product streams; however, some differences between products formed from HZSM-5 and HFER are clear. As illustrated in Figure 5.4, HFER tended to form light gases such as CH_4 and C_{2-4} olefins. The most noticeable difference was the lack of aromatics that formed over HFER, likely due to the restrictiveness of the smaller 8-MR pores.[189] Mihalcik et al. ob-

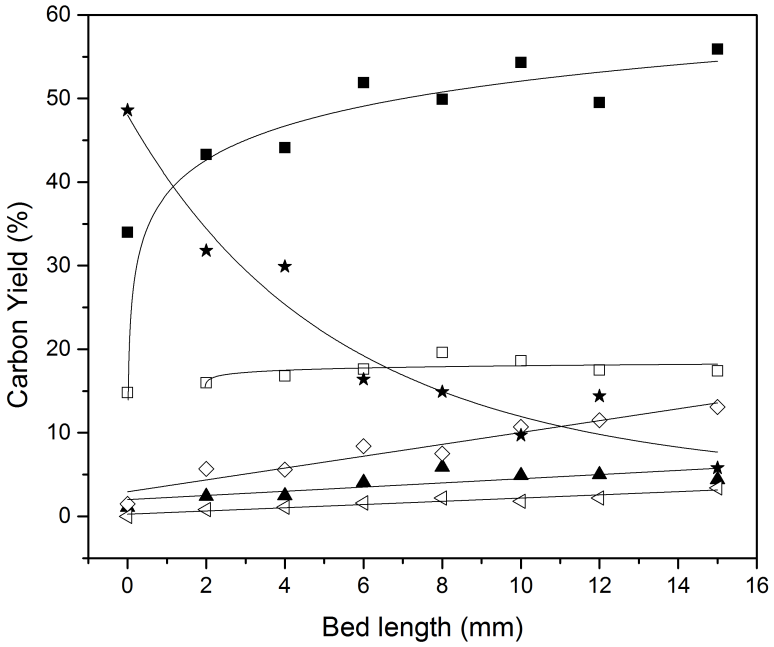

Figure 5.3: Bed length study of HZSM-5/Pt at 30 minutes on stream, illustrating the carbon yield to each product or group of products.

served a similar result while carrying out catalytic pyrolysis of lignocellulosic biomass over HFER and obtained 20 wt% of non-condensable gases and a negligible aromatics yield.[171] Despite the lack of aromatics, the HFER/Pt catalyst was still able to convert 99% of the incoming oxygenate reactant stream, similar to that observed when using HZSM-5/Pt as discussed above.

5.3.5 Performance of USY-based catalysts

Ultra-stabilized Y zeolite (USY) possesses the largest pore diameter of the zeolites tested in this study, with 12-MR pores. Oxygenate yield remained high over USY, increasing from 28% to 37% over 30 minutes of operation. In studies comparing a range of zeolites, zeolite-Y has consistently shown high deoxygenation activity, but low aromatics selectivity,[190–192] consistent with the data shown in Figure 5.5. As with HFER and HZSM-5 experiments, less than 5% CO_2 formed over USY, which catalyzed biomass deoxygenation mainly through CO and H_2O formation. The 28%

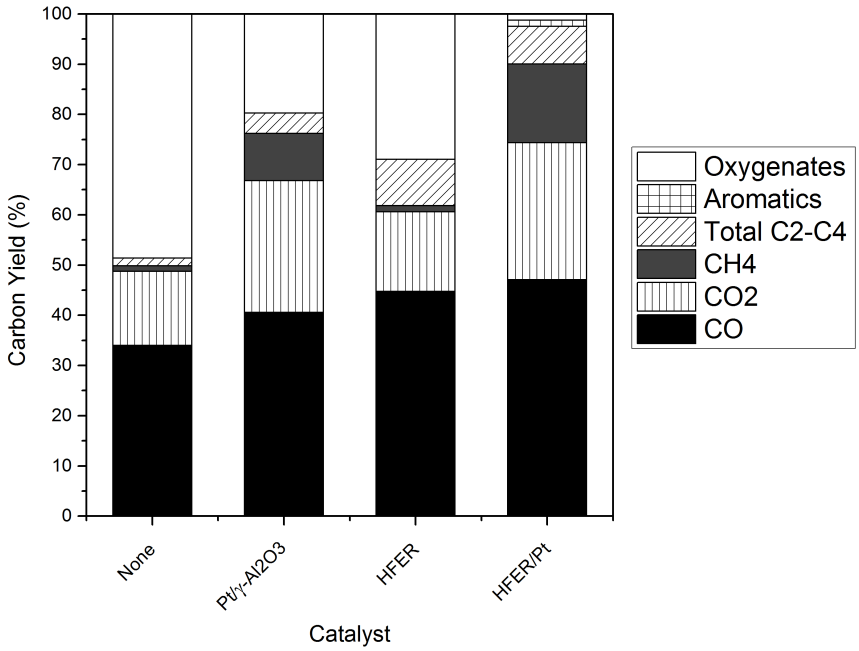

Figure 5.4: Carbon yield to reactor products over control catalysts and HFER at 5 min on stream.

oxygenate yield over 12-MR pore USY is similar to the 29% oxygenate yield over 8-MR pore HFER indicating that the two appear to be equally active for deoxygenation despite large differences in pore size. However, a direct comparison is made difficult by the presence of zeolite deactivation. While larger pore sizes may be more accommodating to a greater number of reactant species, they are also more accommodating to polycyclic aromatics which can quickly deactivate the catalyst.[193] USY may be more active for deoxygenation than HFER but will also deactivate faster so a direct comparison, even at the same time-on-stream, is not feasible. When Pt/γ-Al_2O_3 was added, the oxygenate yield decreased from 28% to 7% leading to an increase in CH_4 and light hydrocarbon production, suggesting that the intrinsic activity of the Pt catalyst affected the conversion of oxygenates to these products. However, it is difficult to determine how the products that form over one catalyst interact with another catalyst when working with a complex feedstock such as cellulose pyrolysis vapors.

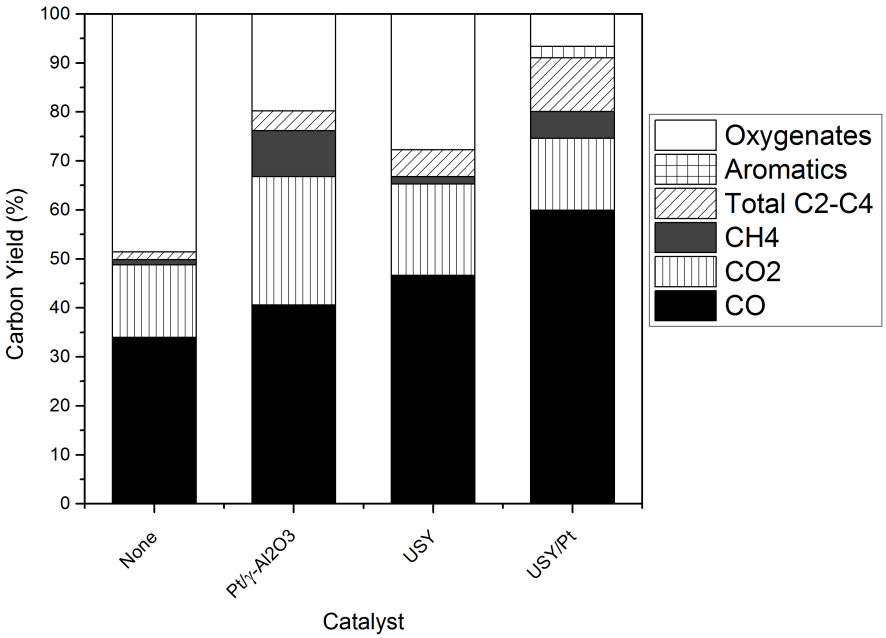

Figure 5.5: Carbon yield to reactor products over control catalysts and USY at 5 min on stream.

5.3.6 Comparison between product yields obtained over monofunctional and bifunctional catalysts

When comparing the performance of the individual components of the bifunctional HZSM-5 with Pt/γ-Al_2O_3 catalyst, we observed a compromise between the behaviors of the two individual catalysts, as well as some synergistic effects. As shown in Table 5.1 and Figure 5.2, complete deoxygenation of the incoming pyrolysis vapors was achieved at 5 minutes on stream over HZSM-5 with Pt/γ-Al_2O_3 while a 20% oxygenate yield remained with Pt/γ-Al_2O_3 separately and a 13% yield with HZSM-5 separately. The addition of Pt active sites while keeping the zeolite loading constant likely explains the increase in conversion of the incoming pyrolysis product stream. The increase in pyrolysis product conversion can also be observed when comparing HFER and HUSY with their bifunctional counterparts.

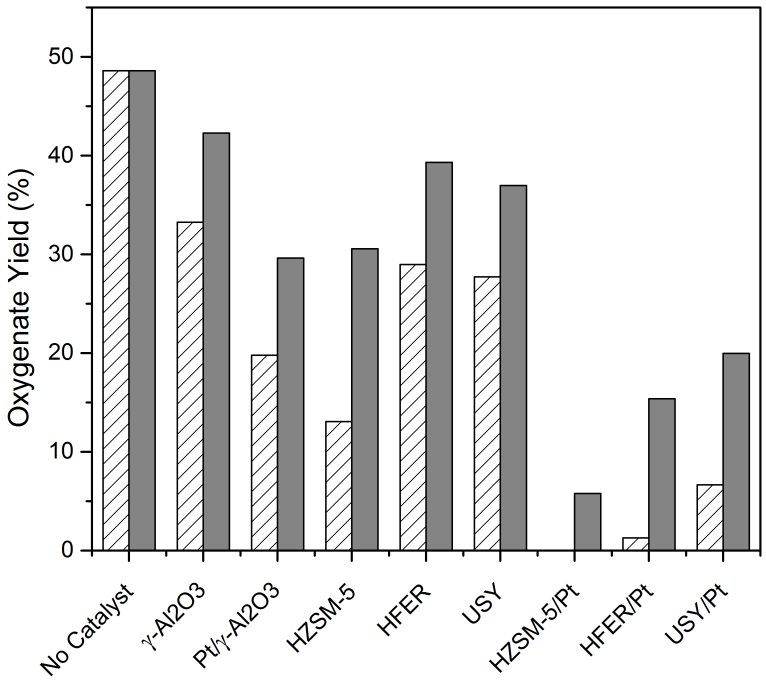

Figure 5.6: Carbon yield of oxygenates as a function of catalyst and time-on-stream. Stripes: 5 min, Solid: 30 min.

5.3.7 Catalyst Deactivation

Deactivation (illustrated in Figure 5.6) occurred from 5 to 30 minutes on-stream as shown by an increase in oxygenate yield. Deactivation is a phenomenon frequently observed in bio-oil upgrading, and generally occurs due to the buildup of polycyclic aromatic species, or coke. Carbonaceous deposits can be of thermal or catalytic origin, and can be found on the catalyst surface, around pore openings, and inside the pores themselves.[71,169,174,194] Acetaldehyde and furfural have been shown to contribute to coke formation, due to the reactivity of acetaldehyde and tendency to form thermal coke, and the tendency of furans to polymerize.[71] Both acetaldehyde and furans were found to form over each catalyst tested.

As shown previously,[44,50] the pyrolysis stage of the reactor does not deactivate because coke formation is not thermodynamically predicted at the temperatures that are observed over the Pt sphere bed (~700 °C). All of the catalysts in the zeolite stage showed some degree of deactivation. Superior deoxygenation performance and

a slower rate of deactivation were observed over bifunctional catalysts when compared with monofunctional catalysts. The decreased rate of deactivation may be a result of hydrogenation reactions that have been shown to remove species that promote coke formation in the temperature range of our experiment.[131] The tendency for oxygenated reactants to form coke and deactivate zeolites may necessitate future solid acid-based catalysts to include a metal component. With each zeolite tested, the oxygenate selectivity was observed to be lower over a bifunctional catalyst than a monofunctional catalyst regardless of the zeolite type. The combination of two catalytic functions may enable the catalyst to process a wider array of reactants, a property especially necessary when converting complex feedstocks such as cellulose pyrolysis vapors.

Despite the deactivation that occurs, coke formation is not significant. We found coke not to exceed 2 wt% of the products as measured by coke burnoff experiments. By contrast, Sharma et al. obtained 30 wt% of coke from upgrading of aspen-derived bio-oil over HZSM-5 at 410 °C.[195] Similarly, Vispute et al. upgraded water-soluble bio-oil derived from pine wood over HZSM-5 at temperatures ranging from 120 to 250 °C, and pressures ranging from 52 to 100 bar[196] and found coke yields ranging from 12 to 50% depending on the type of bio-oil and the presence of Pt or Ru addition to the catalyst. One possible explanation to account for the differences in observed coke formation is that the bio-oil used by most of these groups is lignocellulosic and contains aromatics that are known coke precursors. By contrast, we use pyrolysis vapors obtained from pure cellulose, which contains no aromatics.

An additional possibility is the presence of water in our system. Water has been used to attenuate coke formation in systems that convert methanol and bio-oil to hydrocarbons. Water and olefins are believed to compete for adsorption onto the same sites thus limiting the tendency of oligomers to form coke.[197] Sharma and Bakhshi found that when reacting bio-oil from aspen wood over HZSM-5 at 410 °C, 3.6 h^{-1}, and at atmospheric pressure, the coke yield decreased from 36 to 21% with the addition of 17 wt% of steam. Gayubo et al. found that when reacting synthetic bio-oil, an increase in steam addition from 1.25 to 9 weight ratio of water to bio oil lead to a decrease in coke deposition from 8 to 3 wt%.[71] While Vispute et al. fed pinewood-derived bio-oil diluted with water in a 1:4 weight ratio,[196] water is generated in our system by H_2 oxidation as a sacrificial fuel reaction. Assuming a stoichiometric reaction of sacrificial H_2 and O_2 to water and assuming negligible amounts of water is formed by

cellulose pyrolysis, the pyrolysis vapor feed to the zeolite would contain an additional 65 wt% of water which is ~3 times higher than the wt% of water used by Vispute et al. in their studies. A combination of these possibilities may account for the low rates of coke formation in the autothermal staged reactor.

5.3.8 Proof of concept for autothermal operation

The results thus far have been collected in an autothermal reactor that had the second stage heated with heating tape to mitigate the effect of thermal fluctuations and gradients. The temperatures used in the study, however, are achievable in a heat-integrated configuration if the zeolite bed is placed in the appropriate position downstream of the first stage. A 15 mm bed of HZSM-5/Pt was inserted 4 cm downstream of the first stage and the reactor was run at the same flow rates as the controlled studies. Temperatures at the front and back face of the zeolite bed were 540 and 500 °C, respectively. Carbon selectivity to oxygenates was 2% at 5 minutes, 11% at 60 minutes, and 30% at 150 minutes. As observed in temperature-controlled studies, the CO_2 yield was 25% initially, but dropped to a steady 20% in the first 30 minutes. Methane and light hydrocarbon yields were both initially 10% and reduced to 2 and 6% at 150 minutes on stream, respectively. The performance of the reactor in a fully heat-integrated configuration confirmed the results obtained in the previous sections, namely that a noble metal CPO catalyst and bi-functional zeolite/Pt catalyst can be used in concert to perform catalytic pyrolysis and upgrading of cellulose.

5.4 Conclusions

Oxidative pyrolysis of cellulose was combined with zeolite-catalyzed pyrolysis vapor upgrading in a staged autothermal reactor. Complete conversion of oxygenated bio-oil species to a mixture of CO, CO_2, methane, ethane, propane, and aromatics was obtained over a combination of HZSM-5 and Pt/γ-Al_2O_3 at 500 °C. The majority of deoxygenation was accomplished through decarbonylation and dehydration and not decarboxylation. Deactivation was observed over all catalysts within 30 minutes on stream but had the slowest rate over the bifunctional catalysts, possibly due to the hydrogenation of coke precursors over Pt. Of the bifunctional catalysts, HZSM-

5/Pt was the most selective for aromatics indicating that the pore structure is an important factor in pyrolysis vapor upgrading. Heat-integrated autothermal operation was demonstrated over HZSM-5/Pt with no observable differences in oxygenate conversion or product yields. These results show that high-throughput processing of cellulose to valuable chemicals can be accomplished in a small-scale, high-throughput reactor at atmospheric pressure without external heat input and less deactivation than conventional reactors.

CHAPTER

SIX

CONVERSION OF GLYCEROL TO LIGHT OLEFINS AND GASOLINE PRECURSORS

Autothermal staged reactors are discussed in Chapters 2, 3, and 5. In this chapter, a staged reactor that also combines metal and acid functionalities is applied to the development of a glycerol-to-olefins process. An autothermal capability was not required and so the staged reactor employed was isothermal. We explore a glycerol-to-olefins process in a reactor containing dehydration, hydrogenation, and upgrading stages in series. Glycerol, co-fed with H_2 over HZSM-5 (1.0 g, Si/Al=11.5, 400 °C), was first dehydrated to yield a mixture of acetaldehyde, acrolein, and hydroxypropanone. Acrolein was hydrogenated to propanal over a Pd/α-Al_2O_3 catalyst and the effluent was passed to a third stage which served to further upgrade propanal to olefins. Rapid third stage deactivation was observed, although we obtained a maximum 70% yield of light olefins from a propanal stream reacted over HBEA (0.5 g, 500 °C) with minimal CO production. A decrease in propanal conversion and C_{2-3} olefin yield was observed along with a corresponding increase in C_{4-5} olefin yield as time-on-stream increased to 150 min. We conclude that propanal condensed over Brϕnsted acid sites to form C_{4-5} olefins, which subsequently cracked at high conversion to form C_{2-3} olefins. Increasing the temperature from 400-500 °C also decreased the C_{4-5} olefin yield from 13 to 9% while increasing C_{2-3} olefin yield from 4-15%. C-C bond formation occurred during glycerol upgrading in a staged reactor configuration and negligible carbon is lost as CO.

6.1 Introduction

Global energy challenges has led to heightened interest in the development of renewable carbon-based fuels such as biodiesel as a replacement or supplement for conventional fossil fuels. However, approximately 10 wt% of crude glycerol is obtained as a byproduct of conventional biodiesel production processes,[35,36] limiting process efficiency. Supplanting only a small percentage of petroleum diesel usage with biodiesel would result in an oversupply of glycerol[36] creating an economic obstacle that could prevent wide-spread biodiesel production. Significant research has been devoted to finding new markets for glycerol in an attempt to surmount the glycerol surplus obstacle and help make biodiesel production more economically viable.[36] Additionally, glycerol is a simple sugar and can function as a surrogate for glucose in carbohydrate conversion to hydrocarbons research. While new processes are being explored to convert glycerol into products such as ethers,[198] ethanol,[199] 1,2-propanediol,[200] syngas,[201] and aromatics,[202] one process that has received less attention is olefin production. Light olefins such as ethylene and propylene are common polymer precursors while C_{4-6} olefins can be used in alkylation reactions to produce gasoline-range hydrocarbons through methods such as the Mobil Olefin to Gasoline/Distillate process.[203] Zakaria et al. obtained a maximum 15% olefin yield from glycerol at 600 °C and 105 h^{-1} over Cr/HZSM-5 and Cu/HZSM-5.[204] Corma et al. obtained a maximum 30% yield of ethylene and propylene at 700 °C over HZSM-5 at 30 seconds on stream in a microactivity test reactor,[205] but with 42% of carbon lost as CO. We explore the possibility of developing a tunable process capable of converting glycerol to even higher yields of C_{2-6} olefins with minimal CO production in the interest of finding new pathways for glycerol consumption.

The process we explore utilizes glycerol dehydration and hydrogenation of the ensuing products to form propanal that is further upgraded to olefins by aldol condensation, a reaction that can produce liquid alkanes by C-C bond formation.[206] Glycerol dehydration has been studied in the liquid phase[207,208] and gas phase.[202,209,210] We chose to carry out glycerol dehydration using zeolites because vapor phase glycerol dehydration tends to yield acrolein yields greater than 50% that are stable for more than 2 h on stream.[202] For example, Hoang et al. obtained a 60% yield of acrolein from glycerol at 100% conversion over HZSM-5 at 400 °C, 2 h^{-1}, 2 MPa, and 3 h on stream.[202] The products of glycerol dehydration over HZSM-5 did not react with each

other at times on stream greater than 250 min resulting in a stable product output.

We have identified experimental conditions to aid us in developing a method of processing glycerol into high yields of olefins at temperatures where dealumination is not as predominant, requiring less frequent catalyst replacement. We demonstrate one such approach using a three-staged reactor. The first stage contained a zeolite such as HZSM-5 which served as a glycerol dehydration catalyst, producing stable yields of acrolein and acetaldehyde. A second stage containing a noble metal catalyst, operating at a lower temperature, served as a hydrogenation catalyst to convert acrolein to propanal. A third stage containing HBEA catalyzed the propanal aldol condensation. We also show that a propanal stream in the absence of acetaldehyde fed to HBEA can be converted to ethylene and propylene with yields of up to 70%. Thus, we demonstrate a prototypical tunable system capable of converting glycerol → propanal → olefins assuming removal of acetaldehyde at low temperatures with higher yields.

6.2 Materials and Methods

6.2.1 Catalyst Preparation

The catalysts used were prepared in the same manner as described previously.[47,48] The zeolites used were HBEA (CP814E*; Si/Al=12.5) and HZSM-5 (CBV 2314; Si/Al=11.5). Samples of 1 wt% Pt and Pd were prepared from H_2PtCl_6 (8 wt% in H_2O, Sigma Aldrich) and $PdNO_3$ (4.1 wt% in H_2O, Sigma Aldrich) respectively on γ-Al_2O_3 (Alfa Aesar) and α-Al_2O_3 (Mager Scientific) supports.

6.2.2 Apparatus and Analytical Methods

The three-stage reactor system was constructed, as shown in Figure 6.1, from three quartz tubes (10 mm OD) connected in series. Catalyst particles were situated in each tube between a back-face ceramic foam monolith (α-Al_2O_3, 80 pores per linear inch) and a quartz wool plug front-face. The first stage catalyst contained HZSM-5 (1.0 g), the second stage contained either Pt or Pd impregnated on either α- or γ-Al_2O_3 pellets (1.0 g). The third stage contained 0.5 g of HBEA. The entire assembly was wrapped with heating tape and 1/16" thermocouples (Omega K-type Inconel) were inserted at the back-faces of each catalyst stage and used to control the temperature with

Omega CSC32 Benchtop Controllers. The first and second stage thermocouples were sealed to prevent leakage while the third stage thermocouple was inserted through the reactor outlet. N_2 and H_2 were fed at 1.5 and 0.5 standard liters per minute (SLPM) respectively through a stainless steel nebulizer consisting of concentric ⅛" and 1⁄16" tubes by mass flow controllers (MKS Mass-Flo) along with 40 μL min^{-1} of glycerol by a Valco M50 pump. The nebulizer was inserted through a quartz annulus and 0.2 SLPM of Ar was fed from upstream of the annulus to prevent flow of glycerol vapor back through the reactor. A reactor configuration identical to the one used by Blass et al.[47] was used for experiments using a pure propanal feed (57.3 μL min^{-1}) with an additional 0.2 SLPM of CH_4 fed as an internal standard. Staged reactor product analysis was carried out on a HP 6890 gas chromatograph (GC) equipped with a HP PLOT/Q column (30×0.32×20) and TCD and FID detectors in series. Product identification was aided by a GC/mass spectrometer (HP 5890 GC / 5970 MSD, He carrier). Experiments with a pure propanal feed were analyzed on a HP 5890 GC containing an Alltech Heliflex capillary AT-1 column (60×0.32×1.0) and an FID detector. Mass balances closed to within 15%.

6.2.3 Experimental Procedure

As glycerol was fed to the first stage, samples were analyzed on a GC at 20 min intervals until 160 min on stream. For experiments with two stages, the first stage was aged for 20 min with glycerol prior to introducing additional stages to ensure a steady state production of acrolein and acetaldehyde without aromatics formation that occurs at smaller times-on-stream. After aging, the glycerol feed was turned off and restarted after the additional stages were connected and heated. Hydrogenation of glycerol dehydration products was carried out over Pt or Pd on α- or γ-Al_2O_3 from 100 to 300 °C at 10 and 30 min on stream. The product spectrum was analyzed at the end of each experiment to ensure that the first stage remained at steady state throughout the duration of the experiment. After each experiment, the second stage was removed from the apparatus and separately regenerated at 500 °C with 1.0 SLPM of N_2 and 0.1 SLPM O_2 for 30 min to burn off any coke that formed. The O_2 feed was replaced with 0.1 SLPM of H_2 for an additional 30 min to reduce the catalyst. The first and third stage catalysts containing zeolites were replaced and not regenerated after deactivation.

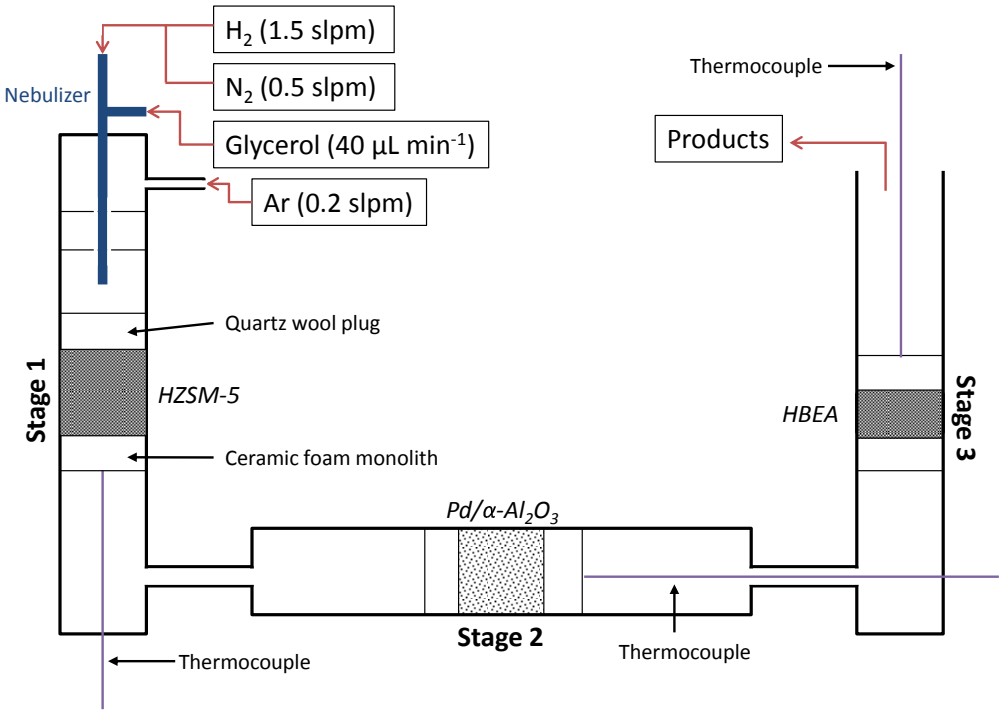

Figure 6.1: Staged reactor schematic used for a glycerol feed.

6.3 Results and Discussion

6.3.1 Glycerol dehydration (one stage)

Previous attempts to convert glycerol to olefins have not produced olefins with yields greater than 30%. As described above, Corma et al. obtained a 30% yield of ethylene and propylene from glycerol in a microactivity test reactor at 700 °C, 30 h^{-1} and 30 s on stream.[205] However, dealumination of the zeolite can occur at these conditions[211,212] requiring frequent catalyst replacement. As a baseline, we show in Figure 6.2 the results of glycerol dehydration over HZSM-5 at 500 °C. The acrolein and acetaldehyde yields reached a steady state of approximately 68% and 30%, respectively, by 100 min on stream. Complete glycerol conversion was observed for the entirety of the experiment and is outlined stoichiometrically in Equation 6.1.

It is unlikely, however, that steady-state yields of acrolein and acetaldehyde are possible due to the likely creation of a staged bed at 100% conversion. A 20% yield of C_{2-4} olefins was obtained at 20 min on stream but the yield decreased to 5% by 60 min and became negligible for the remainder of the experiment. At 500 °C and 20 min on stream, 30% aromatics were formed from glycerol dehydration. The aromatics yield became negligible by 40 minutes on stream with only acrolein and acetaldehyde remaining suggesting that acrolein and acetaldehyde can undergo further cyclization and dehydrogenation to form aromatics. Hoang et al. obtained an initial 40% aromatics yield and 17% light olefin yield over HZSM-5 at 400 °C and 0.1 h^{-1}.[202] They observed that both aromatics and olefin yields became negligible over time while acrolein and acetaldehyde yields increased to steady state values of ~80% and 20% respectively.

While olefins and aromatics were formed at short times on stream, it is likely the available pore structure was disrupted as zeolite coking lead to decreased aromatics formation. The decreasing availability of pore structure resulted in simpler reactions like dehydration, reactions that are not as dependent as aromatization on pore structure, becoming more prevalent.[213] While many kinds of solid acids can catalyze dehydration,[47,72,214] far fewer can catalyze aromatization.[64] The low olefin yields obtained by others from glycerol[202,204,205] help illustrate the difficulty of producing olefins directly from glycerol because, while some olefins and aromatics are formed at small times on stream, deoxygenation reactions to form acrolein and acetaldehyde remain dominant for most of the experiment.

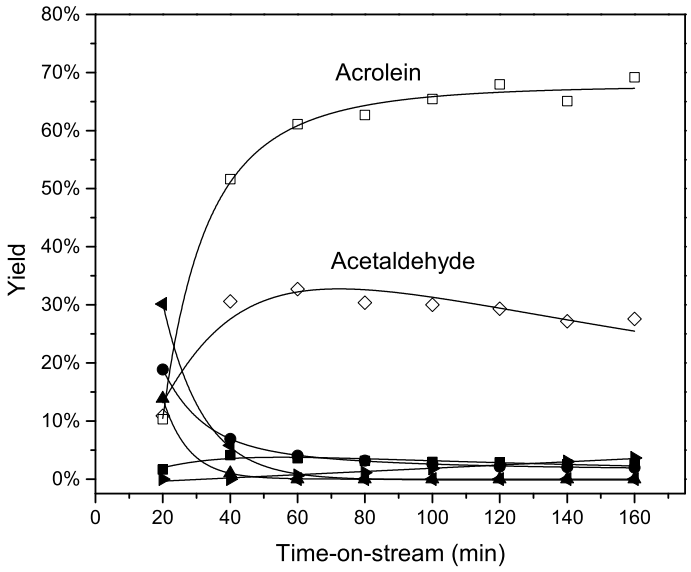

Figure 6.2: Conversion of glycerol with time over HZSM-5 at 500 °C and 3.0 h^{-1} to form acrolein (□), acetaldehyde (◇), C_{2-4} olefins (●), aromatics (◀), CO (▲), hydroxypropanone (▶), and propanal (■).

$$C_3H_8O_3 \longrightarrow 0.33C_2H_4O + 0.72C_3H_4O + 0.055C_3H_6O_2 + 1.8H_2O \tag{6.1}$$

6.3.2 Glycerol dehydration and hydrogenation (two stages)

After dehydration, the next step towards conversion of glycerol to olefins is the hydrogenation of acrolein to propanal which can undergo aldol condensation to form C–C bonds and, subsequently, olefins. Pt/α-Al_2O_3, Pt/γ-Al_2O_3, Pd/α-Al_2O_3, and Pd/γ-Al_2O_3 were evaluated for use in the hydrogenation stage. The temperature of the hydrogenation stage was also varied from 100 to 300 °C. Over both Pt or Pd on either support, lower temperatures favored acrolein hydrogenation while higher temperatures favored C–C bond scission and hydrogenolysis to form smaller molecules such as ethylene, CH_4, and CO (Figure 6.3). Additional pathways for acrolein consumption can be activated at higher temperatures leading to products with smaller sizes.

While all catalysts exhibited similar trends with temperature, Pd was the most

selective for acrolein hydrogenation to propanal. As shown in Figure 6.3, the propanal selectivity from acrolein at 115 °C over Pd/γ-Al_2O_3 and Pd/α-Al_2O_3 was 99% at 115°C and only 70% over Pt on both α-Al_2O_3 and γ-Al_2O_3 at 115 °C. The remaining acrolein was converted to other products such as CO and C_{2-4} paraffins. Others have also shown Pd to be more selective for hydrogenation of the acrolein C=C over the C=O bond.[215,216] Győrffy et al. obtained ~76% selectivity to propanal from acrolein at 97% conversion over Pd colloidal particles and ~40% selectivity to propanal at 89% conversion over Pt colloidal particles at 50 °C.[216] Hydrogenolysis becoming more prevalent at higher temperatures was also observed by Győrffy et al. who obtained ~70% selectivity of ethane from hydrogenolysis of acrolein at 94% conversion as the temperature was increased to 200 °C over Pd.

The support material also had a significant effect on the product distribution over Pt and Pd with temperature. γ-Al_2O_3 is known to have a surface area considerably higher than α-Al_2O_3 which also improves the dispersion and, consequently, activity of impregnated metals.[217] As the temperature increased, the CO yield obtained was 48% at 300 °C over Pt/γ-Al_2O_3 and 23% over Pt/α-Al_2O_3, indicating higher reforming activity over Pt/γ-Al_2O_3 than over Pt/α-Al_2O_3. Similarly, the CO yield obtained was 30% over Pd/γ-Al_2O_3 and 15% over Pd/α-Al_2O_3. Perhaps the most important feature of Figure 6.3 is the hydrogenation selectivity of Pd with temperature. As shown in Figures 6.3c and 6.3d, the propanal yield decreased to 30% over γ-Al_2O_3 and was invariant over α-Al_2O_3 as the temperature was increased from 100 to 200 °C. Concurrently, the propanal yield decreased from 45% to 30% over Pt/γ-Al_2O_3 and remained invariant over Pt/α-Al_2O_3 as the temperature was increased from 100 to 200 °C. Only at 300 °C did the propanal yield begin to decrease over both Pt/α-Al_2O_3 and Pd/α-Al_2O_3. It is possible that higher metal dispersions on γ-Al_2O_3 at temperatures greater than 200 °C made the catalyst too active for selective hydrogenation.

However, lower metal dispersions on α-Al_2O_3 caused the catalyst to be less active, resulting in more selective hydrogenation reactions. Hydrogenolysis requires more contiguous active sites than hydrogenation which only requires one.[218,219] Therefore, a catalyst with a lower dispersion may be more selective for hydrogenation because the relative lack of sites may limit the extent of competing reactions such as hydrogenolysis. Ribeiro et al. found that the extent of hydrogenolysis of hexane over Pt-Re foils at 467 °C decreased as the platinum cluster size decreased with sulfur poisoning leaving only active hydrogenation reactions.[219] Thus, Pd/α-Al_2O_3 was se-

lected for use as the second stage catalyst in all subsequent experiments because it had the highest hydrogenation selectivity over the widest range of temperatures. Flexibility in hydrogenation temperatures is necessary in a system in which compounds like glycerol might be present to prevent any condensation in the reactor which may potentially lead to plugging. For example, second stage temperatures of 140 °C or greater are needed for the glycerol vapor pressure, calculated from Antoine coefficients available from NIST,[220] to be greater than its partial pressure under our experimental conditions assuming differential conversion. Pd/α-Al_2O_3 is capable of selective hydrogenation at those conditions.

All catalysts also produced C_{2-4} compounds besides CO and propanal. As shown in Figures 6.3a and 6.3c, 50% and 40% yields of C_{2-4} compounds were obtained over Pt/γ-Al_2O_3 and Pd/γ-Al_2O_3, respectively, at 300 °C and 10 min on stream. As the second stage temperature increased to 300 °C, the rate of hydrogenolysis to remove oxygen likely also increased, resulting in more deoxygenated product formation. However, the increase in the hydrogenoloysis rate was eclipsed by the increase in the hydrogenation rate which led to all deoxygenated compounds being converted to paraffins. Dehydrogenation of the paraffins formed over noble metals to olefins is considerably more difficult than the reverse reaction because thermodynamic equilibrium favors paraffins at 400 °C and atmospheric pressure. Therefore, an effective glycerol-to-olefins process cannot proceed through a paraffin intermediate so experimental conditions which limit paraffin formation are desirable. However, as shown below, reactions of propanal over zeolites such as HBEA can result in high yields of olefins with minimal paraffin formation.

6.3.3 Glycerol dehydration, hydrogenation, and aldol condensation (three stages)

A third stage was connected to the outlet of the second stage so the acrolein in the second stage effluent could undergo aldol condensation and cracking to form olefins. As shown in Figure 6.4a, propanal and hydroxypropanone appeared to be the most reactive species in the third stage. The propanal yield from glycerol as measured after the third stage decreased by about 5% to 66% at a third stage temperature of 400 °C and to 40% at 500 °C as propanal was consumed in the third stage to form olefins. The hydroxypropanone yield, already small to begin with (~6%), became negligible

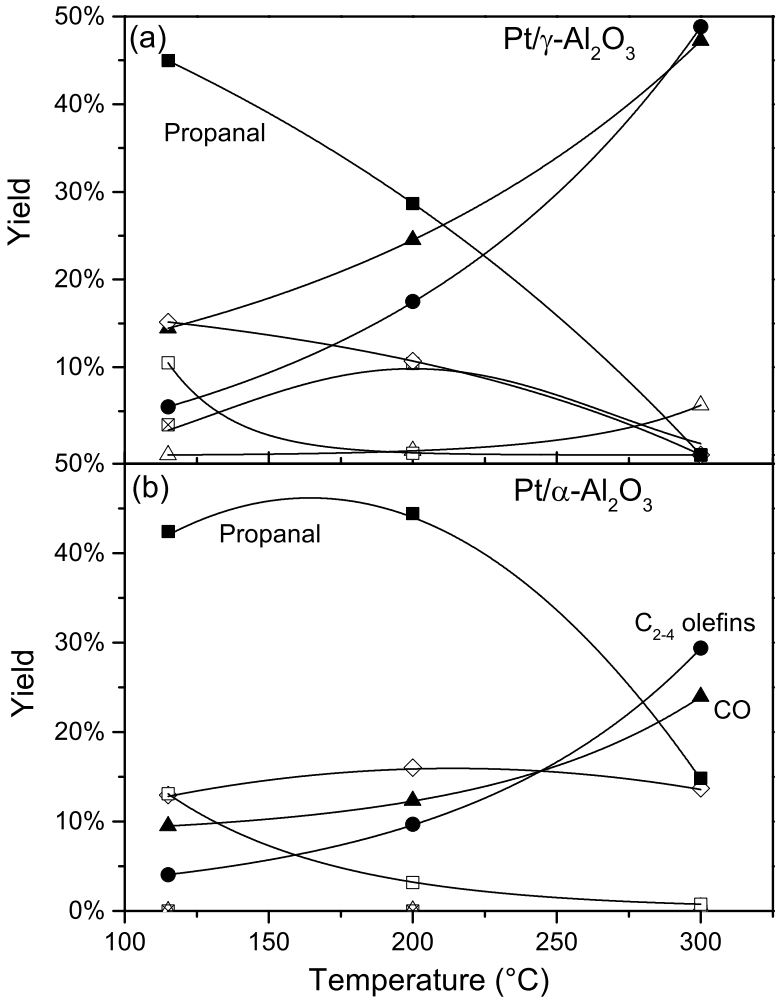
(a)
Pt/γ-Al2O3
Propanal
(b)
Pt/α-Al2O3
Propanal
C2-4 olefins
CO
Yield
Yield
50%
40%
30%
20%
10%
0%
100
150
200
250
300
Temperature (°C)

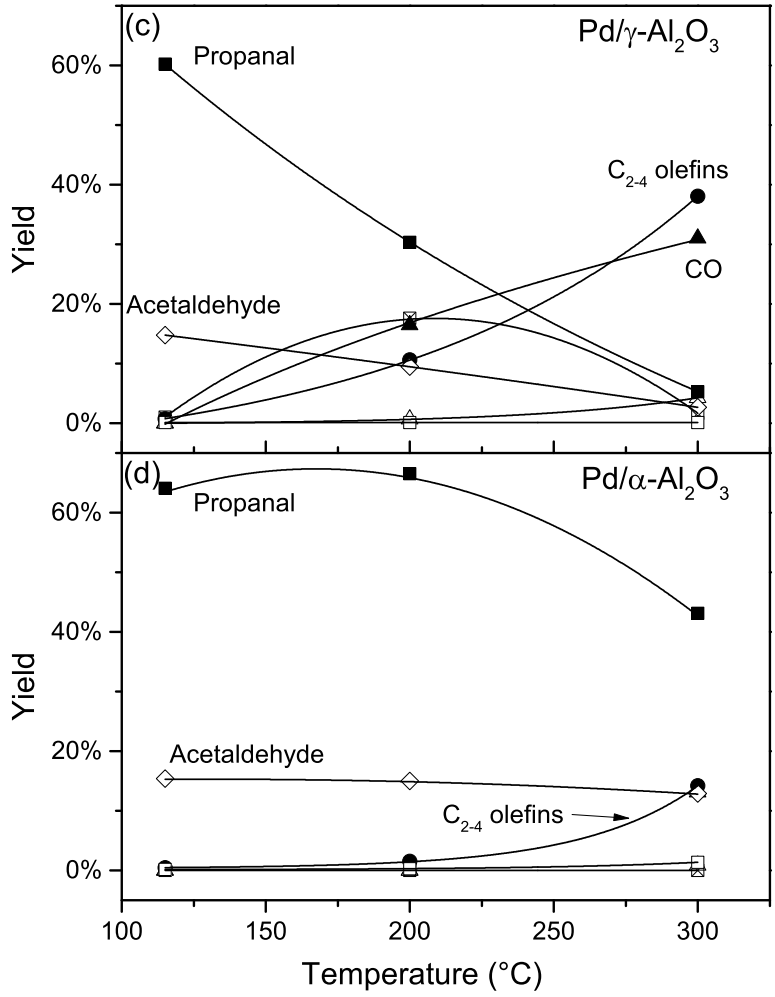

Figure 6.3: Propanal (■), CO (▲), C_{2-4} olefins (●), acetaldehyde (◇), acrolein (□), propanol (⊠), and CH_4 (△) selectivities at different temperatures over second stage noble metal catalysts. Time-on-stream = 10 min, WHSV = 3.0 h^{-1}.

with the introduction of the third stage. The acetaldehdye yield remained relatively constant regardless of the third stage temperature with about 3% of acetaldehyde produced from the first two stages being consumed in the third stage at a temperature of 500 °C. We infer from the results that the majority of products formed in the third stage originated from propanal and hydroxypropanone consumption. The trends are understandable considering that propanal has been shown to undergo aldol condensation and aromatization over zeolites under similar conditions.[78,80,221]

6.3.4 Upgrading of propanal to olefins

We chose to feed 99% pure propanal to the third stage catalyst, bypassing the first two stages, because there are few examples of processes capable of dehydrating glycerol selectively to acrolein. Experiments with a propanal feed were carried out assuming a 100% conversion of glycerol to acrolein with subsequent selective and complete hydrogenation to propanal. These conditions enabled us to simulate an ideal scenario in which acetaldehyde was removed after the second stage to prevent interference with propanal self-condensation. Propanal condensation was carried out over different temperatures and over a range of zeolites with different pore sizes.

Reactivities of propanal from glycerol in a staged reactor and pure propanal feeds

The yields of condensation products formed from propanal in a staged reactor configuration with glycerol as a feed are compared with products formed from reaction of a pure propanal feed over a single stage in Figure 6.4b over HBEA at 10 min on stream and at 400 and 500 °C. The yields obtained in a staged reactor configuration with a glycerol feed were divided by 0.70 to account for the 70% propanal yield from glycerol after two stages. As shown in Figure 6.4b, olefin yields from a pure propanal feed over a single stage are significantly higher than yields in a staged reactor configuration. Conversion increased from 20% and 38% to 50% and 76% at 400 and 500 °C, respectively, upon switching to a pure propanal feed. Meanwhile, the C_{2-5} olefin yield increased from 16% to 45% and 27% to 68% at 400 and 500 °C, respectively. The C_{2-3} also increased from 4% and 11% to 10% and 46% at 400 and 500 °C, respectively. The C_{6-7} compounds consisted of a mixture of aromatics, olefins, and oxygenates while C_{8-9} compounds were almost exclusively aromatics. In all cases, the C_{6-9} yields

were small compared to the C_{2-5} yields. We infer from the results that removal of acetaldehyde is necessary for obtaining desirable yields of olefins from glycerol.

Effect of time-on-stream on product distribution from propanal condensation

While HBEA carrying out propanal upgrading to olefins deactivates within 10 min in the presence of acetaldehyde in a staged reactor configuration with a glycerol feed, conversion of a 99% pure propanal feed over a single stage can continue for at least as long as 150 min, as shown in Figure 6.5. We suspect acetaldehyde may have caused rapid deactivation because propanal upgrading in the absence of acetaldehyde can run for significantly longer times-on-stream. It is possible the acetaldehyde inhibited the self-condensation of propanal by co-adsorption, thus blocking the adsorption of a second propanal molecule. While this inhibition mechanism has not been verified, Yang et al. observed a 40X decrease in the rate of base-catalyzed ethanol conversion to 1-butanol over a Rb-Na exchanged zeolite X at 420 °C upon co-feeding acetaldehyde. They observed the same effect upon co-feeding crotonaldehyde with ethanol over Rb-LiX at the same conditions and suspected crotonaldehyde had a poisoning effect on the ethanol condensation.[222]

When a pure stream of propanal is fed to HBEA, an 83% selectivity at 86% conversion (70% yield) of ethylene and propylene was obtained at 10 min on stream. As time-on-stream increased to 150 min, propanal conversion decreased from 86 to 54% and the C_{2-3} selectivity dropped from 83% to 36% as the catalyst deactivated. Concurrently, the C_{4-5} selectivity increased to 42% at 150 min from 6%. We conclude from the trends in product selectivities with time-on-stream that C_{2-3} are formed from cracking of C_{4-5} olefins which form initially from propanal condensation. We propose that the mechanisms governing the formation of olefins from propanal are similar to those for acetone, an isomer of propanal. There are few studies concerning propanal reactions over HBEA, however, acetone reactions over various zeolite frameworks at similar reaction conditions have produced high selectivities of olefins such as isobutene.

For example, Hutchings et al. obtained an 87% selectivity of isobutene at 49% conversion from acetone condensation over HBEA at 400 °C and 1.6 h^{-1} with the remainder of the products consisting of C_{3-6} compounds.[158,223] Corma et al. proposed that acetone dimerized and cracked to form isobutene and acetic acid[205] in contrast

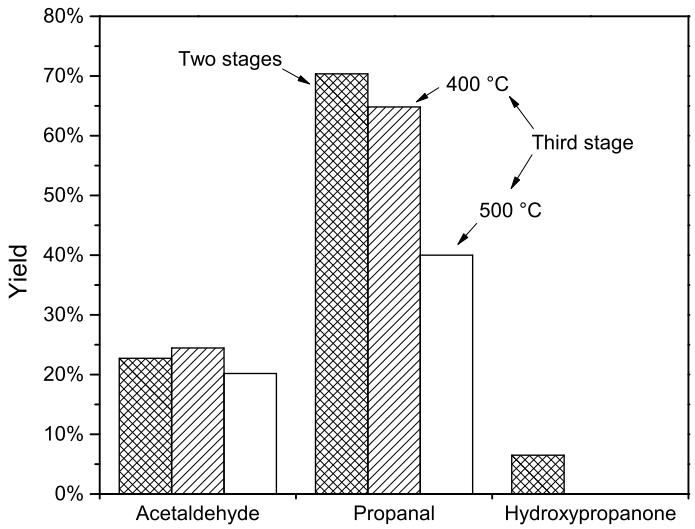

(a) Comparison of reactivities of glycerol dehydration products in staged reactor configuration with two stages (⊠) and three stages at a third stage temperature of 400 °C (⧄) and 500 °C (□). Time-on-stream = 10 min, WHSV = 11.2 h^{-1}.

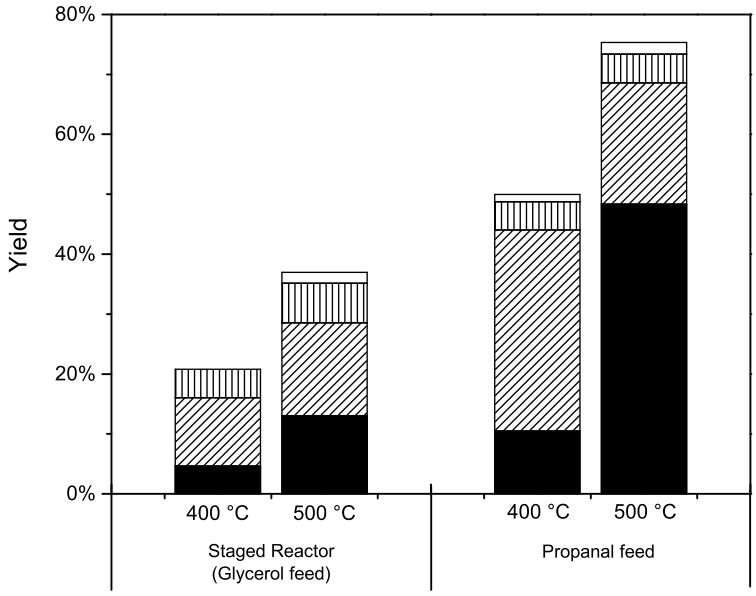

(b) Comparison of propanal condensation products C_{2-3} (■), C_{4-5} (▨), C_{6-7} (▥), and C_{8-9} (□) olefins formed in a staged reactor configuration with a glycerol feed and in a single stage reactor with a pure propanal feed over HBEA. Time-on-stream = 10 min, WHSV = 11.2 h^{-1}.

Figure 6.4

with Hutchings et al. who proposed the formation of isobutene and CO from acetone through an isophorone intermediate.[158] Propanal has been shown to form higher oxygenates through aldol condensation over mixed oxides[224] and zeolites while HBEA and HZSM-5 have been shown to catalyze formation of higher oxygenates but coupled with subsequent cracking of these products to form olefins and aromatics.[158,223] Hoang et al. compared the reactivities of propene and propanal over HZSM-5 at 400 °C and found that propanal had a higher conversion compared to propene and made more aromatics.[80] They obtained ~40% selectivity of aromatics from propanal at 76% conversion (400 °C, 60 min on stream, 7.7 h^{-1}) compared to 1% selectivity at 41% conversion from propene and attributed the difference to the trimerization and dehydration of propanal to mesitylene, among other aromatics. While Hoang et al. obtained high selectivities of aromatics over HZSM-5, we found high olefin yields are possible when reacting propanal over HBEA. Hoang et al. obtained a maximum olefin yield of 20% over HZSM-5 at 400 °C and 100% conversion[78] while we obtained a maximum olefin yield of 71% over HBEA. Therefore, we suggest that propanal also undergoes acid-catalyzed aldol condensation reactions over HBEA but with a higher olefin yield over HBEA than over HZSM-5.

Effect of pore size and temperature on propanal condensation

We varied the pore size and temperature by reacting propanal over HBEA HZSM-5 at 400 and 500 °C to determine experimental conditions which maximize the olefin yield. The products formed over both HBEA and HZSM-5 consisted of largely C_{2-5} olefins with only traces of aromatics. Conversion increased over both HBEA and HZSM-5 as the temperature was increased from 400 to 500 °C along with a corresponding increase in C_{2-3} olefin yield. C_{2-3} yield increased from 6 to 14% over HZSM-5 and from 4 to 15% over HBEA as temperature was increased. Correspondingly, the C_{4-5} olefin yield decreased, likely due to C_{2-3} olefin formation from cracking, further supporting the same conclusion drawn previously from Figure 6.5. The data from Figure 6.6 demonstrates how the tunability of olefin formation from propanal depends on the pore size of the zeolite used as well as the temperature. The product spectrum was shifted to light olefins at higher temperatures and C_{4-5} olefins at lower temperatures.

Pore size also had an effect on the product distribution. The C_{6-9} yields were greater over HBEA than over HZSM-5 possibly because the 12-member ring (12-MR) HBEA pore structure is more accommodating of larger products than the 10-MR

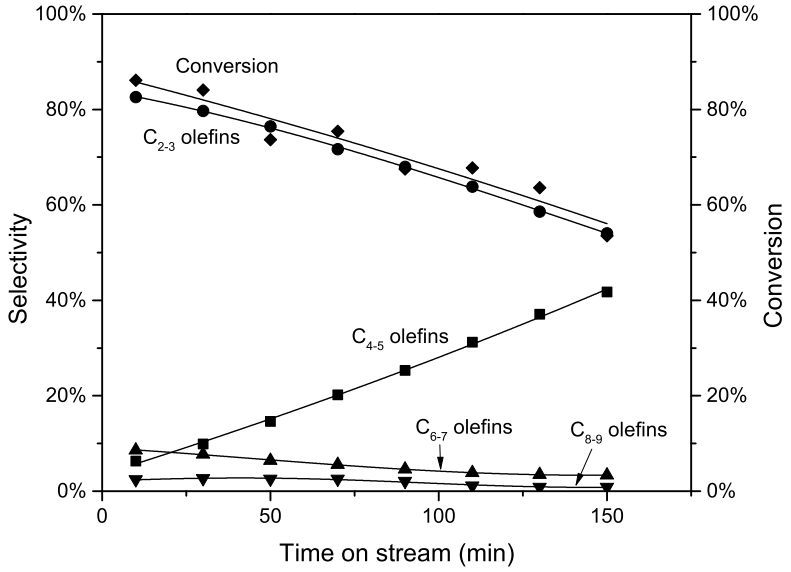

Figure 6.5: Conversion (◆) and C_{2-3} (●), C_{4-5} (■), C_{6-7} (▲), and C_{8-9} (▼) selectivities as a function of time-on-stream for propanal upgrading over HBEA at 500 °C, WHSV = 5.6 h^{-1}.

HZSM-5. The pore size is also important in determining aromatics yields. Hutchings et al. obtained a 46% aromatics selectivity and a 40% C_{4-5} olefins selectivity from acetone over HZSM-5 compared with 3% aromatics and 90% C_{4-5} olefins over HBEA at 378 °C and similar conversions (~62%).[158,223] We observed aromatics yields less than 5% for all zeolites, possibly because the products were evaluated at a time on stream long enough (150 min) to sufficiently deactivate the catalysts, limiting aromatics formation. Thus, the product distribution of a process upgrading propanal to olefins can be tuned by a variation in both pore size and temperature.

6.4 Conclusions

We evaluate the feasibility of a glycerol-to-olefins process in a staged reactor configuration. Glycerol was converted to acetaldehyde, hydroxypropanone, and propanal, of which the latter can undergo aldol condensation and cracking to form C_{2-5} olefins with minimal aromatics and CO production. A high olefin yield can be obtained by propanal conversion in the absence of acetaldehyde over HBEA although deactivation

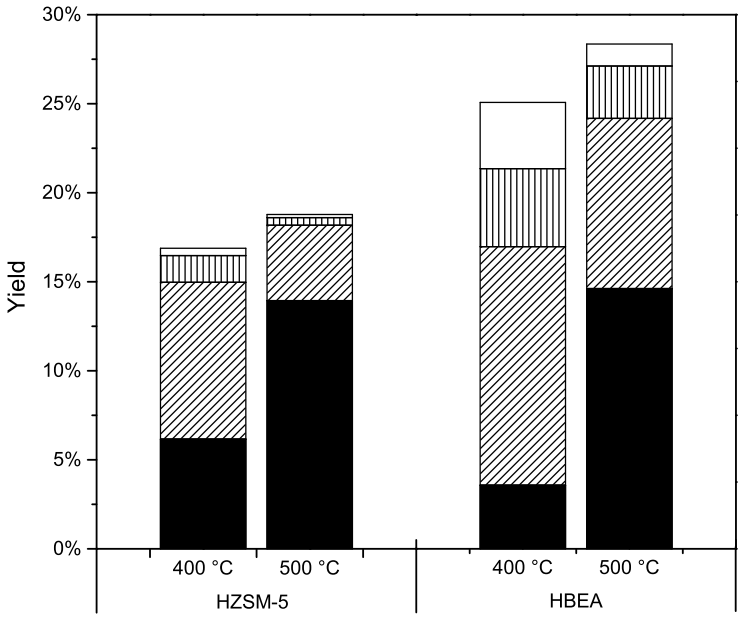

Figure 6.6: Effect of pore size and temperature on C_{2-3} (■), C_{4-5} (▨), C_{6-7} (▥), and C_{8-9} (□) olefin yields. Time-on-stream = 150 min, WHSV = 11.2 h^{-1}.

due to coke formation causes a decrease in propanal conversion with time on stream. The olefin formation process is tunable by varying the temperature and zeolite pore size. For example, the product distribution can be shifted to C_{2-3} olefins at higher temperatures and C_{4-5} olefins at lower temperatures. C_{6-9} products were formed when the zeolite pore size was increased from 10-MR in HZSM-5 to 12-MR in HBEA, likely because larger pores can accommodate larger products. Glycerol-to-olefins is a process that represents a new potential route for glycerol consumption and may aid in the reduction of economic obstacles currently preventing wide-spread biodiesel production.

CHAPTER

SEVEN

FUTURE WORK

7.1 Autothermal staged reactors

7.1.1 Lignocellulosic feed

An autothermal staged reactor was developed for converting a cellulose feed to olefins and aromatics and is described in Chapter 5. While the system worked as intended, the aromatics and olefin yield was quite low and deactivation was rapid. The maximum aromatic yield obtained was 12% over HZSM-5 at 500 °C and 10 min on stream. By subtracting the amount of CO and CO_2 formed from the initial oxidative cellulose pyrolysis, the aromatics yield is approximately doubled to 24%. Deactivation, however, was rapid as evidenced by the increase in the oxygenate yield from 6% to 30% as time-on-stream increased to 30 min. Over Pt/HZSM-5, oxygenates increased to 4% as time-on-stream increased to 30 min but the aromatics yield obtained was only 5%, or 10% when not accounting for the initial CO and CO_2 yields. While the aromatics yield over HZSM-5 was similar to yields observed by others at similar conditions,[184] the yield we obtained over Pt/HZSM-5 was considerably lower. The low olefin and aromatics yields might be attributed to the fact that a pure cellulose feed was used while most biomass upgrading studies use bio-oil generated from lignocellulosic biomass, a feedstock more similar to real biomass than pure cellulose. Lignocellulose contains more phenolic-based aromatics than cellulose which may explain the increased amounts of aromatics found by others.

Considering the low rate of deactivation observed over Pt/HZSM-5, possibly due

to Pt breaking up coke precursors, we propose a lignocellulosic feed to the autothermal staged reactor containing Pt/HZSM-5 in the second stage. A lignocellulosic feed to an autothermal staged reactor may result in higher aromatic yields than a cellulose feed. The reaction can also be carried out at higher pressures because higher hydrogen pressures have been shown to reduce deactivation of hydrocarbon hydroprocessing over bifunctional zeolites.[85] Successful resolution of this project would result in a reactor that can autothermally convert lignocellulosic biomass into a stream of aromatics with a low rate of deactivation and negligible coke formation.

7.1.2 Methane-to-benzene

Another potential application of staged reactors is the dehydroaromatization reaction of methane to benzene, toluene, and xylenes (BTX) shown in Equations 7.1-7.3. Methane, the primary component in natural gas, is abundant and inexpensive and methane coupling to ethylene and benzene, common polymer precursors, is an active area of research. Zeolites such as Mo-exchanged HZSM-5 have emerged as potential methane-coupling catalysts, however, the reaction requires temperatures ~700 °C and equilibrium conversion is limited to 10%.[81] In an autothermal staged reactor, methane-to-benzene is coupled with upstream methane CPO. The downstream stage would consist of Mo-exchanged HZSM-5 synthesized with the same method used by Bedard et al. for the co-processing of oxygenates with methane.[81,82]

The environment of a CPO reactor may be useful for creating the conditions needed for the methane-to-benzene reaction to work. Methane, unconverted from CPO in the first stage, will pass over the second stage heated by the CPO process heat. The Mo in the zeolite pore, capable of C-H bond activation, will catalyze methane coupling to form ethylene. The ethylene formed can then cyclize to form benzene as well as smaller amounts of toluene and xylenes. The formation of benzene shifts the equilibrium of methane to ethylene towards products by consuming ethylene in cyclization reactions.[81,82] For a methane-to-benzene application of a staged autothermal reactor, Pt/α-Al_2O_3 spheres would be loaded into a reactor and serve as a combustion catalyst. Pt was chosen because lower H_2 selectivities are obtained from methane CPO over Pt than Rh due to the decreased extent of endothermic reforming reactions over Pt.[225] The methane-to-benzene equilibrium can be shifted towards reactants and reduce the ethylene yield in the presence of H_2, consequently,

less H_2 formation from methane CPO is desirable.

The yields of ethylene and BTX would be observed as a function of C/O. The experiments would be repeated at a constant C/O because varying the C/O also changes the temperature and the amount of H_2 produced which would change the equilibrium. A successfully coupled methane-to-benzene reactor would be capable of autothermal production of ethylene and benzene from methane.

$$2\,CH_4 \longrightarrow C_2H_4 + 2\,H_2 \tag{7.1}$$

$$3\,C_2H_4 \longrightarrow C_6H_6 + 3\,H_2 \tag{7.2}$$

$$6\,CH_4 \longrightarrow C_6H_6 + 9\,H_2 \tag{7.3}$$

7.1.3 Oxidative Coupling of Methane

Oxidative coupling of methane (OCM) is a reaction that uses methane combustion to generate high temperatures that promote homolytic cleavage of C-H bonds. The initial generation of $CH_3\cdot$ radicals is believed to occur in the gas phase with subsequent $CH_3\cdot$ coupling occurring as a surface reaction on a catalyst.[226] A number of catalysts have been shown to display $CH_3\cdot$ coupling activity with Li/MgO[227] and Sr/La_2O_3[228] being the most common. La_2O_3 without a strontium promoter has also been shown to be catalytically active for the OCM reaction.[229] The best ethylene yields have been limited so far to about 15% because of undesired ethylene oxidation to CO and CO_2.[226] OCM typically requires temperatures from 675-900 °C[226] and an oxidative atmosphere – conditions easily attainable in a SCTR. OCM can also occur thermally and was first demonstrated for acetylene production from methane CPO by Hohn et al. in 1998.[230] A maximum 20% yield of C_2 olefins (15% acetylene and 5% ethylene) was obtained at high gas hourly space velocities ($> 3 \times 10^5$ h^{-1}) and ~1580 °C.

In principle, a high enough methane CPO space velocity ($> 2 \times 10^5$ over 3 wt% Pt/α-Al_2O_3) can result in O_2 breakthrough[225] creating an atmosphere directly below the CPO catalyst that would contain CH_4 and O_2 at temperatures that can exceed 1500 °C—conditions that could be used for OCM. The proposed reactor, an extension of the autothermal staged reactor, will combine both the thermal OCM capability of CPO as demonstrated by Hohn et al.[230] and the surface methane coupling over a

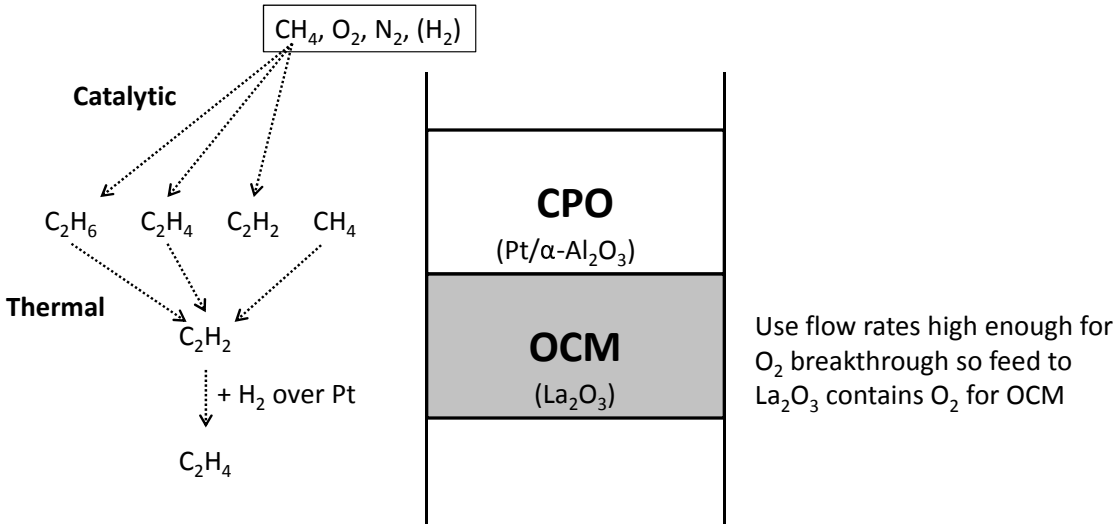

Figure 7.1: Schematic representation of a staged OCM reactor.

conventional downstream OCM catalyst such as Li/MgO or Sr/La_2O_3. As shown schematically in Figure 7.1, methane CPO will be carried out at the same conditions used by Hohn et al.[230] The effluent, containing O_2 due to O_2 breakthrough and up to 20% ethylene and acetylene, will pass through a La_2O_3 bed.

The objective of coupling both CPO and OCM into a staged autothermal reactor is for the OCM catalyst to obtain a higher C_2 yield than has been obtained over either method individually. The temperature of the OCM catalyst can be lowered by increasing the inter-stage distance and relying on radial heat loss to cool the catalyst. This technique was employed in Chapter 3 to change the zeolite temperature and is necessary because the CPO temperature required (> 1500 °C)[230] is greater than conditions used by others over La_2O_3.[227–229,231]

7.2 Isothermal staged reactors

7.2.1 Glycerol upgrading

A glycerol-to-olefins process was discussed in Chapter 6, however, the olefin yield from propanal derived from glycerol was limited to ~40% at 500 °C and 10 min on stream. Upon feeding pure propanal to the same catalyst used in the third stage of the reactor (HBEA), a maximum 70% yield of C_{2-3} was observed and the catalyst lifetime was extended from 10 min to at least 150 min. The acetaldehyde was proposed to be responsible for interfering with the propanal aldol condensation by either coke formation or by blocking propanal molecules from adsorbing to sites containing other

propanal molecules. The water produced from glycerol dehydration (Equation 6.1) is a product of propanal condensation and may have inhibited the reaction.

The first proposed experiment will be a propanal and water co-feed to HBEA at 400 °C. The olefin yield will be measured as a function of the water/propanal ratio. Lower olefin yields should be obtained with increasing proportions of water if water is indeed responsible for inhibiting the reaction. The second experiment will be a propanal and acetaldehyde co-feed to check for acetaldehyde inhibition of propanal condensation. The low boiling point of acetaldehyde (20 °C) makes feeding by pump difficult, therefore, a saturator will have to be employed to obtain steady acetaldehyde flow. If the olefin yield is found to decrease with increasing proportions of acetaldehyde, methods would need to be developed for removing acetaldehyde from the glycerol dehydration effluent to make a glycerol-to-olefins process more feasible such as by liquid condensation or membrane separation. The last possibility is finding a way of producing acrolein selectively from glycerol, a difficult prospect considering the mechanism of glycerol dehydration proposed by Corma et al. shows that acetaldehyde production occurs via a pathway parallel to acrolein production.[205] Despite this difficulty, a selective stream of acrolein from glycerol was reported by Freund et al. at 180 °C over silica.[232]

BIBLIOGRAPHY

[1] Jacobson, M. Z. (2009) Review of solutions to global warming, air pollution, and energy security. *Energy & Environmental Science 2*, 148–173.

[2] Chakrabarti, R., Colby, J. L., and Schmidt, L. D. (2011) Effects of biomass inorganics on rhodium catalysts: I. Steam methane reforming. *Applied Catalysis B: Environmental 107*, 88–94.

[3] Chakrabarti, R., Tupy, S. A., and Schmidt, L. D. (2011) Effects of Biomass Inorganics on Rhodium Catalysts: II. Autothermal Reforming of Ethanol. *Energy & Fuels 25*, 4763–4769.

[4] Alex Marvin, W., Schmidt, L. D., Benjaafar, S., Tiffany, D. G., and Daoutidis, P. (2012) Economic optimization of a lignocellulosic biomass-to-ethanol supply chain. *Chemical Engineering Science 67*, 68–79.

[5] Marvin, W. A., Schmidt, L. D., and Daoutidis, P. (2012) Biorefinery location and technology selection through supply chain optimization. *Industrial & Engineering Chemistry Research 52*, 3192–3208.

[6] Mohan, D., Pittman Jr, C. U., and Steele, P. H. (2006) Pyrolysis of wood/biomass for bio-oil: a critical review. *Energy & Fuels 20*, 848–889.

[7] Huber, G. W., Iborra, S., and Corma, A. (2006) Synthesis of transportation fuels from biomass: chemistry, catalysts, and engineering. *Chemical reviews 106*, 4044–4098.

[8] Devi, L., Ptasinski, K. J., and Janssen, F. J. (2003) A review of the primary

measures for tar elimination in biomass gasification processes. *Biomass and Bioenergy 24*, 125–140.

[9] Sipilä, K., Kuoppala, E., Fagernäs, L., and Oasmaa, A. (1998) Characterization of biomass-based flash pyrolysis oils. *Biomass and Bioenergy 14*, 103–113.

[10] Hickman, D., and Schmidt, L. (1993) Production of syngas by direct catalytic oxidation of methane. *Science 259*, 343–346.

[11] Krummenacher, J., West, K., and Schmidt, L. (2003) Catalytic partial oxidation of higher hydrocarbons at millisecond contact times: decane, hexadecane, and diesel fuel. *Journal of Catalysis 215*, 332–343.

[12] Krummenacher, J., and Schmidt, L. (2004) High yields of olefins and hydrogen from decane in short contact time reactors: rhodium versus platinum. *Journal of Catalysis 222*, 429–438.

[13] Dauenhauer, P. J., Colby, J. L., Balonek, C. M., Suszynski, W. J., and Schmidt, L. D. (2009) Reactive boiling of cellulose for integrated catalysis through an intermediate liquid. *Green Chemistry 11*, 1555–1561.

[14] Dry, M. E. (2002) The Fischer–Tropsch process: 1950–2000. *Catalysis today 71*, 227–241.

[15] Schulz, H. (1999) Short history and present trends of Fischer–Tropsch synthesis. *Applied Catalysis A: General 186*, 3–12.

[16] McKendry, P. (2002) Energy production from biomass (part 1): overview of biomass. *Bioresource Technology 83*, 37 – 46.

[17] Kerr, R. A. (1998) The next oil crisis looms large - and perhaps close. *Science 281*, 1128–1131.

[18] Bardi, U. (2009) Peak oil: The four stages of a new idea. *Energy 34*, 323–326.

[19] Administration, U. E. I. *International Energy Outlook 2013 (IEO2013)*, 2013. `http://www.eia.gov/forecasts/ieo/pdf/0484(2013).pdf`.

[20] International Energy Agency, *World Energy Outlook*, 2007.

[21] Kessel, D. G. (2000) Global warming - facts, assessment, countermeasures. *Journal of Petroleum Science and Engineering 26*, 157–168.

[22] National Energy Board, *Canada's Oil Sands: Opportunities and Challenges to 2015*, `http://www.neb.gc.ca/clf-nsi/rnrgynfmtn/nrgyrprt/lsnd/pprtntsndchllngs20152006/pprtntsndchllngs20152006-eng.pdf`, 2005.

[23] Charpentier, A. D., Bergerson, J. A., and MacLean, H. L. (2009) Understanding the Canadian oil sands industry's greenhouse gas emissions. *Environmental Research Letters 4*, 014005.

[24] Colborn, T., Kwiatkowski, C., Schultz, K., and Bachran, M. (2011) Natural gas operations from a public health perspective. *Human and Ecological Risk Assessment: An International Journal 17*, 1039–1056.

[25] Peng, B., Dhar, N., Liu, H., and Tam, K. (2011) Chemistry and applications of nanocrystalline cellulose and its derivatives: a nanotechnology perspective. *The Canadian Journal of Chemical Engineering 89*, 1191–1206.

[26] Himmel, M. E., Ding, S.-Y., Johnson, D. K., Adney, W. S., Nimlos, M. R., Brady, J. W., and Foust, T. D. (2007) Biomass recalcitrance: engineering plants and enzymes for biofuels production. *Science 315*, 804–807.

[27] Fengel, D., and Wegener, G. *Wood: Chemistry, Ultrastructure, Reactions*; Walter de Gruyter, 1983.

[28] Schmer, M. R., Vogel, K. P., Mitchell, R. B., and Perrin, R. K. (2008) Net energy of cellulosic ethanol from switchgrass. *Proceedings of the National Academy of Sciences 105*, 464–469.

[29] Hill, J., Nelson, E., Tilman, D., Polasky, S., and Tiffany, D. (2006) Environmental, economic, and energetic costs and benefits of biodiesel and ethanol biofuels. *Proceedings of the National Academy of Sciences 103*, 11206–11210.

[30] Administration, U. E. I. *CO2 Emissions from the Consumption of Petroleum*, 2011.

[31] Perlack, R. D., Wright, L. L., Turhollow, A. F., Graham, R. L., Stokes, B. J., and Erbach, D. C. *Biomass as feedstock for a bioenergy and bioproducts industry: the technical feasibility of a billion-ton annual supply*; Technical Report, 2005.

[32] Clydesdale, F. M., and Francis, F. J. Food vs. Fuel. In *Food Nutrition and Health*; Springer, 1985; pp 254–263.

[33] Ma, F., and Hanna, M. A. (1999) Biodiesel production: a review. *Bioresource technology 70*, 1–15.

[34] Kulkarni, M. G., and Dalai, A. K. (2006) Waste cooking oil an economical source for biodiesel: a review. *Industrial & engineering chemistry research 45*, 2901–2913.

[35] Thompson, J., and He, B. (2006) Characterization of crude glycerol from biodiesel production from multiple feedstocks. *Applied Engineering in Agriculture 22*, 261.

[36] Johnson, D. T., and Taconi, K. A. (2007) The glycerin glut: Options for the value-added conversion of crude glycerol resulting from biodiesel production. *Environmental Progress 26*, 338–348.

[37] Hamelinck, C. N., and Faaij, A. P. (2006) Outlook for advanced biofuels. *Energy Policy 34*, 3268–3283.

[38] Wang, M., Wu, M., and Huo, H. (2007) Life-cycle energy and greenhouse gas emission impacts of different corn ethanol plant types. *Environmental Research Letters 2*, 024001.

[39] Yang, B., and Wyman, C. E. (2008) Pretreatment: the key to unlocking low-cost cellulosic ethanol. *Biofuels, Bioproducts and Biorefining 2*, 26–40.

[40] McGovern, P. E., Zhang, J., Tang, J., Zhang, Z., Hall, G. R., Moreau, R. A., Nuñez, A., Butrym, E. D., Richards, M. P., and Wang, C. (2004) Fermented beverages of pre-and proto-historic China. *Proceedings of the National Academy of Sciences of the United States of America 101*, 17593–17598.

[41] Sutton, D., Kelleher, B., and Ross, J. R. (2001) Review of literature on catalysts for biomass gasification. *Fuel Processing Technology 73*, 155–173.

[42] Asadullah, M., Miyazawa, T., Ito, S.-i., Kunimori, K., and Tomishige, K. (2003) Demonstration of real biomass gasification drastically promoted by effective catalyst. *Applied Catalysis A: General 246*, 103–116.

[43] Aznar, M. P., Caballero, M. A., Gil, J., Martín, J. A., and Corella, J. (1998) Commercial steam reforming catalysts to improve biomass gasification with steam-oxygen mixtures. 2. Catalytic tar removal. *Industrial & engineering chemistry research 37*, 2668–2680.

[44] Balonek, C. M., Colby, J. L., Persson, N. E., and Schmidt, L. D. (2010) Rapid ablative pyrolysis of cellulose in an autothermal fixed-bed catalytic reactor. *ChemSusChem 3*, 1355–8.

[45] Huber, G. W., and Corma, A. (2007) Synergies between Bio-and Oil Refineries for the Production of Fuels from Biomass. *Angew. Chem., Int. Ed. 46*, 7184–7201.

[46] Mullen, C. A., Boateng, A. A., Goldberg, N. M., Lima, I. M., Laird, D. A., and Hicks, K. B. (2010) Bio-oil and bio-char production from corn cobs and stover by fast pyrolysis. *biomass and bioenergy 34*, 67–74.

[47] Blass, S. D., Rosenthal, C., Bhan, A., and Schmidt, L. D. (2013) Reductive dehydration of butanone to butane over Pt/-Al2O3 and HZSM-5. *Catalysis Communications 42*, 54 – 57.

[48] Persson, N. E., Blass, S. D., Rosenthal, C., Bhan, A., and Schmidt, L. D. (2013) On-line deoxygenation of cellulose pyrolysis vapors in a staged autothermal reactor. *RSC Adv. 3*, 20163–20170.

[49] Salge, J., Dreyer, B., Dauenhauer, P., and Schmidt, L. (2006) Renewable hydrogen from nonvolatile fuels by reactive flash volatilization. *Science 314*, 801–804.

[50] Dauenhauer, P. J., Dreyer, B. J., Degenstein, N. J., and Schmidt, L. D. (2007) Millisecond reforming of solid biomass for sustainable fuels. *Angewandte Chemie (International ed. in English) 46*, 5864–7.

[51] Hickman, D., and Schmidt, L. D. (1992) Synthesis gas formation by direct oxidation of methane over Pt monoliths. *Journal of Catalysis 138*, 267–282.

[52] Michael, B. C., Donazzi, A., and Schmidt, L. D. (2009) Effects of H2O and CO2 addition in catalytic partial oxidation of methane on Rh. *Journal of catalysis 265*, 117–129.

[53] Horn, R., Williams, K., Degenstein, N., Bitsch-Larsen, A., Dalle Nogare, D., Tupy, S., and Schmidt, L. (2007) Methane catalytic partial oxidation on autothermal Rh and Pt foam catalysts: Oxidation and reforming zones, transport effects, and approach to thermodynamic equilibrium. *Journal of Catalysis 249*, 380–393.

[54] Michael, B. C., Nare, D. N., and Schmidt, L. D. (2010) Catalytic partial oxidation of ethane to ethylene and syngas over Rh and Pt coated monoliths: Spatial profiles of temperature and composition. *Chemical Engineering Science 65*, 3893–3902.

[55] Panuccio, G., Williams, K., and Schmidt, L. (2006) Contributions of heterogeneous and homogeneous chemistry in the catalytic partial oxidation of octane isomers and mixtures on rhodium coated foams. *Chemical engineering science 61*, 4207–4219.

[56] Kruger, J. S., Rennard, D. C., Josephson, T. R., and Schmidt, L. D. (2011) Effect of Functional Groups on Autothermal Partial Oxidation of Bio-oil. Part 1: Role of Catalyst Surface and Molecular Oxygen. *Energy & Fuels 25*, 3157–3171.

[57] Kruger, J. S., Rennard, D. C., Josephson, T. R., and Schmidt, L. D. (2011) Effect of Functional Groups on Autothermal Partial Oxidation of Bio-oil. part 2: Role of homogeneous and support-mediated reactions. *Energy & Fuels 25*, 3172–3185.

[58] Rennard, D. C., Dauenhauer, P. J., Tupy, S. A., and Schmidt, L. D. (2008) Autothermal catalytic partial oxidation of bio-oil functional groups: Esters and acids. *Energy & Fuels 22*, 1318–1327.

[59] Kruger, J. S., Chakrabarti, R., Hermann, R. J., and Schmidt, L. D. (2012) Autothermal partial oxidation of butanol isomers. *Applied Catalysis A: General 411*, 87–94.

[60] Chakrabarti, R., Kruger, J. S., Hermann, R. J., and Schmidt, L. D. (2012) Autothermal reforming of isobutanol. *RSC Advances 2*, 2527–2533.

[61] Wheeler, C. (2004) The watergas-shift reaction at short contact times. *Journal of Catalysis 223*, 191–199.

[62] Balonek, C. M. Ph.D. thesis, University of Minnesota, 2011.

[63] Sun, H., Rosenthal, C., and Schmidt, L. D. (2012) Oxidative Pyrolysis of Polystyrene into Styrene Monomers in an Autothermal Fixed-Bed Catalytic Reactor. *ChemSusChem 5*, 1883–1887.

[64] Bhan, A., and Nicholas Delgass, W. (2008) Propane Aromatization over HZSM-5 and Ga/HZSM-5 Catalysts. *Catalysis Reviews 50*, 19–151.

[65] Kaeding, W., Chu, C., Young, L., and Butter, S. (1981) Shape-selective reactions with zeolite catalysts: II. Selective disproportionation of toluene to produce benzene and p-Xylene. *Journal of Catalysis 69*, 392–398.

[66] Weitkamp, J., Jacobs, P. A., and Martens, J. A. (1983) Isomerization and hydrocracking of C9 through C16 n-alkanes on Pt/HZSM-5 zeolite. *Applied catalysis 8*, 123–141.

[67] Denayer, J. F., Souverijns, W., Jacobs, P. A., Martens, J. A., and Baron, G. V. (1998) High-temperature low-pressure adsorption of branched C5-C8 alkanes on zeolite beta, ZSM-5, ZSM-22, zeolite Y, and mordenite. *The Journal of Physical Chemistry B 102*, 4588–4597.

[68] Ji-Lu, Z. (2007) Bio-oil from fast pyrolysis of rice husk: Yields and related properties and improvement of the pyrolysis system. *Journal of Analytical and Applied Pyrolysis 80*, 30–35.

[69] Gayubo, A., Aguayo, A., Atutxa, A., Aguado, R., Olazar, M., and Bilbao, J. (2004) Transformation of oxygenate components of biomass pyrolysis oil on a HZSM-5 zeolite. II. Aldehydes, ketones, and acids. *Industrial & Engineering Chemistry Research 43*, 2619–2626.

[70] Gayubo, A. G., Aguayo, A. T., Atutxa, A., Aguado, R., and Bilbao, J. (2004) Transformation of Oxygenate Components of Biomass Pyrolysis Oil on a HZSM-5 Zeolite. I. Alcohols and Phenols. *Industrial & Engineering Chemistry Research 43*, 2610–2618.

[71] Gayubo, A. G., Aguayo, A. T., Atutxa, A., Valle, B., and Bilbao, J. (2005) Undesired components in the transformation of biomass pyrolysis oil into hydrocarbons on an HZSM-5 zeolite catalyst. *Journal of Chemical Technology & Biotechnology 80*, 1244–1251.

[72] Sun, H., Blass, S., Michor, E., and Schmidt, L. (2012) Autothermal reforming of butanol to butenes in a staged millisecond reactor: Effect of catalysts and isomers. *Appl. Catal., A 445 - 446*, 35 – 41.

[73] Ramesh, K., Hui, L. M., Han, Y.-F., and Borgna, A. (2009) Structure and reactivity of phosphorous modified H-ZSM-5 catalysts for ethanol dehydration. *Catalysis Communications 10*, 567–571.

[74] Chiang, H., and Bhan, A. (2010) Catalytic consequences of hydroxyl group location on the rate and mechanism of parallel dehydration reactions of ethanol over acidic zeolites. *Journal of Catalysis 271*, 251–261.

[75] DeWilde, J. F., Chiang, H., Hickman, D. A., Ho, C. R., and Bhan, A. (2013) Kinetics and Mechanism of Ethanol Dehydration on γ-Al2O3: The Critical Role of Dimer Inhibition. *ACS Catalysis 3*, 798–807.

[76] Biaglow, A., Sepa, J., Gorte, R., and White, D. (1995) A 13C NMR Study of the Condensation Chemistry of Acetone and Acetaldehyde Adsorbed at the Brnsted Acid Sites in H-ZSM-5. *J. Catal. 151*, 373 – 384.

[77] Veloso, C., Monteiro, J., and Sousa-Aguiar, E. (1994) Aldol condensation of acetone over alkali cation exchanged zeolites. *Stud. Surf. Sci. Catal. 84*, 1913–1920.

[78] Hoang, T. Q., Zhu, X., Lobban, L. L., Resasco, D. E., and Mallinson, R. G. (2010) Effects of HZSM-5 crystallite size on stability and alkyl-aromatics product distribution from conversion of propanal. *Catal. Commun. 11*, 977 – 981.

[79] Dumitriu, E., Hulea, V., Fechete, I., Auroux, A., Lacaze, J.-F., and Guimon, C. (2001) The aldol condensation of lower aldehydes over MFI zeolites with different acidic properties. *Microporous Mesoporous Mater. 43*, 341 – 359.

[80] Hoang, T. Q., Zhu, X., Sooknoi, T., Resasco, D. E., and Mallinson, R. G. (2010) A comparison of the reactivities of propanal and propylene on HZSM-5. *Journal of Catalysis 271*, 201–208.

[81] Bedard, J., Hong, D.-Y., and Bhan, A. (2013) CH4 dehydroaromatization on Mo/H–ZSM-5: 1. Effects of co-processing H2 and CH3COOH. *Journal of Catalysis 306*, 58–67.

[82] Bedard, J., Hong, D.-Y., and Bhan, A. (2013) Co-processing CH4 and oxygenates on Mo/H-ZSM-5: 2. CH4-CO2 and CH4-HCOOH mixtures. *Phys. Chem. Chem. Phys. 15*, 12173–12179.

[83] Skinner, M. J., Michor, E. L., Fan, W., Tsapatsis, M., Bhan, A., and Schmidt, L. D. (2011) Ethanol dehydration to ethylene in a stratified autothermal millisecond reactor. *ChemSusChem 4*, 1151–6.

[84] Makarova, M., Paukshtis, E., Thomas, J., Williams, C., and Zamaraev, K. (1994) Dehydration of n-Butanol on Zeolite H-ZSM-5 and Amorphous Aluminosilicate: Detailed Mechanistic Study and the Effect of Pore Confinement. *J. Catal. 149*, 36 – 51.

[85] Scherzer, J., and Gruia, A. J. *Hydrocracking science and technology*; CRC Press, 1996; Vol. 66.

[86] Coonradt, H. L., and Garwood, W. E. (1964) Mechanism of hydrocracking. Reactions of Paraffins and Olefins. *Industrial & Engineering Chemistry Process Design and Development 3*, 38–45.

[87] Weisz, P., and Swegler, E. (1957) Stepwise reaction on separate catalytic centers: isomerization of saturated hydrocarbons. *Science 126*, 31–32.

[88] Sun, H., and Schmidt, L. D. (2011) Methanol dehydration to dimethyl ether in a staged autothermal millisecond residence time reactor. *Applied Catalysis A: General 404*, 81 – 86.

[89] Weber, C., Farwick, A., Benisch, F., Brat, D., Dietz, H., Subtil, T., and Boles, E. (2010) Trends and challenges in the microbial production of lignocellulosic bioalcohol fuels. *Applied Microbiology and Biotechnology 87*, 1303–1315.

[90] Garca, V., Pkkil, J., Ojamo, H., Muurinen, E., and Keiski, R. L. (2011) Challenges in biobutanol production: How to improve the efficiency? *Renewable and Sustainable Energy Reviews 15*, 964–980.

[91] Atsumi, S., Wu, T.-Y., Eckl, E.-M., Hawkins, S., Buelter, T., and Liao, J. (2010) Engineering the isobutanol biosynthetic pathway in Escherichia coli by comparison of three aldehyde reductase/alcohol dehydrogenase genes. *Applied Microbiology and Biotechnology 85*, 651–657.

[92] Atsumi, S., Hanai, T., and Liao, J. C. (2008) Non-fermentative pathways for synthesis of branched-chain higher alcohols as biofuels. *Nature 451*, 86–89.

[93] Williams, C., Makarova, M. A., Malysheva, L. V., Paukshtis, E. A., Zamaraev, K. I., and Thomas, J. M. (1990) Mechanistic studies of the catalytic dehydration of isobutyl alcohol on NaH-ZSM-5. *J. Chem. Soc.{,} Faraday Trans. 86*, 3473–3485.

[94] Shi, B., Dabbagh, H., and Davis, B. (2002) Catalytic Dehydration of Alcohols. Kinetic Isotope Effect for the Dehydration of t-Butanol. *Topics in Catalysis 18*, 259–264.

[95] Zhang, D., Al-Hajri, R., Barri, S. A. I., and Chadwick, D. (2010) One-step dehydration and isomerisation of n-butanol to iso-butene over zeolite catalysts. *Chem. Commun. 46*, 4088–4090.

[96] Houvi?ka, J., Hansildaar, S., and Ponec, V. (1997) The Shape Selectivity in the Skeletal Isomerisation ofn-Butene to Isobutene. *Journal of Catalysis 167*, 273–278.

[97] Cheng, Z. X., and Ponec, V. (1994) Selective Isomerization of Butene to Isobutene. *Journal of Catalysis 148*, 607–616.

[98] Xu, W.-Q., Yin, Y.-G., Suib, S. L., Edwards, J. C., and OYoung, C.-L. (1995) n-Butene Skeletal Isomerization to Isobutylene on Shape Selective Catalysts: Ferrierite/ZSM-35. *The Journal of Physical Chemistry 99*, 9443–9451.

[99] Macho, V., Krlik, M., Jurecekova, E., Hudec, J., and Jurecek, L. (2001) Dehydration of {C4} alkanols conjugated with a positional and skeletal isomerisation of the formed {C4} alkenes. *Applied Catalysis A: General 214*, 251–257.

[100] Bond, J. Q., Alonso, D. M., Wang, D., West, R. M., and Dumesic, J. A. (2010) Integrated catalytic conversion of γ-valerolactone to liquid alkenes for transportation fuels. *Science 327*, 1110–1114.

[101] Mantilla, A., Tzompantzi, F., Ferrat, G., Lpez-Ortega, A., Alfaro, S., Gmez, R., and Torres, M. (2005) Oligomerization of isobutene on sulfated titania: Effect of reaction conditions on selectivity. *Catalysis Today 107108*, 707–712.

[102] Quann, R. J., Green, L. A., Tabak, S. A., and Krambeck, F. J. (1988) Chemistry of olefin oligomerization over ZSM-5 catalyst. *Industrial & Engineering Chemistry Research 27*, 565–570.

[103] Jones, D. S. J., and Pujado, P. R. *Handbook of Petroleum Processing*; Springerlink, 2006; pp 356–360.

[104] Nel, R. J. J., and de Klerk, A. (2007) FischerTropsch Aqueous Phase Refining by Catalytic Alcohol Dehydration. *Industrial & Engineering Chemistry Research 46*, 3558–3565.

[105] Colby, J. L., Dauenhauer, P. J., and Schmidt, L. D. (2008) Millisecond autothermal steam reforming of cellulose for synthetic biofuels by reactive flash volatilization. *Green Chemistry 10*, 773.

[106] Kruger, J. Ph.D. thesis, University of Minnesota, 2011.

[107] Traxel, B., and Hohn, K. (2003) Partial oxidation of methanol at millisecond contact times. *Applied Catalysis A: General 244*, 129–140.

[108] Zhang, D., Barri, S. A., and Chadwick, D. (2011) n-Butanol to iso-butene in one-step over zeolite catalysts. *Applied Catalysis A: General 403*, 1–11.

[109] Guisnet, M. (1996) Skeletal Isomerization ofn-Butenes I. Mechanism ofn-Butene Transformation on a Nondeactivated H-Ferrierite Catalyst. *Journal of Catalysis 158*, 551–560.

[110] de Ménorval, B., Ayrault, P., Gnep, N., and Guisnet, M. (2006) n-Butene skeletal isomerization over HFER zeolites: Influence of Si/Al ratio and of carbonaceous deposits. *Applied Catalysis A: General 304*, 1–13.

[111] Makarova, M., Paukshtis, E., Thomas, J., Williams, C., and Zamaraev, K. (1994) Dehydration of n-Butanol on Zeolite H-ZSM-5 and Amorphous Aluminosilicate: Detailed Mechanistic Study and the Effect of Pore Confinement. *Journal of Catalysis 149*, 36 – 51.

[112] Makarova, M. A., Williams, C., Zamaraev, K. I., and Thomas, J. M. (1994) Mechanistic study of sec-butyl alcohol dehydration on zeolite H-ZSM-5 and amorphous aluminosilicate. *Journal of the Chemical Society, Faraday Transactions 90*, 2147.

[113] Makarova, M., Paukshtis, E., Thomas, J., Williams, C., and Zamaraev, K. (1991) In situ FTIR kinetic studies of diffusion, adsorption and dehydration reaction of tert-butanol on zeolite NaH-ZSM-5. *Catalysis Today 9*, 61–68.

[114] Williams, C., Makarova, M., Malysheva, L., Paukshtis, E., Talsi, E., Thomas, J., and Zamaraev, K. (1991) Kinetic studies of catalytic dehydration of tert-butanol on zeolite NaHZSM-5. *Journal of Catalysis 127*, 377 – 392.

[115] Chiang, H., and Bhan, A. (2011) Catalytic consequences of hydroxyl group location on the kinetics of n-hexane hydroisomerization over acidic zeolites. *Journal of Catalysis 283*, 98–107.

[116] Macht, J., Carr, R. T., and Iglesia, E. (2009) Consequences of Acid Strength for Isomerization and Elimination Catalysis on Solid Acids. *Journal of the American Chemical Society 131*, 6554–6565.

[117] Deluga, G., Salge, J., Schmidt, L., and Verykios, X. (2004) Renewable hydrogen from ethanol by autothermal reforming. *Science 303*, 993.

[118] Subramanian, R., and Schmidt, L. D. (2005) Renewable Olefins from Biodiesel by Autothermal Reforming. *Angewandte Chemie International Edition 44*, 302–305.

[119] Subramanian, R., Panuccio, G., Krummenacher, J., Lee, I., and Schmidt, L. (2004) Catalytic partial oxidation of higher hydrocarbons: reactivities and selectivities of mixtures. *Chemical Engineering Science 59*, 5501–5507.

[120] Williams, K., and Schmidt, L. (2006) Catalytic autoignition of higher alkane partial oxidation on Rh-coated foams. *Applied Catalysis A: General 299*, 30–45.

[121] Sukovich, D., Seffernick, J., Richman, J., Hunt, K., Gralnick, J., and Wackett, L. (2010) Structure, function, and insights into the biosynthesis of a head-to-head hydrocarbon in Shewanella oneidensis strain MR-1. *Applied and Environmental Microbiology 76*, 3842–3849.

[122] Frias, J., Richman, J., Erickson, J., and Wackett, L. (2011) Purification and characterization of OleA from Xanthomonas campestris and demonstration of a non-decarboxylative Claisen condensation reaction. *Journal of Biological Chemistry 286*, 10930.

[123] Gates, B. (1995) Supported metal clusters: synthesis, structure, and catalysis. *Chemical Reviews 95*, 511–522.

[124] de Lucas, A., Valverde, J., Sánchez, P., Dorado, F., and Ramos, M. (2004) Influence of the binder on the n-octane hydroisomerization over palladium-containing zeolite catalysts. *Industrial & Engineering Chemistry Research 43*, 8217–8225.

[125] Weisz, P., and Swegler, E. (1957) Stepwise reaction on separate catalytic centers: isomerization of saturated hydrocarbons. *Science 126*, 31–32.

[126] Chu, H., Rosynek, M., and Lunsford, J. (1998) Skeletal isomerization of hexane over Pt/H-beta zeolites: Is the classical mechanism correct? *Journal of Catalysis 178*, 352–362.

[127] Lonyi, F., Kovacs, A., Szegedi, Á., and Valyon, J. (2009) Activation of Hydrogen and Hexane over Pt, H-Mordenite Hydroisomerization Catalysts. *Journal of Physical Chemistry C 113*, 10527–10540.

[128] Labinger, J., and Bercaw, J. (2002) Understanding and exploiting C–H bond activation. *Nature 417*, 507–514.

[129] Kopinke, F. D., Zimmermann, G., Reyniers, G. C., and Froment, G. F. (1993) Relative rates of coke formation from hydrocarbons in steam cracking of naphtha. 2. Paraffins, naphthenes, mono-, di-, and cycloolefins, and acetylenes. *Ind. Eng. Chem. Res. 32*, 56–61.

[130] Pereira, R., and Pasa, V. (2006) Effect of mono-olefins and diolefins on the stability of automotive gasoline. *Fuel 85*, 1860–1865.

[131] Frye, C. G., Barger, B. D., Brennan, H. M., Coley, J. R., and Gutberlet, L. C. (1963) Hydroisomerization of Olefins. *Industrial & Engineering Chemistry Product Research and Development 2*, 40–42.

[132] Wittenbrink, R., Ryan, D., and Silverberg, S. *Hydroisomerization of a predominantly N-paraffin feed to produce high purity solvent compositions*, 1999, US Patent 5,866,748.

[133] Calemma, V., Peratello, S., Stroppa, F., Giardino, R., and Perego, C. (2004) Hydrocracking and hydroisomerization of long-chain n-paraffins. Reactivity and reaction pathway for base oil formation. *Industrial & Engineering Chemistry Research 43*, 934–940.

[134] Froment, G. (1987) Kinetics of the hydroisomerization and hydrocracking of paraffins on a platinum containing bifunctional Y-zeolite. *Catalysis Today 1*, 455–473.

[135] Bodke, A., Bharadwaj, S., and Schmidt, L. (1998) The effect of ceramic supports on partial oxidation of hydrocarbons over noble metal coated monoliths. *Journal of Catalysis 179*, 138–149.

[136] Eder, F., Stockenhuber, M., and Lercher, J. A. (1997) Brnsted Acid Site and Pore Controlled Siting of Alkane Sorption in Acidic Molecular Sieves. *Journal of Physical Chemistry B 101*, 5414–5419.

[137] Narbeshuber, T., Vinek, H., and Lercher, J. (1995) Monomolecular Conversion of Light Alkanes over H-ZSM-5. *Journal of Catalysis 157*, 388 – 395.

[138] Kotrel, S., Rosynek, M. P., and Lunsford, J. H. (1999) Intrinsic Catalytic Cracking Activity of Hexane over HZSM-5, HBEA and HY Zeolites. *Journal of Physical Chemistry B 103*, 818–824.

[139] Eder, F., and Lercher, J. A. (1997) On the Role of the Pore Size and Tortuosity for Sorption of Alkanes in Molecular Sieves. *Journal of Physical Chemistry B 101*, 1273–1278.

[140] Hoang, T. Q., Zhu, X., Sooknoi, T., Resasco, D. E., and Mallinson, R. G. (2010) A comparison of the reactivities of propanal and propylene on HZSM-5. *Journal of Catalysis 271*, 201 – 208.

[141] Buchanan, J., Santiesteban, J., and Haag, W. (1996) Mechanistic Considerations in Acid-Catalyzed Cracking of Olefins. *Journal of Catalysis 158*, 279 – 287.

[142] Steijns, M., Froment, G., Jacobs, P., Uytterhaeven, J., and Weitkamp, J. (1981) Hydroisomerization and hydrocracking. 2. Product distributions from n-decane and n-dodecane. *Industrial & Engineering Chemistry Product Research and Development 20*, 654–660.

[143] Denayer, J. F., Baron, G. V., Souverijns, W., Martens, J. A., and Jacobs, P. A. (1997) Hydrocracking of n-Alkane Mixtures on Pt/HY Zeolite: Chain Length Dependence of the Adsorption and the Kinetic Constants. *Industrial & Engineering Chemistry Research 36*, 3242–3247.

[144] Martens, J., Jacobs, P., and Weitkamp, J. (1986) Attempts to rationalize the distribution of hydrocracked products. I qualitative description of the primary hydrocracking modes of long chain paraffins in open zeolites. *Applied Catalysis 20*, 239 – 281.

[145] van de Runstraat, A., Kamp, J., Stobbelaar, P., van Grondelle, J., Krijnen, S., and van Santen, R. (1997) Kinetics of Hydro-isomerization of n-Hexane over Platinum Containing Zeolites. *Journal of Catalysis 171*, 77 – 84.

[146] Degnan, T. F., and Kennedy, C. R. (1993) Impact of catalyst acid/metal balance in hydroisomerization of normal paraffins. *AIChE Journal 39*, 607–614.

[147] Weisz, P. (1962) Polyfunctional heterogeneous catalysis. *Advances in Catalysis 13*, 137–190.

[148] Bhasin, M., McCain, J., Vora, B., Imai, T., and Pujado, P. (2001) Dehydrogenation and oxydehydrogenation of paraffins to olefins. *Applied Catalysis A: General 221*, 397–419.

[149] Thybaut, J., Narasimhan, C., Denayer, J., Baron, G., Jacobs, P., Martens, J., and Marin, G. (2005) Acid-metal balance of a hydrocracking catalyst: Ideal versus nonideal behavior. *Industrial & Engineering Chemistry Research 44*, 5159–5169.

[150] Min, H.-K., and Hong, S. B. (2011) Mechanistic Investigations of Ethylbenzene Disproportionation over Medium-Pore Zeolites with Different Framework Topologies. *Journal of Physical Chemistry C 115*, 16124–16133.

[151] Novakova, J., Bosáček, V., Dolejšek, Z., and Kubelkova, L. (1993) Interaction of acetone with ammonia and alcohols over a HZSM-5 zeolite: Part 1. Methanol. *Journal of Molecular Catalysis 78*, 43–55.

[152] Denayer, J. F., Baron, G. V., Jacobs, P. A., and Martens, J. A. (2000) Competitive physisorption effects in hydroisomerisation of n-alkane mixtures on Pt/Y and Pt/USY zeolite catalysts. *Physical Chemistry Chemical Physics 2*, 1007–1014.

[153] Sinha, N. K., and Neurock, M. (2012) A first principles analysis of the hydrogenation of C1-C4 aldehydes and ketones over Ru(0 0 0 1). *J. Catal. 295*, 31 – 44.

[154] Wei, H., Gomez, C., Liu, J., Guo, N., Wu, T., Lobo-Lapidus, R., Marshall, C. L., Miller, J. T., and Meyer, R. J. (2013) Selective hydrogenation of acrolein on supported silver catalysts: A kinetics study of particle size effects. *J. Catal. 298*, 18 – 26.

[155] Alotaibi, M. A., Kozhevnikova, E. F., and Kozhevnikov, I. V. (2012) Hydrogenation of methyl isobutyl ketone over bifunctional Ptzeolite catalyst. *J. Catal. 293*, 141 – 144.

[156] Chaminand, J., aurent Djakovitch, L., Gallezot, P., Marion, P., Pinel, C., and Rosier, C. (2004) Glycerol hydrogenolysis on heterogeneous catalysts. *Green Chem. 6*, 359–361.

[157] Chang, C. D., and Silvestri, A. J. (1977) The conversion of methanol and other O-compounds to hydrocarbons over zeolite catalysts. *J. Catal. 47*, 249 – 259.

[158] Hutchings, G., Johnston, P., Lee, D., Warwick, A., Williams, C., and Wilkinson, M. (1994) The Conversion of Methanol and Other O-Compounds to Hydrocarbons over Zeolite Beta. *J. Catal. 147*, 177 – 185.

[159] Šepa, J., Lee, C., Gorte, R., White, D., Kassab, E., Evleth, E., Jessri, H., and Allavena, M. (1996) carbonyl 13C shielding tensors and heats of adsorption of

acetone adsorbed in silicalite and the 1: 1 stoichiometric complex in H-ZSM-5. *J. Phys. Chem. 100*, 18515–18523.

[160] Knözinger, H., Bühl, H., and Kochloefl, K. (1972) The dehydration of alcohols on alumina: XIV. Reactivity and mechanism. *J. Catal. 24*, 57–68.

[161] Huber, G. W., Iborra, S., and Corma, A. (2006) Synthesis of transportation fuels from biomass: chemistry, catalysts, and engineering. *Chemical reviews 106*, 4044.

[162] Lynd, L. R., Cushman, J. H., Nichols, R. J., and Wyman, C. E. (1991) Fuel ethanol from cellulosic biomass. *Science 251*, 1318–1323.

[163] Bridgwater, A. V. (1995) The technical and economic feasibility of biomass gasification for power generation. *Fuel 74*, 631–653.

[164] Anderson, N. G. (2001) Practical Use of Continuous Processing in Developing and Scaling Up Laboratory Processes. *Organic Process Research & Development 5*, 613–621.

[165] Mullen, C. A., and Boateng, A. A. (2008) Chemical Composition of Bio-oils Produced by Fast Pyrolysis of Two Energy Crops. *Energy & Fuels 22*, 2104–2109.

[166] Adjaye, J., and Bakhshi, N. (1995) Production of hydrocarbons by catalytic upgrading of a fast pyrolysis bio-oil. Part I: Conversion over various catalysts. *Fuel Processing Technology 45*, 161–183.

[167] Diebold, J., and Scahill, J. Biomass to Gasoline. In *Pyrolysis Oils from Biomass*; American Chemical Society, 1988; Vol. 376, pp 23–264.

[168] Foster, A. J., Jae, J., Cheng, Y.-T., Huber, G. W., and Lobo, R. F. (2012) Optimizing the aromatic yield and distribution from catalytic fast pyrolysis of biomass over ZSM-5. *Applied Catalysis A: General 423424*, 154–161.

[169] Horne, P. A., and Williams, P. T. (1995) The effect of zeolite ZSM-5 catalyst deactivation during the upgrading of biomass-derived pyrolysis vapours. *Journal of Analytical and Applied Pyrolysis 34*, 65–85.

[170] Adjaye, J., and Bakhshi, N. (1995) Production of hydrocarbons by catalytic upgrading of a fast pyrolysis bio-oil. Part II: Comparative catalyst performance and reaction pathways. *Fuel Processing Technology 45*, 185–202.

[171] Mihalcik, D. J., Mullen, C. a., and Boateng, A. a. (2011) Screening acidic zeolites for catalytic fast pyrolysis of biomass and its components. *Journal of Analytical and Applied Pyrolysis 92*, 224–232.

[172] Dejaifve, P., Auroux, A., Gravelle, P. C., Vdrine, J. C., Gabelica, Z., and Derouane, E. (1981) Methanol conversion on acidic ZSM-5, offretite, and mordenite zeolites: A comparative study of the formation and stability of coke deposits. *Journal of Catalysis 70*, 123 – 136.

[173] Thring, R. W., Katikaneni, S. P., and Bakhshi, N. N. (2000) The production of gasoline range hydrocarbons from Alcell® lignin using HZSM-5 catalyst. *Fuel Processing Technology 62*, 17–30.

[174] Mores, D., Stavitski, E., Kox, M. H. F., Kornatowski, J., Olsbye, U., and Weckhuysen, B. M. (2008) Space- and time-resolved in-situ spectroscopy on the coke formation in molecular sieves: methanol-to-olefin conversion over H-ZSM-5 and H-SAPO-34. *Chemistry (Weinheim an der Bergstrasse, Germany) 14*, 11320–7.

[175] Elordi, G., Olazar, M., Lopez, G., Castaño, P., and Bilbao, J. (2011) Role of pore structure in the deactivation of zeolites (HZSM-5, Hβ and HY) by coke in the pyrolysis of polyethylene in a conical spouted bed reactor. *Applied Catalysis B: Environmental 102*, 224–231.

[176] Vitolo, S., Bresci, B., Seggiani, M., and Gallo, M. G. (2001) Catalytic upgrading of pyrolytic oils over HZSM-5 zeolite: behaviour of the catalyst when used in repeated upgradingregenerating cycles. *Fuel 80*, 17–26.

[177] Hong, D.-Y., Miller, S. J., Agrawal, P. K., and Jones, C. W. (2010) Hydrodeoxygenation and coupling of aqueous phenolics over bifunctional zeolite-supported metal catalysts. *Chemical communications (Cambridge, England) 46*, 1038–40.

[178] Gayubo, A. G., Aguayo, A. T., Atutxa, A., Aguado, R., Olazar, M., and Bilbao, J. (2004) Transformation of oxygenate components of biomass pyrolysis oil

on a HZSM-5 zeolite. II. Aldehydes, ketones, and acids. *Industrial & engineering chemistry research 43*, 2619–2626.

[179] Balonek, C. M., Lillebø, A. H., Rane, S., Rytter, E., Schmidt, L. D., and Holmen, A. (2010) Effect of alkali metal impurities on Co–Re catalysts for Fischer–Tropsch synthesis from biomass-derived syngas. *Catalysis letters 138*, 8–13.

[180] Graham, R. G., Mok, L. K., Bergougnou, M. A., De Lasa, H. I., and Freel, B. A. (1984) Fast pyrolysis (ultrapyrolysis) of cellulose. *Journal of Analytical and Applied Pyrolysis 6*, 363–374.

[181] Saiz-Jimenez, C., and De Leeuw, J. W. (1986) Lignin pyrolysis products: Their structures and their significance as biomarkers. *Organic Geochemistry 10*, 869–876.

[182] Amen-Chen, C., Pakdel, H., and Roy, C. (2001) Production of monomeric phenols by thermochemical conversion of biomass: a review. *Bioresource Technology 79*, 277–299.

[183] Y., C. N., E., W. D., and R., K. L. Fluidized-Bed Upgrading of Wood Pyrolysis Liquids and Related Compounds. In *Pyrolysis Oils from Biomass*; American Chemical Society, 1988; Vol. 376, pp 24–277.

[184] Adjaye, J. D., Katikaneni, S. P., and Bakhshi, N. N. (1996) Catalytic conversion of a biofuel to hydrocarbons: effect of mixtures of HZSM-5 and silica-alumina catalysts on product distribution. *Fuel Processing Technology 48*, 115–143.

[185] Laurent, E., and Delmon, B. (1994) A Study of the hydrodeoxygenation of carbonyl , carboxylic and guaiacyl groups over sulfided CoMo/y-Al2O3 catalysts. I. Catalytic reaction schemes. *Applied Catalysis A: General 109*, 77–96.

[186] Fisk, C. A., Morgan, T., Ji, Y., Crocker, M., Crofcheck, C., and Lewis, S. A. (2009) Bio-oil upgrading over platinum catalysts using in situ generated hydrogen. *Applied Catalysis A: General 358*, 150–156.

[187] Nimmanwudipong, T., Runnebaum, R. C., Block, D. E., and Gates, B. C. (2011) Catalytic Conversion of Guaiacol Catalyzed by Platinum Supported on Alumina: Reaction Network Including Hydrodeoxygenation Reactions. *Energy & Fuels 25*, 3417–3427.

[188] Danuthai, T., Jongpatiwut, S., Rirksomboon, T., Osuwan, S., and Resasco, D. E. (2009) Conversion of methylesters to hydrocarbons over an H-ZSM5 zeolite catalyst. *Applied Catalysis A: General 361*, 99–105.

[189] Rollmann, L. D. (1977) Systematics of shape selectivity in common zeolites. *Journal of Catalysis 47*, 113–121.

[190] Park, H. J., Jeon, J.-K., Kim, J. M., Lee, H. I., Yim, J.-H., Park, J., and Park, Y.-K. (2008) Synthesis of Nanoporous Material from Zeolite USY and Catalytic Application to Bio-Oil Conversion. *Journal of Nanoscience and Nanotechnology 8*, 5439–5444.

[191] Lappas, A. A., Samolada, M. C., Iatridis, D. K., Voutetakis, S. S., and Vasalos, I. A. (2002) Biomass pyrolysis in a circulating fluid bed reactor for the production of fuels and chemicals. *Fuel 81*, 2087–2095.

[192] Corma, A., Huber, G. W., Sauvanaud, L., and O'Connor, P. (2007) Processing biomass-derived oxygenates in the oil refinery: Catalytic cracking (FCC) reaction pathways and role of catalyst. *Journal of Catalysis 247*, 307–327.

[193] Li, C., and Stair, P. C. (1997) Ultraviolet Raman spectroscopy characterization of coke formation in zeolites. *Catalysis Today 33*, 353 – 360, Catalysis and Photocatalysis on Metal Oxides: Recent Developments.

[194] Guisnet, M., and Magnoux, P. (2001) Organic chemistry of coke formation. *Applied Catalysis A: General 212*, 83–96.

[195] Sharma, R., and Bakhshi, N. (1991) Upgrading of wood-derived bio-oil over HZSM-5. *Bioresource Technology 35*, 57–66.

[196] Vispute, T. P., Zhang, H., Sanna, A., Xiao, R., and Huber, G. W. (2010) Renewable chemical commodity feedstocks from integrated catalytic processing of pyrolysis oils. *Science (New York, N.Y.) 330*, 1222–7.

[197] Gayubo, A. G., Aguayo, A. T., Morán, A. L., Olazar, M., and Bilbao, J. (2002) Role of water in the kinetic modeling of catalyst deactivation in the MTG process. *AIChE Journal 48*, 1561–1571.

[198] Karinen, R., and Krause, A. (2006) New biocomponents from glycerol. *Applied Catalysis A: General 306*, 128 – 133.

[199] Dharmadi, Y., Murarka, A., and Gonzalez, R. (2006) Anaerobic fermentation of glycerol by Escherichia coli: A new platform for metabolic engineering. *Biotechnology and Bioengineering 94*, 821–829.

[200] Gandarias, I., Arias, P., Requies, J., Doukkali, M. E., and Gemez, M. (2011) Liquid-phase glycerol hydrogenolysis to 1,2-propanediol under nitrogen pressure using 2-propanol as hydrogen source. *Journal of Catalysis 282*, 237 – 247.

[201] Rennard, D. C., Kruger, J. S., and Schmidt, L. D. (2009) Autothermal catalytic partial oxidation of glycerol to syngas and to non-equilibrium products. *ChemSusChem 2*, 89–98.

[202] Hoang, T. Q., Zhu, X., Danuthai, T., Lobban, L. L., Resasco, D. E., and Mallinson, R. G. (2010) Conversion of Glycerol to Alkyl-aromatics over Zeolites. *Energy & Fuels 24*, 3804–3809.

[203] Tabak, S. A. *Two stage system for catalytic conversion of olefins with distillate and gasoline modes*, 1984, US Patent 4,433,185.

[204] Zakaria, Z. Y., Amin, N. A. S., and Linnekoski, J. (2013) A perspective on catalytic conversion of glycerol to olefins. *Biomass and Bioenergy 55*, 370–385.

[205] Corma, A., Huber, G., Sauvanaud, L., and O'Connor, P. (2008) Biomass to chemicals: Catalytic conversion of glycerol/water mixtures into acrolein, reaction network. *Journal of Catalysis 257*, 163–171.

[206] Huber, G. W., Chheda, J., Barrett, C., and Dumesic, J. A. (2005) Production of liquid alkanes by aqueous-phase processing of biomass-derived carbohydrates. *Science 308*, 1446–2079.

[207] Ott, L., Bicker, M., and Vogel, H. (2006) Catalytic dehydration of glycerol in sub- and supercritical water: a new chemical process for acrolein production. *Green Chem. 8*, 214–220.

[208] Ramayya, S., Brittain, A., DeAlmeida, C., Mok, W., and Jr, M. J. A. (1987) Acid-catalysed dehydration of alcohols in supercritical water. *Fuel 66*, 1364 – 1371.

[209] Chai, S.-H., Wang, H.-P., Liang, Y., and Xu, B.-Q. (2007) Sustainable production of acrolein: investigation of solid acid-base catalysts for gas-phase dehydration of glycerol. *Green Chem. 9*, 1130–1136.

[210] Tsukuda, E., Sato, S., Takahashi, R., and Sodesawa, T. (2007) Production of acrolein from glycerol over silica-supported heteropoly acids. *Catalysis Communications 8*, 1349 – 1353.

[211] Campbell, S. M., Bibby, D. M., Coddington, J. M., Howe, R. F., and Meinhold, R. H. (1996) Dealumination of HZSM-5 Zeolites: I. Calcination and Hydrothermal Treatment. *Journal of Catalysis 161*, 338 – 349.

[212] Marques, J. P., Gener, I., Ayrault, P., Bordado, J. C., Lopes, J. M., Ribeiro, F. R., and Guisnet, M. (2005) Dealumination of HBEA zeolite by steaming and acid leaching: distribution of the various aluminic species and identification of the hydroxyl groups. *Comptes Rendus Chimie 8*, 399–410.

[213] Bhattacharya, D., and Sivasanker, S. (1995) A Comparison of Aromatization Activities of the Medium Pore Zeolites, ZSM-5, ZSM-22, and Eu-1. *Journal of Catalysis 153*, 353 – 355.

[214] Blass, S. D., Bhan, A., and Schmidt, L. D. (2013) Hydroconversion of liquid hydrocarbons in a staged autothermal reactor. *Applied Catalysis A: General 451*, 153 – 159.

[215] Delbecq, F., and Sautet, P. (1995) Competitive C-C and C-O Adsorption of -- Unsaturated Aldehydes on Pt and Pd Surfaces in Relation with the Selectivity of Hydrogenation Reactions: A Theoretical Approach. *Journal of Catalysis 152*, 217 – 236.

[216] Győrffy, N., and Paal, Z. (2008) Acrolein hydrogenation on PdPt powder catalysts prepared by colloid synthesis. *Journal of Molecular Catalysis A: Chemical 295*, 24–28.

[217] Degenstein, N., Subramanian, R., and Schmidt, L. (2006) Partial oxidation of n-hexadecane at short contact times: Catalyst and washcoat loading and catalyst morphology. *Applied Catalysis A: General 305*, 146–159.

[218] Biloen, P., Dautzenberg, F., and Sachtler, W. (1977) Catalytic dehydrogenation of propane to propene over platinum and platinum-gold alloys. *Journal of Catalysis 50*, 77 – 86.

[219] Ribeiro, F., Bonivardi, A., Kim, C., and Somorjai, G. (1994) Transformation of Platinum into a Stable, High-Temperature, Dehydrogenation-Hydrogenation Catalyst by Ensemble Size Reduction with Rhenium and Sulfur. *Journal of Catalysis 150*, 186–198.

[220] National Institute of Standards and Technology, *NIST Chemistry WebBook: Glycerin*, `http://webbook.nist.gov/chemistry`, 2011.

[221] Zhu, X., Lobban, L. L., Mallinson, R. G., and Resasco, D. E. (2010) Tailoring the mesopore structure of HZSM-5 to control product distribution in the conversion of propanal. *Journal of Catalysis 271*, 88–98.

[222] Yang, C., and Meng, Z. (1993) Bimolecular condensation of ethanol to 1-butanol catalyzed by alkali cation zeolites. *Journal of Catalysis 142*, 37–44.

[223] Hutchings, G. J., Johnston, P., Lee, D. F., and Williams, C. D. (1993) Acetone conversion to isobutene in high selectivity using zeolite β catalyst. *Catalysis Letters 21*, 49–53.

[224] Gangadharan, A., Shen, M., Sooknoi, T., Resasco, D. E., and Mallinson, R. G. (2010) Condensation reactions of propanal over CexZr1xO2 mixed oxide catalysts. *Applied Catalysis A: General 385*, 80 – 91.

[225] Horn, R., Williams, K., Degenstein, N., Bitsch-Larsen, A., Dalle Nogare, D., Tupy, S., and Schmidt, L. (2007) Methane catalytic partial oxidation on autothermal Rh and Pt foam catalysts: Oxidation and reforming zones, transport effects, and approach to thermodynamic equilibrium. *Journal of Catalysis 249*, 380–393.

[226] Lunsford, J. H. (1995) The catalytic oxidative coupling of methane. *Angewandte Chemie International Edition in English 34*, 970–980.

[227] Amin, N. A. S., and Pheng, S. E. (2006) Influence of process variables and optimization of ethylene yield in oxidative coupling of methane over Li/MgO catalyst. *Chemical Engineering Journal 116*, 187–195.

[228] Marafee, A., Liu, C., Xu, G., Mallinson, R., and Lobban, L. (1997) An experimental study on the oxidative coupling of methane in a direct current corona discharge reactor over Sr/La2O3 catalyst. *Industrial & engineering chemistry research 36*, 632–637.

[229] Conway, S., Greig, J., and Thomas, G. (1992) Comparison of lanthanum oxide and strontium-modified lanthanum oxide catalysts for the oxidative coupling of methane. *Applied Catalysis A: General 86*, 199–212.

[230] Hohn, K., Witt, P., Davis, M., and Schmidt, L. (1998) Methane coupling to acetylene over Pt-coated monoliths at millisecond contact times. *Catalysis letters 54*, 113–118.

[231] Le Van, T., Che, M., Kermarec, M., Louis, C., and Tatibouet, J. (1990) Structure sensitivity of the catalytic oxidative coupling of methane on lanthanum oxide. *Catalysis Letters 6*, 395–400.

[232] Erich, F. *Production of unsaturated organic compounds*, 1928, US Patent 1,672,378.